DISSERTATION

submitted to the

Combined Faculties for the Natural Sciences and for Mathematics

of the Ruperto-Carola University of Heidelberg, Germany

for the degree of

Doctor of Natural Sciences

presented by

M.Sc. Lídia Silva

Born in Covilhã, Portugal

Oral examination: September 20th, 2017

Branched-chain amino acid metabolism in the tumor microenvironment interaction

Referees: Prof. Dr. Rüdiger Hell

Dr. Christiane Opitz

Declaration

I hereby declare that I have written the submitted dissertation “Branched-chain amino acid metabolism in the tumor microenvironment interaction” myself and in this process have not used any other sources than those expressly indicated.

I hereby declare that I have not applied to be examined at any other institution, nor have I used the dissertation in this or any other form at any other institution as an examination paper, nor submitted it to any other faculty as a dissertation.

_____

Lídia Silva

Table of contents

Index of figures

Index of tables

Summary

Glioblastoma (GBM) is a highly aggressive tumor that leads to the patient's deaths within approximately one year. Despite recent considerable advances in our understanding of the pathogenetic alterations present in the tumor cells and the nature of the glioblastoma microenvironment, it has not been yet possible to develop effective therapies. The role of tumor-derived metabolites in the interaction of the tumor cells with cells of the tumor stroma, e.g. immune cells, are a promising aspect of glioblastoma biology for defining new therapeutic targets.

This thesis explores different approaches to characterize the branched-chain amino acid (BCAA) metabolism in the tumor-stroma interaction. In the first part I investigated whether and how branched-chain ketoacids (BCKAs), generated in the first step of the BCAA catabolism, are excreted from glioblastoma cells. I found that while the monocarboxylate transporters MCT1 and MCT4 are both capable and sufficient to transport BCKAs across the membranes of living cells, excretion of BCKAs from glioblastoma cells appears to be mediated mostly by MCT1. Additionally, I could show that MCT1 locates in close proximity to the BCKA-generating branched-chain transaminase 1 (BCAT1), suggesting possible functional interaction of the proteins. In the second part I investigated the fate and function of tumor-secreted BCKAs in the tumor-stroma interaction using macrophages as a model of the stroma compartment. Using *in vitro* isotope tracing analysis, it was demonstrated that BCKAs are taken up by macrophages and catabolized to BCAAs. Additionally, exposure to BCKAs reduced the phagocytic activity of macrophages suggesting that in glioblastoma, tumor cell-secreted BCKAs might be able to modulate the tumor-associated macrophages/microglia, contributing to their role in tumor immune suppression and supporting glioblastoma tumor growth and progression. Furthermore, I was able to provide evidence, that the manipulation of BCAT1 expression in the tumor compartment can impact the immune phenotype of tumor-associated macrophages of the stroma compartment via BCKAs and likely other diffusible factors.

Ultimately, this study provides further evidence for the eminent role of BCAA catabolism in glioblastoma by demonstrating that tumor-excreted BCKAs might have a direct role in tumor immune suppression.

Zusammenfassung

Das Glioblastom ist ein höchst aggressiver Tumor, der innerhalb von einem Jahr zum Tod des Patienten führt. Trotz neuester beachtlicher Fortschritte in unserem Verständnis der pathogenetischen Veränderungen in Tumorzellen sowie der Mikroumgebung der Glioblastome, gibt es bislang keine wirksamen Therapien. Ein vielversprechender Ansatzpunkt für neue therapeutische Zielmoleküle liegt in Metaboliten, die vom Tumor abstammen und eine Rolle in der Wechselwirkung zwischen Tumorzellen und Zellen im Tumor umgebenden Gewebe, wie z.B. Immunzellen, spielen.

Die vorliegende Dissertation ermittelt verschiedene Ansätze, um den Metabolismus von verzweigtkettigen Aminosäuren (branched chain amino acids, BCAAs) im Hinblick auf deren Interaktion zwischen Tumor und Stroma zu charakterisieren. Im ersten Teil untersuchte ich, ob und in welchem Ausmaß verzweigtkettige Aminosäuren, die im ersten Schritt des BCAA-Katabolismus entstehen, von Glioblastomzellen ausgeschieden werden. Ich habe herausgefunden, dass die Ausschüttung von verzweigtkettigen Ketonsäuren (BCKAs) aus Glioblastomzellen hauptsächlich durch den Monocarbontransporter MCT1 erfolgt, obwohl sowohl MCT1 als auch MCT4 allein jeweils ausreichend sind, um BCKAs über die Membranen lebender Zellen zu transportieren. Darüber hinaus konnte ich zeigen, dass MCT1 in räumlicher Nähe zum Enzym branched-chain transaminase 1 (BCAT1) liegt, das für die Entstehung von BCKAs zuständig ist, und somit einen Funktionszusammenhang der Proteine vermuten lässt. Im zweiten Teil der Arbeit habe ich Makrophagen als Modell für das Stromakompartiment verwendet, um Schicksal und Funktion der vom Tumor abgesonderten BCKAs hinsichtlich Tumor-Stroma-Wechselwirkung zu untersuchen. Mittels *in vitro* Isotopentracings konnte gezeigt werden, dass BCKAs durch Makrophagen aufgenommen und zu BCAAs abgebaut werden. Außerdem wird die Phagozytoseaktivität von Makrophagen durch die Exposition zu BCKAs reduziert, was darauf hindeutet, dass die von Tumorzellen sekretierten BCKAs in Glioblastomen möglicherweise in der Lage sind, tumor-assoziierte Makrophagen/Mikrogliazellen zu regulieren, indem sie zu ihrer immunsuppressiven Rolle beitragen und das Fortschreiten des Tumorwachstums unterstützen. Zusätzlich konnte ich nachweisen, dass die Manipulation von BCAT1 Expression im Tumorkompartiment den Immunphenotyp der Tumor assoziierten

Makrophagen im Stroma mittels BCKAs und möglicher anderer diffusionsfähiger Faktoren beeinflussen kann.

Zusammenfassend liefert diese Dissertation den Nachweis für die bedeutende Rolle des BCAA Katabolismus in Glioblastomen, indem gezeigt wurde, dass vom Tumor sezernierte BCKAs eine direkte Rolle in der Immunsuppression spielen.

Abbreviations

2-HG	2-hydroxyglutarate
ARF1	ADP-ribosylation factor 1
BCA	Bicinchoninic acid
BCAA	Branched-chain amino acid
BCAT	Branched-chain aminotransferase/transaminase
BCKA	Branched-chain ketoacid
BCKD	Branched-chain α-ketoacid dehydrogenase
BLAST	Basic Local Alignment Search Tool
BSA	Bovine serum albumin
BTSC	Brain tumor stem cell-like
CA	Carbonic anhydrase
CAF	Cancer associated fibroblasts
cBCAT	Cytosolic branched chain aminotransferase
CCL2	C-C Motif Chemokine Ligand 2
CFSE	Carboxyfluorescein succinimidyl ester
CHC	α-cyano-4-hydroxycinnamate
CNS	Central nervous system
coA	Coenzyme A
cRNA	Coding RNA
CSF-1	Colony-stimulating factor 1
DBDS	4,4′-dibenzamidostilbene-2,2′-disulphonate
DIDS	4,4'-Diisothiocyano-2,2'-stilbenedisulfonic acid
DMB	1,2-diamino-4,5-methylendioxybenzene
DMEM	Dulbecco’s modified eagle medium
DMSO	Dimethyl sulphoxide
DNA	Deoxyribonucleic acid
dNTP	Deoxynucleotide
DTT	Dithiothreitol
EDTA	Ethylendiaminetetracetate
EdU	5-ethynyl-2´-deoxyuridine
EGFR	Epidermal growth factor receptor
EI	Electron ionization
ER	Estrogen receptor
ES	Enrichment score
FBS	Fetal bovine serum
FCS	Fetal calf serum
FD	Fast digest
FDA	Food and Drug Administration
FDR	False discovery rate
GAM	Glioma-infiltrating macrophages/microglia
G-CIMP	Glioma-CpG Island Methylator Phenotype
GC-MS	Gas Chromatography-Mass Spectrometry
Glu	Glutamate
GLUT	Glucose transporter
GM-CSF	Granulocyte-macrophage colony-stimulating factor
GPCF	Genomics and Proteomics Core Facility

GPI	Glycosyl-phosphatidyl-inositol
GPNMB	Glycoprotein NMB
GRO	C-X-C motif chemokine ligand 1
GSEA	Gene Set Enrichment Analysis
HIF	Hypoxia-inducible factor
HRP	Horse-raddish peroxidase
HS	Human serum
IDH	Isocitrate dehydrogenase
IGFBP2	Insulin Like Growth Factor Binding Protein 2
IL	Interleukin
INF	Interferon
KIC	α-ketoisocaproate
KIV	α-ketoisovalerate
KMV	α-keto-β-methylvalerate
LB	Luria Bertani
LDHA	Lactate dehydrogenase A
LDHB	Lactate dehydrogenase B
Mac	Macrophages
mBCAT	Mitochondrial branched chain aminotransferase
MCP1	Monocyte chemoattractant protein 1
M-CSF	Macrophage colony-stimulating factor
MCT	Monocarboxylate transporter
MMP	Matrix metalloproteinase
MSUD	Maple syrup urine disease
NAP2	Neutrophil activating protein-2
NB	Normal brain
NES	Normalized enrichment score
NF1	Neurofibromin 1
NSCLC	Non-small cell lung cancer
nt	Non-target
OAA	Oxaloacetate
OPD	O-Phenylendiamine
P/S	Penicillin and streptomycin
PBMC	Peripheral blood mononuclear cells
PBS	Phosphate buffered saline
PCR	Polymerase chain reaction
PDAC	Pancreatic ductal adenocarcinoma
PDGFRA	Platelet-derived growth factor receptor A
PE	Phycoerythrin
PFA	Paraformaldehyde
PGK1	Phosphoglycerate kinase 1
PI	Propidium iodide
PIC	Protease and phosphatase inhibitor cocktail
PLA	Proximity ligation assay
PMA	Phorbol 12-myristate 13-acetate
PR	Progesterone receptor
PTEN	Phosphatase and tensin homolog
qPCR	Quantitative Real Time PCR
RNA	Ribonucleic acid
RPMI	Roswell Park Memorial Institute
RT	Room temperature

RTK	Receptor tyrosine kinase
SD	Standard deviation
SDS	Sodium dodecyl sulfate
SE	Standard error
sh	Short-hairpin
SPP1	Secreted phosphoprotein 1
TAM	Tumor-associated macrophages
TBE	TRIS-borat-EDTA
TBP	TATA-box binding protein
TBS	TRIS-buffered saline
TBS-T	TRIS-buffered saline-Tween
TCA	Tricarboxylic acid
TCGA	The Cancer Genome Atlas
TCM	Tumor-conditioned medium
TM	Transmembrane
TMZ	Temozolomide
TNBC	Triple negative breast cancer
TRIS	Tris-(hydroxymethyl)-aminomethan
UBL	Ubiquitin-like protein
UPLC	Ultra-performance liquid chromatography
VEGF	Vascular endothelial growth factor
WHO	World Health Organization
α-KG	Alpha-ketoglutarate

1. Introduction

1.1. Glioma

Glioma is the most common type of primary brain tumors, accounting for around 70% of primary central nervous system (CNS) neoplasms with an incidence of 5 – 10 people per 100000 annually (DeAngelis, 2001; Louis et al., 2007). Gliomas originate from precursors of glial cells (DeAngelis, 2001) and the vast majority is characterized by diffuse infiltrative growth into the surrounding CNS parenchyma . Diffuse gliomas are traditionally typed as astrocytomas, oligodendrogliomas or as mixed gliomas/oligoastrocytomas based on histopathological features. However, the latter diagnosis is disappearing due to the recent progress made on molecular testing that provides an unambiguous diagnosis of either astrocytic or oligodendroglial tumor (Lenting et al., 2017; Louis et al., 2016). Furthermore, a malignancy grade is assigned to diffuse gliomas (World Health Organization (WHO) grade II-IV) (Lenting et al., 2017). Considering the gliomas with a circumscribed rather than diffuse infiltrative growth pattern, the most frequent examples are pilocytic astrocytoma (WHO grade I) and different variants of ependymoma (WHO grade I-III) (Lenting et al., 2017). The WHO grade is one indicator of the patient prognosis. Patients with grade I glioma survive, on average, for more than 10 years whereas for patients with grade II glioma this value decreases to 5 years. The survival of patients with grade III tumors is around 2-3 years and patients with grade IV glioma, also known as glioblastoma, present the poorest prognosis, frequently succumbing to the disease within 1 year (Louis et al., 2007).

Recently, multiple studies contributed to the identification of molecular events on the basis of gliomagenesis and on their clinical relevance as diagnostic, prognostic and predictive markers. The recently published new WHO classification utilizes some of these markers for the definition of particular glioma entities (Louis et al., 2016). One example are the metabolic enzymes isocitrate dehydrogenase 1 (IDH1) and 2 (IDH2). Mutations in *IDH* genes have been implicated in the pathogenesis of malignant gliomas (Yan et al., 2009). Gliomas with *IDH* mutations are clinically and genetically distinct from gliomas carrying wild-type *IDH* genes (Yan et al., 2009). Point mutations in cytoplasmic IDH1 and, less frequently, mitochondrial IDH2

occur in 70-80% of WHO grade II or III diffuse gliomas (astrocytomas and oligodendroglial tumors) (Yan et al., 2009) and are rare (7-12%) in glioblastoma (Balss et al., 2008; Li et al., 2015; Ohgaki and Kleihues, 2013; Parsons et al., 2008). These mutations cause a gain of a novel enzymatic activity. Instead of isocitrate being converted to α-ketoglutarate (α-KG) with NADPH production, α-KG is converted to 2-hydroxyglutarate (2-HG) with NADPH consumption. In normal cells and tissues, the concentration of 2-HG is low. However, in patients with somatic *IDH1* or *IDH2* mutations, 2-HG levels are high in glioma tissues and support tumor progression (Cairns et al., 2011). Furthermore, these mutations have important consequences for the epigenome and cause extensive DNA methylation in IDH-mutant diffuse gliomas ('glioma-CpG island methylator phenotype'/G-CIMP) (Ceccarelli et al., 2016; Noushmehr et al., 2010).

1.2. Glioblastoma

Glioblastoma (GBM) is the highest grade (WHO grade IV) and most aggressive glioma. Despite aggressive treatment including surgery, adjuvant Temozolomide-based chemotherapy and radiotherapy, the median survival of patients after diagnosis is only around 15 months (Ohka et al., 2012).

According to the 2016 CNS WHO classification, glioblastomas are divided into (1) glioblastoma IDH-wildtype (about 90% of cases); (2) glioblastoma IDH-mutant (about 10% of cases) and (3) glioblastoma NOS, referring to tumors for which full IDH evaluation cannot be performed (Louis et al., 2016).

1.2.1. Subtype classification of GBM

A gene expression-based molecular classification of glioblastoma into proneural, neural, classical and mesenchymal subtypes was proposed by Verhaak et al., 2010 (Verhaak et al., 2010). Aberrations and gene expression of *EGFR*, *NF1*, and *PDGFRA/IDH1* each define the classical, mesenchymal, and proneural subtypes, respectively, whereas no distinctive mutations have yet been found in neural GBMs (Verhaak et al., 2010). Additionally, it was shown that the subtypes have specific differentiation characteristics suggesting alternative cells of origin. The comprehensive genomic- and genetic based classification of GBM is of major importance for investigation of targeted therapies and could ultimately result in personalized therapies for determined groups of patients with GBM (Verhaak et al., 2010).

More recently, DNA methylation profiling studies have identified related but different subgroups of GBM (Noushmehr et al., 2010; Sturm et al., 2012). Specifically, a distinct glioma-CpG Island Methylator Phenotype (G-CIMP)-positive cluster consisting of IDH-mutated tumors was identified, while the remaining, non-mutated tumors were G-CIMP negative. Furthermore, a separate cluster of tumors containing alterations in *PDGFRA*, called "receptor tyrosine kinase I (RTK-I)," emerged corresponding to the proneural IDH wild-type subgroup proposed by Verhaak et al, 2010. The remaining clusters, designated "receptor tyrosine kinase II (RTK-II)," which is enriched for tumors carrying *EGFR* alterations and "mesenchymal," containing many *PTEN* and *NF1* altered tumors, were similar to the classical and mesenchymal subgroups proposed by Verhaak et al, 2010.

1.2.2. Current treatment options

The standard treatment protocol for GBM has not changed since the Food and Drug Administration (FDA) approval of temozolomide (TMZ) in 2005. The current treatment strategy for GBM comprises surgical debulking of the tumor, radiation therapy and chemotherapy. However, the current state of care only slightly prolongs survival, meaning that novel therapeutics are urgently required for the treatment of GBM.

Several reasons contribute to the lack of approved drug-based treatment strategies. On the one hand, it is the high diversity in genetic aberrations in glioma combined with substantial intratumoral heterogeneity and the relatively low incidence of diffuse gliomas (Lenting et al., 2017). On the other hand, gliomas are heterogeneous tumors that contain, among other stromal cells, a high proportion of glioma-associated macrophages and microglia that are highly modulated by glioma-secreted factors, including metabolites. So, with this work we aim to provide additional support for the concept of developing alternative therapy for glioma treatment based on the metabolite exchange between tumor and stromal cells.

1.3. Branched-chain amino acid (BCAA) metabolism in cancer

In contrast to most normal tissues, rapidly proliferating types of cancer have shown to exhibit characteristic alterations of metabolism that encompass an increased consumption of glucose that is mostly metabolized into lactate even in the presence of ample oxygen (Koppenol et al., 2011; Warburg, 1924). This phenotype is termed aerobic glycolysis or the Warburg effect

(Warburg, 1956). Additionally, cancers cells have been shown to exhibit an increased dependence on amino acid metabolism (Dang, 2012). As a consequence, cancer cells typically display elevated uptake of amino acids, in particular glutamine and the essential branched-chain amino acids (BCAAs) valine, leucine and isoleucine (Jain et al., 2012; Mayers et al., 2016). BCAAs participate directly and indirectly in a variety of crucial biochemical functions in the brain and other tissues. These include protein synthesis, the production of energy, the compartmentalization of glutamate, the transfer of nitrogen between tissues and synthesis of the amine neurotransmitters serotonin and the catecholamines dopamine and norepinephrine (Daikhin and Yudkoff, 2000; Suryawan et al., 1998). In cancer, it has been recently shown that the tissue dictates BCAA metabolism, i.e. non-small cell lung cancer (NSCLC) tumors displayed increased uptake of BCAA compared with normal lung, whereas pancreatic ductal adenocarcinoma (PDAC) tumors incorporated less BCAAs relative to normal pancreas (Mayers et al., 2016).

A refocused perspective of cancer metabolism that identifies metabolic diversity within a tumor offers novel therapeutic targets. Specifically, cancer cells may be starved from their fuel source and thereby become more sensitive to traditional therapeutic options (Nakajima and Van Houten, 2013).

1.4. BCAT1 reaction

The first step of BCAA catabolism involves the transfer of the primary amino group to α-ketoglutarate, yielding glutamate and the respective branched-chain ketoacids (BCKAs). These reversible transamination reactions are catalyzed by the branched chain aminotransferases BCAT1 and BCAT2 in the cytoplasm and the mitochondria, respectively. Whereas BCAT2 expression is nearly ubiquitous, BCAT1 expression is restricted to a small number of tissues, including the brain (Garcia-Espinosa et al., 2007; Sweatt et al., 2004), where BCAAs constitute a major source of nitrogen for the synthesis of the neurotransmitter glutamate (Garcia-Espinosa et al., 2007; Hutson et al., 2005). After transamination, the resulting branched-chain ketoacids (α-ketoisocaproate (KIC) from leucine, α-ketoisovalerate (KIV) from valine and α-keto-β-methylvalerate (KMV) from isoleucine) undergo oxidative decarboxylation in the reaction catalyzed by branched-chain α-ketoacid dehydrogenase (BCKD) to acetyl coenzyme A (acetyl-coA) and succinyl-coA, which are subsequently oxidized in the tricarboxylic acid (TCA) cycle to

provide macromolecule precursors and energy for ATP synthesis (Figure 1) (Kainulainen et al., 2013; Tönjes et al., 2013).

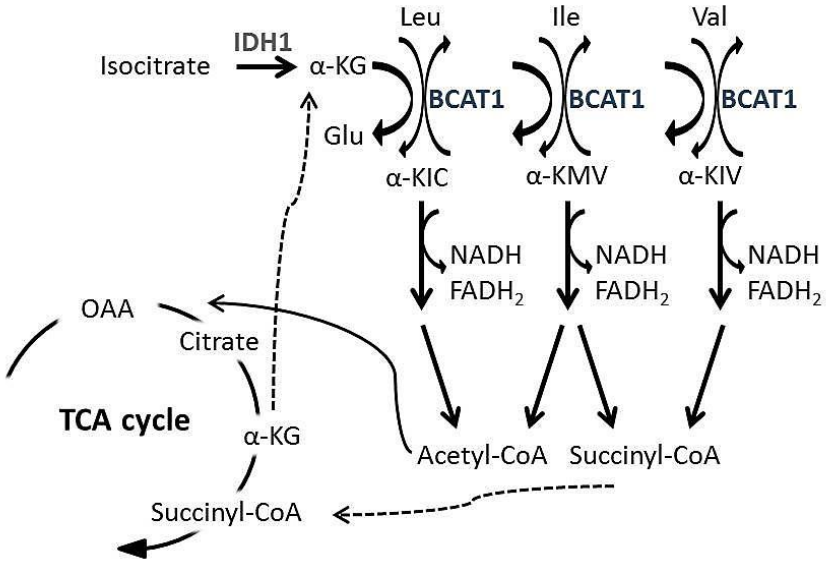

Figure 1 – Schematic representation of BCAA catabolism.

BCAAs are catabolized, especially during exercise, to acetyl-CoA and/or succinyl-CoA, which supply the TCA cycle**.** The cytosolic BCAT1 or mitochondrial BCAT2 isoenzymes catalyze the first step of the BCAA catabolism that consists in the transfer of an α-amino group to α-ketoglutarate, yielding glutamate and the respective branched-chain α-ketoacids. Some steps of the TCA cycle were omitted for simplification. Leu: leucine; Ile: isoleucine; Val: valine; α-KIC: α-ketoisocaproate; α-KMV: α-keto-β-methylvalerate; α-KIV: α**-**ketoisovalerate; α-KG: alpha-ketoglutarate; Glu: glutamate; OAA: oxaloacetate; TCA: tricarboxylic acid. Adapted from Kainulainen et al., 2013 (Kainulainen et al., 2013).

1.4.1. BCAT1 expression in cancer

BCAT1 has been associated with numerous types of tumors (Chang et al., 2016b; Mayers et al., 2016; Xu et al., 2016). BCAT1 expression is upregulated in patients with hepatocellular carcinoma (Xu et al., 2016). It has been recently shown that BCAT1 is overexpressed in NSCLC tumors compared to normal lung tissue (Mayers et al., 2016). BCAT1 overexpression is associated with advanced tumor status and implies adverse clinical outcomes of urothelial carcinoma (Chang et al., 2016b). Others have shown that BCAT1 is strongly

overexpressed in serous epithelial ovarian tumors and associates with cancer progression (Wang et al., 2015). However, BCAT1 role in tumorigenesis was firstly described in glioblastoma (Tönjes et al., 2013). BCAT1 is overexpressed in glioblastoma and required to support the sustained growth of these aggressive tumors with BCAT1 being exclusively expressed in tumors expressing wildtype *IDH* (Tönjes et al., 2013). In contrast, BCAT2 was not differentially expressed in IDH^{wt} glioblastomas compared to normal brain. One implication of the group-specific high BCAT1 expression is its possible use to identify this tumor group in a diagnostic setting (Tönjes et al., 2013). Furthermore, suppression of BCAA catabolism by knockdown of BCAT1 reduces cell proliferation *in vitro* and *in vivo* (Tönjes et al., 2013). The authors proposed that the blockage of BCAA and fatty acid catabolism might lead to reduced flow of acetyl-CoA and succinyl-CoA into the TCA cycle thereby impacting on the synthesis of macromolecules required for cell division (Tönjes et al., 2013). However, one cannot exclude the effects of the tumor derived metabolites in the surrounding cells, especially those from the immune compartment, in modulating tumor growth.

Interestingly, a large proportion of the glutamate produced by BCAT1 was excreted from the glioblastoma cells (Tönjes et al., 2013). Further, it is known that BCKAs, the other product of the BCAT1 reaction, also can be excreted from cells, i.e. during overnight fasting when BCAAs are transaminated to BCKAs in muscle cells, excreted and transported to the liver for further oxidation (Hutson et al., 2005).

1.5. Monocarboxylate transporters (MCTs)

As previously referred, many cancer cells have been shown to exhibit alterations of metabolism including a shift away from oxidative phosphorylation and towards aerobic glycolysis, converting most of the incoming glucose to lactate (Semenza, 2008; Warburg, 1956). As a result lactate is abundantly synthesized from pyruvate (Feron, 2009), which contributes to the intracellular acidification inducing cellular acidosis and triggering apoptosis. Thus, in order to avoid apoptosis, cancer cells must sustain lactate homeostasis (Izumi et al., 2011). To be able to adapt to an acidic environment, cancer cells increase proton efflux through pH regulators such as bicarbonate transporters, proton pumps, sodium-proton exchangers and H^+-linked monocarboxylate transporters, which are described to be upregulated in tumor cells (Izumi et al., 2003). Furthermore, inhibition of these adaptive mechanisms can decrease the cancer cell

viability and increase sensitivity to chemotherapeutic agents (Fais et al., 2007; Fang et al., 2006).

Transport of monocarboxylates through plasma membranes of various cells is mediated by a family of monocarboxylate transporters (MCTs) which can be found in a broad spectrum of organisms (Garcia et al., 1994; Price et al., 1998). The MCTs constitute a family of 14 transmembrane proteins encoded by the *SLC16A* family of genes of which MCT1 – 4 are known to transport monocarboxylates together with H^+ in a 1:1 stoichiometry (Halestrap, 2013; Halestrap and Meredith, 2004).

Although no three-dimensional crystal structure of any member of the MCT family has been reported, theoretical predictions and biochemical assays using MCT1 as a model indicate that all the members of the MCT family share a similar overall structure that consists of 12 transmembrane (TM) helices with intracellular C- and N-termini, two highly conserved sequences in TM1 and TM5 and a large cytosolic loop between TM6 and TM7 (Figure 2) (Halestrap, 2012). 3D models have been proposed based on extensive site-directed mutagenesis and molecular modeling predict that the structure of MCT1 at the plasma membrane alternates between two states: a closed (also designated as “inside-open”) conformation where the substrate-binding site is cytosolic and an open (also designated as “outside open”) conformation where this site is extracellular (Halestrap, 2012).

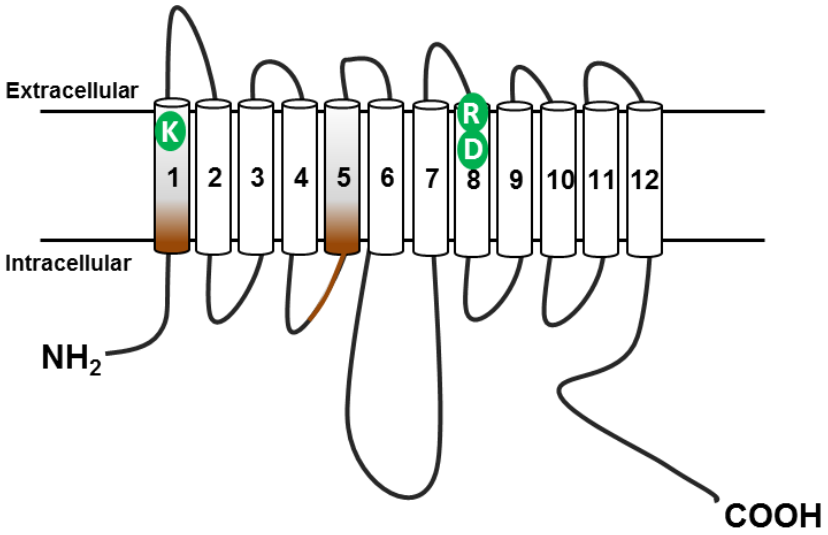

Figure 2 – Schematic representation of the topology of MCTs.

MCTs contain 12 transmembrane (TM) helices (1-12) with intracellular C- and N-termini, two highly conserved sequences in TM1 and TM5 (represented in dark orange) and a large cytosolic loop between TM6 and TM7. The members from the MCT family all contain a lysine (K) in TM1 and an aspartate (D) and arginine (R) in TM 8 that are involved in proton and monocarboxylate binding during the translocation cycle.

1.5.1. Mechanism of activity and regulatory proteins

The transport of lactic acid by human MCT1 through the plasma membrane is based on the predicted open and closed conformation of MCTs and kinetic studies of H^+-linked transport of lactate into erythrocytes. The uptake of lactate by MCT1 is an ordered process that starts with binding of a proton to K38 at the extracellular surface of MCT1, charging positively the lysine (Galic et al., 2003; Manoharan et al., 2006). The subsequent binding of one molecule of lactate forming an ionic pair promotes a change from closed to open conformation. The proton is then transferred to D302 residue and lactate to R306 causing the deprotonation of K38 what induces the return to the closed conformation. The pair H^+/lac^- is then released into the cytoplasm. So, the transport of lactic acid by MCT1 is passive and bidirectional. The intra- and extracellular concentrations of lactate and protons dictate whether import or export is privileged (Halestrap, 2012; Halestrap and Meredith, 2004).

The correct localization and activity of MCTs depends on interactions with ancillary proteins, primarily basigin/CD147 and embigin/gp70 (Poole and Halestrap, 1997; Wilson et al.,

2005). These proteins are anchored to the plasma membrane through a single transmembrane domain containing a conserved glutamate residue and several groups have demonstrated the crucial role of these proteins for the precise localization and activity of MCTs (Kirk et al., 2000; Ovens et al., 2010; Wilson et al., 2005). In the absence of the ancillary proteins, MCTs are not able to reach their final position and accumulate in the Golgi apparatus (Kirk et al., 2000; Wilson et al., 2005). It has been described that basigin is more widely expressed compared to embigin, and appears more frequently as partner for MCT1, MCT3 and MCT4, whereas MCT2 preferentially interacts with embigin (Ovens et al., 2010; Wilson et al., 2005).

Other proteins have been suggested to interact with MCTs. Carbonic anhydrase II (CAII) and CAIV, cytosolic and extracellular CA isoforms, respectively, can also establish interactions with MCT/basigin complexes, enhancing the activity of the transporters (Klier et al., 2014; Klier et al., 2011). It has been proposed that CAs supply MCTs with protons increasing MCT activity (Klier et al., 2014; Klier et al., 2011). Specifically, CAII, directly bound to MCT1, can act as a "H^+-collecting/distributing antenna" increasing the concentration of protons in the vicinity of MCTs to support proton/lactate co-transport (Figure 3) (Becker et al., 2011; Klier et al., 2014).

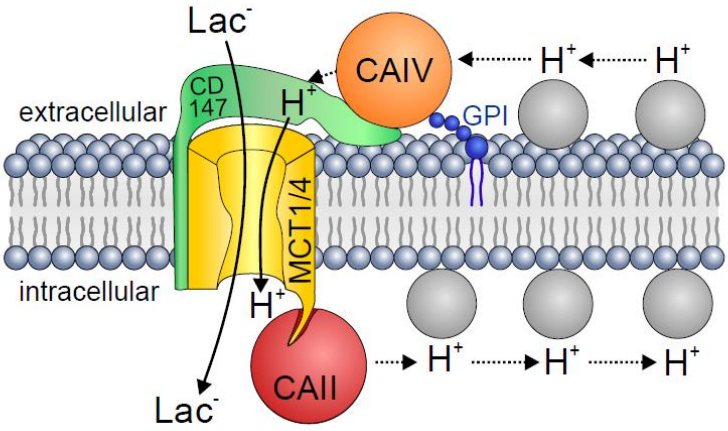

Figure 3 – Hypothetical model of the interaction between MCT1/4, CAII, CAIV.

Extracellular CAIV is anchored to the extracellular side of the plasma membrane by glycosyl-phosphatidyl-inositol (GPI) anchor. CAIV is located close to MCT1 and MCT4 by direct interaction with CD147 (basigin), the chaperon of the two transporters. On the intracellular site CAII is located close to the transporters by binding to their C-terminal tail. In this position, CAIV and CAII can act as an extra- and intracellular proton-collecting antenna for the transporter, which shuttles protons between transport pore and surrounding protonatable residues (gray circles) to facilitate shuttling of H^+ and lactate across the cell membrane. Lac^-: lactic acid. Figure taken from Klier et al., 2014 (Klier et al., 2014).

1.5.2. Substrates

It has been proposed that MCT1 – 4 isoforms show preference for short chain monocarboxylates, including those substituted on positions two and three, such as $_{L}$-lactate, $_{D}$-lactate, pyruvate, β-hydroxybutyrate and acetoacetate. In quantitative terms, lactate has been identified as one of the most important metabolites for these transporters with a stereoselectivity for $_{L}$- over $_{D}$-lactate (Halestrap, 2012).

Previous reports described that MCT4 (*SLC16A3*) preferentially exports lactate, while MCT1 (*SLC16A1*) can facilitate both lactate import and export depending on the pH gradient (Draoui and Feron, 2011). MCT4 has the lowest affinity for lactate, is encoded by a hypoxia-inducible factor (HIF) HIF-1α-target gene (Ullah et al., 2006), and is therefore responsible for the export of lactic acid from glycolytic tumor cells (Dimmer et al., 2000). It has been proposed that MCT4 has a central role in the regulation of intracellular pH although it has only a low affinity for lactate, its high turnover rate ensures efficient proton export (Chiche et al., 2012).

MCT1 has an intermediate affinity for lactate and is ubiquitously expressed in healthy and cancer tissues. In cancer, it was proposed to facilitate lactate uptake fueling the oxidative metabolism of oxygenated tumor cells in a newly described metabolic pathway involving lactate oxidation into pyruvate to fuel the TCA cycle (Sonveaux et al., 2008).

MCT2 is reported to be expressed in the mitochondrial membrane, where it is involved in the import of pyruvate following lactate oxidation (Koukourakis et al., 2006). MCT3 exports lactate, but is only reported to be expressed in retinal pigment epithelium and choroid plexus epithelium (Philp et al., 2001).

Besides their role as lactate transporters, MCTs have affinity for the transport α-ketoacids (Manning Fox et al., 2000). Affinity studies performed on *Xenopus* oocytes indicate K_m values of MCT4 and MCT1 for α-ketoisocaproate of 95mM and 0.7mM, respectively and for α-ketoisovalerate of 113mM and 1.3mM, respectively (Table 1) (Manning Fox et al., 2000).

Furthermore, it was shown that the transport of α-ketoisocaproate (KIC) in neurons involves one of the MCT proteins (Mac et al., 2000).

Table 1 – K_m values of different MCT isoforms for a range of monocarboxylates.

Values are given ± Standard Error (SE). Adapted from Manning Fox et al., 2000 (Manning Fox et al., 2000).

Substrate	MCT4 K_m (Oocytes) (mM)	MCT1 K_m (Tumor cells) (mM)	MCT1 K_m (Oocytes) (mM)	MCT2 K_m (Oocytes) (mM)
Formate	>500	>100	-	-
Bicarbonate	>500	-	-	-
Oxamate	>500	49	-	-
Glyoxylate	>500	63	-	-
$_{L}$-Lactate	28±4	4.5	3.5	0.74
$_{D}$-Lactate	519±33	27.5	>60	-
Pyruvate	153±6	0.7	1.0	0.08
S-Chloropropionate	46±2.5	0.7	-	-
R- Chloropropionate	51±2.6	0.7	-	-
$_{D\text{-}L}$-α-Hydroxybutyrate	56±3	2.6	-	-
$_{L}$-β- Hydroxybutyrate	824±64	11.4	-	1.2
$_{D}$-β- Hydroxybutyrate	130±9.6	10.1	-	1.2
γ- Hydroxybutyrate	>500	7.7	-	-
Acetoacetate	216±27	5.5	-	0.8
α-Ketobutyrate	57±3.3	0.2	-	-
α-Ketoisocaproate	95±5.1	-	0.7	0.1
α-Ketoisovalerate	113±9.6	-	1.3	0.3
β-Phenylpyruvate	>500	-	-	-

K_m values were derived by least-squares regression to the Michaelis-Menten equation.

1.5.3. Inhibitors

Several MCT inhibitors have been identified over the past decades. Phloretin, flavonoids such as quercetin, stilbene disulphonates (including DIDS and 4,4′-dibenzamidostilbene-2,2′-disulphonate [DBDS]), and α-cyano-4-hydroxycinnamate (CHC) and its analogs were the first inhibitors to be described but all have off-target effects (Halestrap, 2012; Halestrap and Price, 1999). More recently other inhibitors have been developed that exhibit high affinity for MCTs (Bola et al., 2014; Ovens et al., 2010). The compound AZD3965 is a dual MCT1 and MCT2 inhibitor that is currently being evaluated as an anticancer agent in Phase I clinical trials for patients with prostate cancer, gastric cancer or diffuse large B cell lymphoma (Polanski et al., 2014). The related compound AR-C155858 is a dual MCT1/2 inhibitor that inhibits preferentially MCT1 (K_i ~ 2nM) but also MCT2 when it is bound to ancillary protein basigin but not when it is bound to its preferred chaperone embigin (Nancolas et al., 2015; Ovens et al., 2010). AR-

C155858 does not inhibit MCT4 and the recent identification of key binding site residues in the intracellular substrate-binding cavity that differ significantly between MCT1/MCT2 and MCT4 can explain the differences in inhibitor binding, contributing to the isoform selectivity of AR-C155858 (Nancolas et al., 2015) (Figure 4). AR-C155858 binds to MCT1 from the intracellular side and involves TMs helices 7-10 and kinetic studies suggest that it is a non-competitive inhibitor (Ovens et al., 2010).

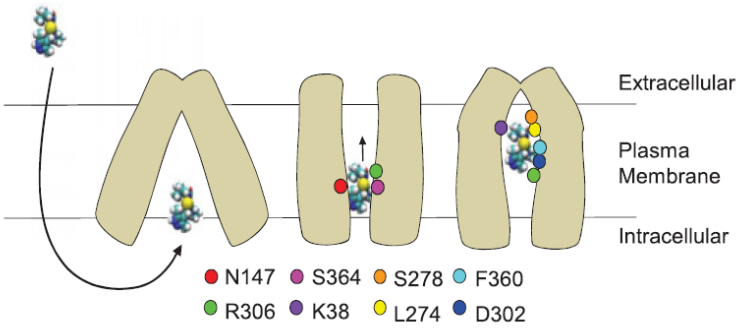

Figure 4 – Schematic representation of the proposed mechanism of inhibition by AR-C155858.
AR-C155858 crosses the plasma membrane to enter MCT1 in the inward-open conformation. An intermediate conformation is adopted, allowing binding of the inhibitor by interaction with residues in the intracellular half including Asn147 (helix 5), Arg306 (helix 8) and Ser364 (helix 10). A further conformational change allows the movement of AR-C155858 into the channel of MCT1, interacting with residues in the extracellular half including Lys38 (helix 1), Asp302 (helix 8), Phe360 (helix 10), Lys274 and Ser278 (helix 7). Figure taken from Nancolas et al,2015 (Nancolas et al., 2015)

1.5.4. Cell-specific distribution

Expression of MCT1 is considered ubiquitous since it is found in several tissues and organs, whereas the expression of the other three members is known to be more restricted (Perez-Escuredo et al., 2016). Focusing on brain, MCT1 is expressed primarily in endothelial cells, while MCT4 is expressed mainly in astrocytes. Neurons, on the other hand, express primarily MCT2. The difference in MCT isoforms between astrocytes and neurons is the basis of the lactate shuttle hypothesis, which states that lactate is produced by astrocytes and used by neurons (1.6.1) (Kennedy and Dewhirst, 2010; Pellerin, 2003).

1.5.5. MCTs expression in cancer

In tumor cells take-up or export of lactate are dependent on oxygen availability, lactate concentration and expression of the MCT subtype at the plasma membrane (Semenza, 2008) Recent data suggest that MCT1 can transport lactate into and out of tumor cells. Whereas most oxidative (opposing to glycolytic) cancer cells import lactate through MCT1 to fuel mitochondrial respiration, the role of MCT1 in glycolysis-derived lactate efflux remains less clear (Boidot et al., 2012).

In tumors, it has been described that MCT1 and MCT4 are overexpressed in the plasma membrane of glioblastomas, compared with non-neoplastic brain tissues (Miranda-Goncalves et al., 2013). Other studies have shown that MCT1 and MCT4 overexpression in human neuroblastoma, cervix and colorectal cancers, was associated with bad prognosis of cancer (Fang et al., 2006; Pinheiro et al., 2009; Pinheiro et al., 2008; Sonveaux et al., 2008). It was also shown that high expression of both MCT1 and MCT4 correlates with the invasiveness of lung cancer cells (Izumi et al., 2011).

A recent study reveals that MCT1 and MCT4 expression is significantly reduced in mutant IDH1 compared to wild-type IDH1 gliomas (Viswanath et al., 2016). This observation suggests that reduced MCT expression is part of the metabolic reprogramming of mutant IDH1 gliomas (Viswanath et al., 2016).

Fewer reports are available that evaluate MCT2 and MCT3 expression in cancer. A recent study pointed to an overexpression of MCT2 in pancreatic cancer and suggested it as a putative biomarker and molecular target (Pertega-Gomes et al., 2015). Others have shown that MCT3 is expressed in both cancer and stromal cells in NSCLC (Eilertsen et al., 2014).

1.6. Metabolite exchange between tissue compartments

1.6.1. Astrocyte-neuron lactate shuttle

MCTs mediate lactate exchange between astrocytes and neurons in the brain (Perez-Escuredo et al., 2016). Astrocytes import glucose via glucose transporters (GLUT) and convert it to pyruvate and ATP via glycolysis, and pyruvate to lactate via lactate dehydrogenase A (LDHA). Lactate is exported together with protons via MCT4. Neurons import lactate via MCT2 and oxidize it to pyruvate via lactate dehydrogenase B (LDHB) fueling the TCA cycle to support ATP production via oxidative phosphorylation (Perez-Escuredo et al., 2016).

1.6.2. BCAT cycle in the brain

An analogous transfer of metabolites, involving the coupled exchange of the amino acids glutamate and glutamine and the branched chain amino acids and ketoacids (BCAT cycle) has been shown to occur in the normal brain and is crucial for maintaining nitrogen balance (Figure 5) (Butt et al., 2012). Exchange of these metabolites between neurons and astrocytes has been demonstrated in co-culture systems (Bak et al., 2013; Leke et al., 2011).

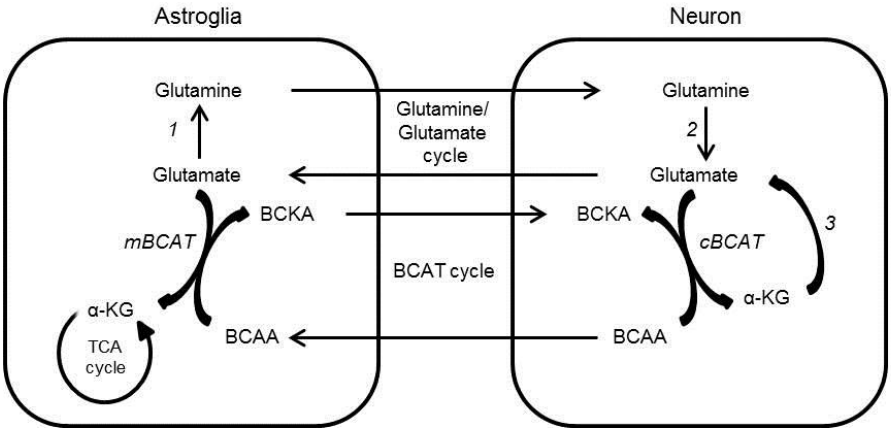

Figure 5 – Cell to cell transfer of branched-chain amino acids (BCAAs) and branched-chain ketoacids (BCKAs) for *de novo* glutamate synthesis in normal brain.

(1) glutamine synthetase; (2) glutaminase; (3) glutamate dehydrogenase. mBCAT, mitochondrial BCAT; cBCAT, cytosolic BCAT; TCA, tricarboxylic cycle; α-KG, α-ketoglutarate. Adapted from Butt et al,2012 (Butt et al., 2012)

1.6.3. Lactate shuttle in tumors

Recent studies suggested that different aspects of tumor metabolism, i.e. lactate production and consumption, are compartmentalized between tumor cells and fibroblast stroma cells in mammary carcinoma. In this model lactate is produced and excreted via MCT4 by stroma cells and taken up by tumor cells via MCT1 for ATP production (Migneco et al., 2010; Nakajima and Van Houten, 2013).

Others have provided evidence for the existence of a lactate shuttle in prostate cancer, with cancer associated fibroblasts (CAFs) excreting lactate, via MCT4, that is imported by the tumor cells via MCT1. Furthermore, high MCT4 expression in CAFs with concomitant strong MCT1 expression in cancer cells was associated with poor clinical outcome (Pertega-Gomes et al., 2014). It has been recently shown that lactate produced by multiple myeloma cell lines and bone marrow stromal cells contributes to the survival of such tumor cells in an autocrine or paracrine manner (Fujiwara et al., 2015).

This exchange of metabolites between tumor and stromal cells provides a system by which cancer cells may adapt to or maximize the use of available resources, thereby increasing their capacity to grow and metastasize. Components involved in this process such as metabolite transporters and enzymes may serve clinically as prognostic indicators and their inhibition as potential therapeutic targets (Nakajima and Van Houten, 2013).

1.7. Glioblastoma microenvironment

The resistance of glioblastoma to standard therapies is believed to result from their heterogeneity and the unique tumor microenvironment composed by multiple types of cells, including malignant cells, extracellular matrix, nonmalignant resident stromal cells such as activated fibroblasts and migratory hematopoietic cells such as macrophages (Figure 6) (Charles et al., 2012; Hanahan and Weinberg, 2011). The interactions among the components of a tumor microenvironment modulate tumor progression, invasion and angiogenesis (Balkwill et al., 2005). The inflammatory microenvironment of tumor tissues consists of macrophages, dendritic cells, mast cells and T cells (Balkwill and Mantovani, 2001; Coussens and Werb, 2002; Nakayama et al., 2004).

Macrophages have traditionally been classified as tumor-suppressive (M1) or tumor-supportive (M2) (Mantovani et al., 2002). M1 macrophages are classically activated by interferon (IFN)-γ, whereas alternative activation by interleukin (IL)-4 and IL-13 drives macrophages toward the M2 phenotype (Mantovani et al., 2002). It is important to note that fully polarized M1 and M2 macrophages are the extremes of a continuum of functional states (Mantovani et al., 2002).

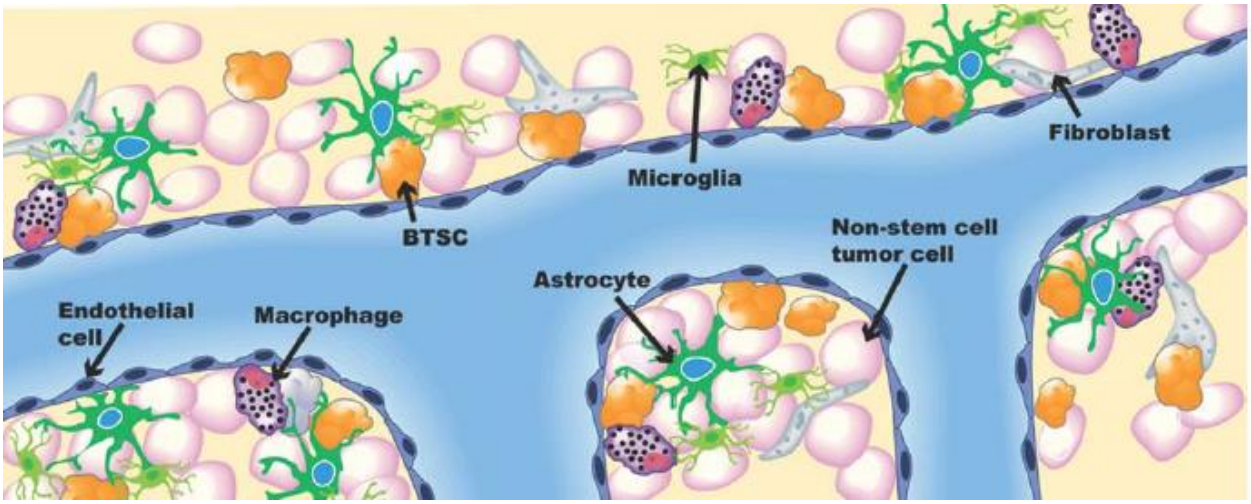

Figure 6 – Schematic representation of glioblastoma microenvironment.

Glioblastoma microenvironment is composed by several stromal cell types that include but are not limited to astrocytes, pericytes, fibroblasts, endothelial cells and macrophages. BTSC: brain tumor stem cell-like. Adapted from Charles et al, 2012 (Charles et al., 2012)

1.7.1. Tumor-associated macrophages/microglia

The interactions of macrophages and microglia with gliomas have been extensively studied, and whether these cells function to suppress or enhance glioma growth is still a matter of debate.

Tumor–associated macrophages (TAMs) are a major component of the tumor leukocyte infiltrate, accumulating in hypoxic areas of tumors (Bingle et al., 2002; Pollard, 2004) due to HIF-1-dependent upregulation of the chemokine receptor CXCR4 (Schioppa et al., 2003). TAMs recruitment and survival is sustained by cytokines present in the tumor microenvironment (Balkwill et al., 2005). It has been described that in response to cytokines such as TGF-β, IL-10 and M-CSF, TAMs acquire M2 properties, promoting tumor proliferation (Pollard, 2004; Wyckoff et al., 2004).

The origin of TAMs and mechanism of their recruitment and differentiation is not entirely clear. There is evidence that both tissue-resident and recruited macrophages may coexist in tumors (Kim and Bae, 2016). On the one hand, there is evidence that resident microglia, and not peripheral macrophages, is the main source of mononuclear cells in gliomas (Muller et al., 2015). Besides brain microglia, lung alveolar and peritoneal macrophages, Kupffer cells and epidermal Langerhans cells, all derived from primitive yolk sac precursors, can be self-

maintained locally (Kim and Bae, 2016). On the other hand, studies performed in mice revealed that mammary tumor growth induces the accumulation of TAMs that are phenotypically and functionally distinct from mammary tissue macrophages and differentiate from $CCR2^{+}$ inflammatory monocytes (Franklin et al., 2014).

In glioma, glioma-infiltrating macrophages and microglia (GAMs) constitute a substantial portion of the tumor mass that can be as high as one in every three cells (Sarkar et al., 2014).

Predominantly, gliomas appear to suppress the immune surveillance functions of macrophages and microglia. It is reported that glioma switches the infiltrating macrophages/microglia toward an immunosuppressive phenotype characterized by reduced phagocytic activity, production of less inflammatory cytokines and secretion of matrix metalloproteinases (MMP) enzymes, thus promoting glioblastoma invasion (Hussain et al., 2006; Li and Graeber, 2012). Others have shown that exposure of microglia to glioblastoma conditioned medium modulates microglia migration and phagocytic activity *in vitro* (D'Alessandro et al., 2013).

In contrast, there is evidence that macrophages and microglia attempt to counteract the activity of glioma cells. Macrophage and microglia factors stimulate the apoptosis of glioma cells in culture (Hwang et al., 2009) and *in vivo* (Brantley et al., 2010) and the toll-like receptor 3 agonist poly(I:C) causes microglia to secrete factors that kill glioma cells in culture (Kees et al., 2012).

1.7.2. Expression profile of glioma associated macrophages/microglia

As previously referred, glioma-associated microglial cells and infiltrating macrophages (GAMs) make up the largest portion of tumor-infiltrating cells, contributing to up to 30% of the entire glioma mass (Charles et al., 2012; Sarkar et al., 2014). Lately, several studies have been conducted in order to refine the phenotypic and/or genotypic characterization of glioblastoma-infiltrating innate immune cells. According to a recent study using genome-wide microarray expression analysis, GAMs display an expression profile different from M1 and M2 polarization and express the pro-tumorigenic genes *GPNMB* and *SPP1* (Szulzewsky et al., 2015). Another recent study, combining immune phenotyping, whole-genome microarray analysis and microRNA expression profiling revealed that glioblastoma-infiltrating innate immune cells resemble, contrary to the current dogma, a nonpolarized M0 macrophage phenotype (Gabrusiewicz et al., 2016).

1.7.3. Effect of tumor secreted factors on macrophage polarization

Tumor cell-derived factors play an important role in tumor cell-macrophage communication.

In glioma, recent findings demonstrate the importance of tumor-cell-derived versican, also known as CSPG2, in tumor-macrophage communication (Hu et al., 2015). Versican released from glioma cells promotes tumor expansion via glioma-associated microglia/macrophages Toll-like receptor 2 signaling (Hu et al., 2015).

Others have shown that the production and release of cytokines by tumor cells can impact on macrophage survival and polarization (Ries et al., 2014; Zhou et al., 2015). Periostin secreted by glioblastoma stem cells recruits M2 tumor-associated macrophages and promotes malignant growth (Zhou et al., 2015). Specifically, the authors showed that glioma stem cells secrete periostin to attract circulating monocytes that are differentiated into M2 TAMs that promote tumor growth. Targeting periostin on glioma stem cells attenuated the differentiation of M2 TAMs and halted tumor progression (Zhou et al., 2015). Additionally, experiments using tumor conditioned media (TCM) from various cell lines derived from different tumor entities revealed that macrophages differentiated with TCM containing high colony-stimulating factor 1 (CSF-1) and low granulocyte-macrophage colony-stimulating factor (GM-CSF) levels displayed an M2-like phenotype, whereas macrophages differentiated with TCM containing high GM-CSF showed a mixed M1/M2 phenotype (Ries et al., 2014). These studies show that the levels of cytokines present in the tumor microenvironment influence and shape the cells from the immune compartment impacting on their anti-tumoral or pro-tumoral state of activation.

Among the tumor-derived signals, metabolites have also been shown to impact on the phenotype of the surrounding stromal cells (Colegio et al., 2014; De Simone et al., 2013; Patel et al., 2017). Lactic acid produced by tumor cells has a critical function as a signaling molecule, namely through the induction of Vascular endothelial growth factor (VEGF) and the M2-like polarization of TAMs (Colegio et al., 2014). Additionally, lactate-induced expression of arginase 1 by macrophages has in turn an important role in promoting tumor growth (Colegio et al., 2014). Branched-chain amino acids influence the immune properties of microglial cells and their responsiveness to pro-inflammatory signals (De Simone et al., 2013). High concentrations of BCAAs (10mM) polarize microglial cells towards the M2 state, with enhanced interleukin (IL) IL-10 expression and phagocytic activity (De Simone et al., 2013).

1.8. Aims of the study

The first aim of the present study is to investigate the involvement of MCTs in the transport of BCKAs across cell membranes using two distinct approaches: 1) heterologous expression of MCTs and BCAT1 in *Xenopus* oocytes and the characterization of BCKAs transport in this model system and 2) modulation of MCTs transport activity in glioblastoma cell lines.

The second aim is to clarify the fate and function of tumor-secreted BCKAs in the tumor-microenvironment interaction using macrophages as a model of the stroma compartment. Specifically, I want to address the question whether stromal cells, i.e. tumor-associated macrophages, take up and metabolize BCKAs and whether BCKAs affect the macrophages' phenotype.

In additional work I aim to evaluate the effect of manipulating BCAT1 expression in tumor cells on the stromal cell phenotype.

Ultimately, this study aims to contribute to the identification of new therapeutic targets for glioblastoma by studying BCAA catabolism in the tumor-stroma interaction.

2. Materials and methods

2.1. Materials

2.1.1. Antibodies

Antibody	Company
anti-β-tubulin	Sigma-Aldrich, Munich, Germany
anti-rabbit IgG-HRP	sc-2004, Santa Cruz Biotechnology, Dallas, TX, USA
anti-mouse IgG-HRP	sc-2005, Santa Cruz Biotechnology, Dallas, TX, USA
anti-BCAT1	Insight Biotechnology limited (Wembley, UK)
anti-MCT1	ab90582, Abcam, Cambridge, UK
anti-MCT1	AB3538P, Millipore
anti-MCT4	sc376140, Santa Cruz Biotechnology, Dallas, TX, USA
anti-PGK1	GTX107614, GeneTex, Irvine, CA, USA
anti-MCT2	PA5-50518, Thermo Fisher Scientific
FITC anti-human CD14	301804, Biolegend, San Diego, CA, USA
FITC Mouse IgG1 κ Isotype Control	555748,BD Biosciences, Heidelberg, Germany
Streptavidin-Phycoerythrin (SAv-PE)	554061, BD Biosciences, Heidelberg, Germany

2.1.2. Buffers and solutions

Solution	Composition
FACS buffer	5 % FCS in PBS 1X
LB (Luria Bertani) medium	0.5 % (w/v) NaCl, 1 % (w/v) Tryptone, 0.5 % (w/v) Yeast extract
LB Agar	0.5 % (w/v) NaCl, 1 % (w/v) Tryptone, 0.5 % (w/v) Yeast extract, 1.6 % (w/v) Agarose
Transfer buffer 1X	25 mM Tris, 200 mM glycine, 20 % methanol
TRIS buffered saline (TBS) 1X	150 mM NaCl, 10 mM Tris, pH 7.5
TRIS-Borat-EDTA (TBE) 1X	0.445 M Tris-Borat, 10 mM EDTA
TBS-T	TBS 1X, 1:1000 (v/v) Tween 20
Stripping buffer	62.5 mM Tris pH 6.8, 2% SDS, 100mM β-mercaptoethanol

2.1.3. Cell culture reagents and material

Reagent/ Material	Distributor
Accutase	Sigma-Aldrich, Munich, Germany
Biocoll	Biochrom GmbH, Berlin, Germany
Carboxyfluorescein succinimidyl ester (CFSE)	BD Biosciences, Heidelberg, Germany
CCL2, human recombinant protein	R&D Systems, Minneapolis, MN, USA
Cell culture flasks and multi-well plates	Tritech Research, Los Angeles, USA
CD14 MicroBeads, human	Miltenyi Biotec, Bergisch Gladbach,

	Germany
ChamberSlides, Lab-Tek II, 8 Kammern, Glas	Thermo Fischer Scientific, Langenselbold, Germany
Corning® Transwell® polycarbonate membrane cell culture inserts 5.0µm pore	Sigma-Aldrich, Munich, Germany
Cryo tubes	Nunc, Wiesbaden, Germany
Dimethyl sulphoxide (DMSO)	Sigma-Aldrich, Munich, Germany
DharmaFECT 1 transfection reagent	Dharmacon Inc., Lafayette, Colorado, EUA
DMEM (Dulbecco's modified eagle medium) 5796	Sigma-Aldrich, Munich, Germany
DMEM 5921	Sigma-Aldrich, Munich, Germany
DMEM 6046	Sigma-Aldrich, Munich, Germany
Doxycycline	Sigma-Aldrich, Munich, Germany
Fetal calf serum (FCS)	Merck Millipore, Darmstadt, Germany
Leucosep™ tubes, 50 mL	Greiner Bio-One International GmbH, Kremsmunster, Austria
L-Glutamine	Thermo Fischer Scientific, Langenselbold, Germany
MACS buffer	Miltenyi Biotec, Bergisch Gladbach, Germany
MACS human CD14 Microbeads	Miltenyi Biotec, Bergisch Gladbach, Germany
MACS LS separation columns	Miltenyi Biotec, Bergisch Gladbach, Germany
MACS Magnet and stand	Miltenyi Biotec, Bergisch Gladbach, Germany
M-CSF, human recombinant	Miltenyi Biotec, Bergisch Gladbach, Germany
Opti-MEM I reduced serum medium	Thermo Fischer Scientific, Langenselbold, Germany
PBS Dulbecco's	Life Technologies, Carlsbad, USA
Penicillin/Streptomycin (10000 U/ml, 100 µg/ml)	Thermo Fischer Scientific, Langenselbold, Germany
Phorbol 12-myristate 13-acetate (PMA)	Sigma-Aldrich, Munich, Germany
RPMI (Roswell Park Memorial Institute) 1640	Life Technologies, Carlsbad, US
Tet system approved Fetal Bovine Serum (FBS)	Clontech/Takara, Saint-Germain-en-Laye France
Trypsin EDTA solution (0.5 %)	Sigma-Aldrich, Munich, Germany
α-Keto-β-methylvaleric acid (KMV) sodium salt	sc-214140, Santa Cruz Biotechnology, Dallas, TX, USA
α-Ketoisovaleric acid (KIV) sodium salt	198994-5G, Sigma-Aldrich, Munich, Germany
α-Ketoisovaleric acid (KIV) sodium salt (13C5,98%)	Cambridge Isotope Laboratories, Inc., Andover, MA, USA
α-Ketoisocaproic acid (KIC) sodium salt	Sigma-Aldrich, Munich, Germany
α-Ketoisocaproic acid (KIC) sodium salt (1,2-13C2, 99%)	Cambridge Isotope Laboratories, Inc., Andover, MA, USA

2.1.4. Cell lines and biological material

Cell line/biological material	Distributor
LN-229	ATCC
One Shot TOP10 Chemically Competent *E.coli*	Life Technologies GmbH
U251-MG	ATCC
U87-MG	ATCC
U937 (GFP transduced)	Provided by Dr.Martina Seiffert, DKFZ, Heidelberg

2.1.5. Chemicals and reagents

Reagent	Distributor
Agarose	Sigma-Aldrich, Munich, Germany
Ampicillin	Roche Diagnostics, Mannheim, Germany
AR-C155858 (MCT1/2 inhibitor)	Tocris Bioscience, Bristol, UK
Bicinchoninic acid (BCA)	Sigma-Aldrich, Munich, Germany
Bovine serum albumin (BSA)	Sigma-Aldrich, Munich, Germany
Copper-(II)-sulphate	Sigma-Aldrich, Munich, Germany
Dithiotreitol (DTT) (0.1 M)	Thermo Fischer Scientific, Langenselbold, Germany
DNA marker (1kb)	Fermentas, St Leon-Rot, Germany
dNTP mix (100 µM each)	Thermo Fischer Scientific, Langenselbold, Germany
Ethanol	Merck Millipore, Darmstadt, Germany
Ethidium bromide	Sigma-Aldrich, Munich, Germany
Ethylendiaminetetracetate (EDTA) (25 mM)	Thermo Fischer Scientific, Langenselbold, Germany
EDTA 1X	Thermo Fischer Scientific, Langenselbold, Germany
FD green buffer (10X)	Thermo Fischer Scientific, Langenselbold, Germany
Formamide	Merck Millipore, Darmstadt, Germany
Glycerol	Carl Roth, Karlsruhe, Germany
Methanol	Sigma-Aldrich, Munich, Germany
NaCl 0.9%	Braun, Melsungen, Germany
Nuclease-free water	Ambion, Austin, USA
NuPAGE® LDS sample buffer (4X)	Life Technologies, Darmstadt, Germany
NuPAGE® SDS running buffer (20X)	Life Technologies, Darmstadt, Germany
Paraformaldehyde (PFA)	Sigma-Aldrich, Munich, Germany
Protease and phosphatase inhibitor cocktail (PIC) (1X)	Thermo Fischer Scientific, Langenselbold, Germany
Pierce ECL Western blotting substrate	Thermo Fischer Scientific, Langenselbold, Germany
Random primer mix	New England Biolabs (NEB), Ipswich, USA
RIPA-lysis buffer	Sigma-Aldrich, Munich, Germany
S.O.C medium	Thermo Fischer Scientific, Langenselbold, Germany
Sodium dodecyl sulfate (SDS)	Sigma-Aldrich, Munich, Germany
Sodium acetate	Carl Roth, Karlsruhe, Germany
Spectra high range multicolor protein ladder	Fermentas, St Leon-Rot, Germany
Tris-(hydroxymethyl)-aminomethan (TRIS)	Carl Roth, Karlsruhe, Germany
Triton X-100	Sigma-Aldrich, Munich, Germany
Tween 20	Sigma-Aldrich, Munich, Germany
Whole milk powder	Carl Roth, Karlsruhe, Germany
β-Mercaptoethanol	Sigma-Aldrich, Munich, Germany

2.1.6. Databases

Database	site
Ensembl	www.ensembl.org
Gene Cards (Human Genes Database)	www.genecards.org/
HMDB	http://www.hmdb.ca/
NCI-60	http://129.187.44.58:7070/NCI60/
PubMed	www.ncbi.nim.nih.gov/PubMed/
R2: Genomics Analysis and Visualization Platform	http://hgserver1.amc.nl/cgi-bin/r2/main.cgi
Universal Probe Library Roche	https://qpcr.probefinder.com/organism.jsp

2.1.7. Enzymes

Enzyme	Supplier
BamHI FastDigest (FD)	Thermo Fischer Scientific, Langenselbold, Germany
DNase I	Thermo Fischer Scientific, Langenselbold, Germany
EUROTAQ DNA polymerase	EuroClone/Biozol, Eching, Germany
HindIII FastDigest (FD)	Thermo Fischer Scientific, Langenselbold, Germany
PRECISOR High-Fidelity DNA Polymerase	BioCat, Heidleberg, Germany
SuperScript II Reverse Transcriptase	Thermo Fischer Scientific, Langenselbold, Germany
T4 DNA ligase	Thermo Fischer Scientific, Langenselbold, Germany

2.1.8. Instruments

Instrument	Distributor
ABI PRISM 7900HT Fast Real Time PCR System	Applied Biosystems / Life Technologies, Carlsbad, USA
Acquity FLR detector	Waters GmbH, Eschborn, Germany
Acquity H-class UPLC system	Waters GmbH, Eschborn, Germany
Agilent 7890 Gas Chromatograph	Agilent Technologies Deutschland GmbH, Waldbronn, Germany
Agilent 5975C Mass Spectrometer	Agilent Technologies Deutschland GmbH, Waldbronn, Germany

Axioplan 2 imaging microscope	Carl Zeiss Microscopy, Jena, Germany
Cell Observer microscope	Carl Zeiss Microscopy, Jena, Germany
Centrifuge Heraeus Sepatech Varifuge 3.0R	M&S Laborgerate GmbH, Wiesloch, Germany
Eppendorf MastercyclerR Thermal Cycler S	Eppendorf, Hamburg, Germany
FACS Canto II™	BD Biosciences, Heidelberg, Germany
Fusion solo S	Vilber Lourmat, Eberhardzell, Germany
Leica DM IRBE microscope	Leica Microsystems, Wetzlar, Germany
NanoDrop ND-1000 Spectrometer	NanoDrop, Wilmington, USA
Pipettes (2µl, 10µl)	Eppendorf, Hamburg, Germany
Pipettes (20µl, 100µl, 200µl, 1000µl)	Gilson, Middleton, Germany
SDS-PAGE Gel Apparatus	Bio-Rad Laboratories, Inc., Hercules, USA
Steri-Cycle CO_2 Cell Culture Incubator	Thermo Fisher Scientific, Waltham, MA, USA
UV-Gel Documentation System	BioRad, Hercules, USA
Vi-CELL XR 2.03	Beckman Coulter GmbH, Krefeld, Germany
Western Blot Transfer Device	Bio-Rad Laboratories, Inc., Hercules, USA

2.1.9. Kits

Kit	Company
ABsolute SYBR® Green ROX mix	Thermo Fischer Scientific, Langenselbold, Germany
BigDye® Terminator sequencing kit	Applied Biosciences, Foster City, USA
Click-iT® EdU proliferation kit (Alexa488)	Life Technologies, Darmstadt, Germany
Cytokine array - Human cytokine antibody	Abcam, Cambridge, UK
DuoLink in situ orange starter kit mouse	Sigma-Aldrich, Munich, Germany
ECL Western Blot detection kit	GE Healthcare Europe GmbH, Freiburg, Germany
EUROTAQ TAQ DNA pol kit	EuroClone/Biozol, Eching, Germany
MagniSort® Human T cell Enrichment Kit	eBioscience, San Diego, CA, USA
Plasmid Maxi kit	Qiagen, Hilden, Germany
Plasmid Mini kit	Qiagen, Hilden, Germany
Precisor high fidelity DNA polymerase kit	Biocat, Heidleberg, Germany
QIAshredder	Qiagen, Hilden, Germany
QiAquick Gel extraction kit	Qiagen, Hilden, Germany
QiAquick PCR purification kit	Qiagen, Hilden, Germany
Rapid DNA ligation kit	Roche, Mannheim, Germany
RNeasy Micro kit	Qiagen, Hilden, Germany
RNeasy Mini kit	Qiagen, Hilden, Germany

2.1.10. Other material

Material	Distributor
0.22µm Millex 4mm Durapore PVDF filters	Merck Millipore,
1.0µm FluoSpheres Biotin-labeled Microspheres	Thermo Fisher Scientific, Waltham, MA, USA ABgene, Epsom, UK
ABgeneTM adhesive PCR plate seals	R. Langenbrinck GmbH, Emmendingen, Germany
Cover slips (24x60 mm) Marienfeld	Dako, Glostrup, Denmark
Dako Pen	Eppendorf, Hamburg, Germany
Eppendorf Safe-Lock microcentrifuge tubes (1.5 mL, 2.0 mL)	BD Bioscience, Heidelberg, Germany
FACS tubes	BD Bioscience, Heidelberg, Germany
Falcon® tubes (15 and 50mL)	Kisker Biotech, Steinfurt, Germany
Fuji X-ray Film Super RX	Life Technologies, Darmstadt, Germany
NuPAGE® antioxidant	Life Technologies, Darmstadt, Germany
NuPAGE® Bis-Tris precast gels (15 or 10 well; 1.5 or 1 mm)	Molecular BioProducts, San Diego, USA
PCR tubes (0.2 ml)	Starlab, Ahrensburg, Germany
Pipette tips (10 µl, 20 µl, 100 µl, 200 µl, 1000 µl)	Sigma Aldrich, Munich, Germany
Polyvinylidene fluoride (PVDF) membrane	Qiagen, Hilden, Germany
QIAshredderTM	Terumo/Novodirect, Kehl/Rhein, Germany
X100 syringe luer centre 1mL	

2.1.11. Plasmids

- pLVX_Puro (Clontech)
- pGEM-He-Juel (obtained from Holger M. Becker, TU Kaiserslautern, Germany)

See appendix for plasmid maps.

Generated plasmids

- pLVX_BCAT1-v1 (previously generated by co-workers. In short, for overexpression of BCAT1, the insert was generated using PCR and subsequently cloned into the XbaI and XhoI sites of the pLVX-puro lentiviral vector (Tönjes et al., 2013).
- pGEM-He-Juel-BCAT1-v6

2.1.12. Primers

Application	Gene name	Oligo Name	Sequence 5' to 3'
qRT-PCR	*SLC16A1*	MCT1-F3	TTGTGGAATGCTGTCCTGTC
		MCT1-R3	ACATGTCATTGAGCCGACCT
	SLC16A3	MCT4-F3	TACCTCACCACTGGGGTCAT
		MCT4-R3	TTCAGCATGATGAGCGAGGG
	SLC16A7	MCT2 Forw 2	CAAAGACTCTGGGACTCTTGGT
		MCT2 Rev 2	TCTGGAGGTGGATGCACAG
	BCAT1	BCAT1_h_rt_fwd1	CAACTATGGAGAATGGTCCTAAGCT
		BCAT1_h_rt_rev1	TGTCCAGTCGCTCTCTTCTCTTC
	ARF1	ARF_h_rt_fwd	GACCACGATCCTCTACAAGC
		ARF_h_rt_rev	TCCCACACAGTGAAGCTGATG
	TBP	TBP_h_rt_fwd	GAACCACGGCACTGATTTTC
		TBP_h_rt_rev	CCCCACCATGTTCTGAATCT
Cloning	*BCAT1*	BCAT1_v6_h_BamHI_fwd	GATCGGATCCATGGATTGCAGTAACGGAT
		BCAT1_h_HindIII_rev	GATCAAGCTTTCAGGATAGCACAATTGTCC
		T7 sequencing primer	TAATACGACTCACTATAGGG

2.1.13. siRNAs

siRNA	target
siRNA sc45892, Santa Cruz	MCT4
siRNA smart pool M-005126-04-0005, Dharmacon	MCT4
siRNA smart pool M-007402-02-0005, Dharmacon	MCT1
non-target #2 siRNA pool D-001206-14-05, Dharmacon	

2.1.14. Software

Software	Company
Basic Local Alignment Search Tool (BLAST)	ncbi.nlm.nih.gov
Empower3 software suite	Waters, Eschborn, Germany
EndNote X7	Thomson ResearchSoft, Carlsbad, USA
FACS-Diva	BD Biosciences, Heidelberg, Germany
Gene Set Enrichment Analysis (GSEA)	http://software.broadinstitute.org/gsea/index.jsp
GraphPad Prism 7	GraphPad, San Diego, USA
Hokawo	Hamamatsu Photonics Germany GmbH
ImageJ	imagej.nih.gov/ij
Ingenuity® Pathway Analysis	Qiagen, Hilden, Germany
Primer-BLAST	ncbi.nlm.nih.gov
SDS 2.4	Applied Biosystems, Foster City, USA

2.2. Methods

2.2.1. Cell Culture Conditions

Human glioblastoma cell lines

- **U87-MG and U251-MG**

Inducible BCAT1 knockdown cells were established as described previously (Tönjes et al., 2013) by infecting U87-MG and U251-MG cells with pLKO-Tet-On non-target (nt) shRNA and pLKO-Tet-On BCAT1 shRNA2 lentiviral particles and selecting with puromycin (1 µg/mL) for 7 days. Induction was achieved by adding 0.1 µg/mL doxycycline to the medium for at least 3 days. Cells were cultured in DMEM containing 1 g/L glucose (D5921, Sigma) supplemented with 10% Tetracycline-free fetal bovine serum (Tet-free FBS), 1% penicillin and streptomycin (P/S) mix and glutamine (0.5 mM). Cell lines were cultivated at 37 °C in a humidified incubator with 10% CO_2.

- **LN-229**

Cells were cultured in DMEM containing 4.5 g/L glucose (D5796, Sigma) supplemented with 10% Fetal calf serum (FCS) and 1%P/S. Cells were cultivated at 37 °C in a humidified incubator with 10% CO_2.

Monocytic cell lines

- **U937**

Cells were cultured in RPMI (1640) supplemented with 10%FCS and 1%P/S. Cells were cultivated at 37 °C in a humidified incubator with 5% CO_2. Differentiation to macrophages was obtained by treatment with 5 nM phorbol 12-myristate 13-acetate (PMA) for 48h.

2.2.2. Cell number and viability measurements

The viability and absolute number of cells was determined using a Vi-CELL XR 2.03 cell counter (Beckman Coulter). Viability was assessed using trypan blue dye exclusion method and only cell suspensions with a viability of at least 90% were used for experiments.

2.2.3. Metabolite quantification using ultra performance liquid chromatography (UPLC)

To quantitatively analyze BCKAs KIV, KIC and KMV, we established protocols for ultra-performance liquid chromatography (UPLC) separation coupled to fluorescence detection using either O-Phenylendiamine (OPD) or 1,2-diamino-4,5-methylendioxybenzene (DMB) as derivatization agents. The DMB method was used to quantify intracellular BCKA concentrations whereas the OPD method was used to quantify other metabolites, including pyruvate, ketobutyrate and glyoxalate (Supplementary table 1) (Appendix).

For derivatization with OPD (o-phenylendiamine) reagent, 100 µL of cell culture supernatant were mixed with 200 µL ice-cold 1M perchloric acid for protein precipitation. After centrifugation at 4°C and 16 400 g for 10 min, 150 µL of the supernatant were mixed with an equal volume of OPD derivatization solution and (25 mM OPD in 2M HCl) and derivatized by incubation at 50°C for 30 min. After centrifugation for 10 min, the derivatized ketoacids were separated by reversed phase chromatography on an Acquity HSS T3 column (100 mm x 2.1 mm, 1.7 µm, Waters) connected to an Acquity H-class UPLC system. Prior separation, the column was heated to 40°C and equilibrated with 5 column volumes of solvent A (0.1% formic acid in 10% acetonitrile) at a flow rate of 0.55 mL/min. Separation of ketoacid derivates was achieved by increasing the concentration of solvent B (acetonitrile) in solvent A as follows: 2 min 2% B, 5 min 18% B, 5.2 min 22% B, 9 min 40% B, 9.1min 80% B and hold for 2min, and return to 2% B in 2 min.

For determination of intracellular BCKA content, cells were extracted with 200 µL cold 1M perchloric acid. Insoluble material was removed by centrifugation for 10 min at 25.000g. For derivatization with DMB (1,2-diamino-4,5-methylendioxybenzene), 30 µL extract were mixed with 30 µL DMB derivatization reagent (5mM DMB, 20mM sodium hydrosulfite, 1M 2-mercaptoethanol, 1.2M HCl) and incubated at 100°C for 45 min. After 10 min centrifugation, the

reaction was diluted with 240 µL 10% acetonitrile. UPLC system, column and solvent was used as described above. Baseline separation of DMB derivates was achieved by increasing the concentration of acetonitrile (B) in buffer A as follows: 2 min 2% B, 4.5 min 15% B, 10.5 min 38% B, 10.6 min 90% B, hold for 2 min, and return to 2% B in 3.5 min.
BCKAs levels in cell lysates and in supernatants from *Xenopus* oocytes (2.2.7.2) were detected using the derivatization with DMB derivatization reagent as described above.
The separated derivates were detected by fluorescence (Acquity FLR detector, Waters, OPD: excitation: 350 nm, emission: 410 nm; DMB: excitation: 367 nm, emission: 446 nm) and quantified using ultrapure standards (Sigma). Data acquisition and processing was performed with the Empower3 software suite (Waters).

2.2.4. Protein quantification

For protein extraction, cells were washed twice with PBS and resuspended in 40-60µL RIPA-lysis buffer, which was supplemented with 1X protease and phosphatase inhibitor cocktail (PIC) and 1X EDTA. The lysates were centrifuged at 13000 rpm at 4°C for 5 min and the supernatants containing the protein extracts were stored at -80°C. Total protein was quantified using bicinchoninic acid (BCA) method. Protein samples were diluted either 1:2 or 1:4 in RIPA lysis buffer and 1 µL was pipetted into 0.2 µL tube. Bicinchoninic acid and copper sulphate solution mixed in a ratio of 50:1 and 20 µL of this solution was added to each tube. Each sample was measured in duplicate and RIPA buffer was used for the blank measurement. Protein-Cu^{2+} complex form during the subsequent incubation at 37°C for 30 min with consequent reduction of Cu^{2+} to Cu^{1+} by protein in an alkaline environment containing sodium potassium tartrate. BCA reacts with the reduced cation forming a purple-colored complex, the absorption of which was measured at 562 nm. A bovine serum albumin (BSA) based standard curve was used for regression analysis to determine protein concentration.

2.2.5. Western blot

Total protein of cell lines was extracted using RIPA lysis buffer (as described in section 2.2.4). 15 µg of protein was separated by 4-12% SDS-PAGE and transferred to a polyvinylidene difluoride membrane. The membrane was blocked in blocking solution (5% Milk in TBS-T) and incubated with primary antibodies overnight at 4°C. Horseradish peroxidase (HRP)-conjugated

secondary antibodies were incubated for 1h at room temperature (RT) before chemiluminescent detection of protein (ECL kit, GE Healthcare). The following antibodies were used: monoclonal mouse antibody to α-tubulin (1:3000 dilution) (clone DM1A, #T9026, Sigma-Aldrich), anti-MCT4 (sc50329, Santa Cruz) antibody (1:1000 dilution), anti-MCT1 (AB3538P, Millipore) (1:500 dilution), anti-MCT2 (PA5-50518, Thermo Fisher Scientific) (1:1000 dilution). HRP-conjugated antibody to mouse IgG (1:5000 dilution) (sc-2005, Santa Cruz) or HRP-conjugated antibody to rabbit IgG (1:3000 dilution) (sc-2004, Santa Cruz) were used as secondary antibodies.

2.2.6. RNA extraction, RT-PCR and qPCR

RNA extraction

Total RNA was isolated using RNeasy Microkit, Qiagen according to the manufacturer's instructions. RNA concentration was measured using Nanodrop ND-1000 spectrophotometer.
In the preparation of RNA for microarray analysis, cells were lysed in 350 µL RLT buffer (RNeasy Microkit, Qiagen) and the lysate was homogenized by passing through QiashredderTM columns at 13000 rpm for 2 min at RT. DNAse I on column treatment step was performed.

RT-PCR

Total RNA was reverse transcribed using random primers and Superscript II Reverse Transcriptase according to manufacturer's instructions. In short, first, residual DNA was removed by incubation of total RNA with 1 µL DNAse I and 2 µL first strand buffer for 15 min at RT. Samples were then incubated with a random primer mix for 10 min at 65°C and 2 min at RT for primer hybridization. Finally, 1 µL Superscript II Reverse Transcriptase was added and incubation at 42°C for 50 min followed. The reaction was stopped by incubation at 94°C for 10 min. ddH_2O was added to achieve a final cDNA concentration of 16.67 ng/µL.

Quantitative Real Time PCR (qPCR)

Each cDNA sample was analyzed in triplicate with the Applied Biosystems Prism 7900HT Fast Real-Time PCR System using Absolute SYBR Green ROX Mix. Primers were also tested on genomic DNA and ddH_2O. The relative amount of specific mRNA was normalized to *ARF1* and *TBP* mRNA. Primer sequences are given in 2.1.12.

The following amplification protocol was used, with 40 cycles of steps 2 and 3:

Step	Temperature (°C)	Time
1: activation	50	2 min
2: initial denaturation	95	15 min
3: denaturation	95	15 sec
4: annealing/extension	60	1 min

Data was analyzed using the SDS 2.4 software. For relative quantification, mean ratios were calculated between the gene of interest and two housekeeping genes (*ARF1* [ADP-ribosylation factor 1] and *TBP* [TATA-box binding protein]).

2.2.7. Heterologous expression of BCAT1 and MCTs in *Xenopus* oocytes

2.2.7.1. Cloning of human BCAT1-v6 into pGEM-He-Juel vector

BCAT1-version 1 (v1) was previously cloned into pLVX_Puro vector (Tönjes et al., 2013) and this vector was used to subclone human BCAT1-version 6 (v6) into the oocyte expression vector pGEM-He-Juel.

PCR using pLVX_BCAT1-v1 vector and BCAT1_v6_h_BamHI forward primer and BCAT1_h_HindIII reverse primer (2.1.12) using the following reaction mix:

PCR reaction Mix

Reagent	Volume (µL)
HiFi buffer 5X (Biocat)	30
pLVX-BCAT1-v1 (0.01µg/µl)	0.5
dNTPs Mix (Biocat)	1.5
primer BCAT1_v6_h_BamHI_fwd (10µM)	3
primer BCAT1_h_HindIII_rev (10µM)	3
PRECISOR High-fidelity DNA polymerase (Biocat)	3
ddH_2O	109
Total	**150**

PCR program

Temperature (°C)	Time	Cycles
98	30 sec	
98	30 sec	
66	30 sec	35
72	45 sec	
72	10 min	
4	∞	

5 µL of PCR product were analyzed by 1% agarose gel electrophoresis and the remaining volume was purified using QiAquick PCR purification Kit (Qiagen) accordingly to manufacturer's protocol. After purification, PCR product was digested at 37°C 30 min followed by 80°C 10 min using BamHI Fast digest (FD) and HindIII Fast digest (FD) restriction enzymes as follows:

Digestion reaction

	BCAT1-v6 PCR product	**pGEM-He-Juel**	**pGEM-He-Juel**
	Volume (µL)	Volume (µL)	Volume (µL)
DNA	48	1	1
BamHI FD	3	1	-
HindIII FD	3	1	-
FD green buffer (10X)	6	2	2
ddH_2O	-	15	17
Total	**60**	**60**	**60**

Digestion products were analyzed by 1% agarose gel electrophoresis and agarose bands were excised from the gel and DNA was extracted using QiAquick Gel extraction kit (Qiagen) accordingly to manufacturer's protocol. DNA was quantified using Nanodrop ND-1000 spectrophotometer and ligation reaction was performed at RT for 15 min using Rapid DNA ligation kit (Roche) as follows:

Ligation reaction

	pGEM-He-Juel	**BCAT1-v6**
	Volume (µL)	Volume (µL)
DNA (final concentration 50ng/µL)	3	1
1X Dilution buffer (Roche)	6	
T4 DNA ligase buffer (Roche)	10	
T4 DNA ligase (Roche)	1	
Total	**21**	

5 µL of ligation reaction were added to 50 µL of TOP10 *E.coli* (Life Technologies) and transformation was performed as follows: 30 min incubation on ice, 30 sec at 42°C followed by 2 min incubation on ice. 250 µL S.O.C. medium (Thermo Fisher Scientific) were added and cells were incubated 1h at 37°C with agitation (300 rpm). After incubation time 50 µL were plated in Agar plates with ampicillin and incubated ON at 37°C. On the next day, 10 colonies were selected and picked from the agar plates and colony PCR was performed using the following conditions:

Colony PCR Mix

Reagent	Volume (µL)
10X PCR buffer (EUROTAQ kit)	2.5
dNTPs Mix	0.25
$MgCl_2$	0.75
primer BCAT1_v6_h_BamHI_fwd (10µM)	0.5
primer BCAT1_h_HindIII_rev (10µM)	0.5
EUROTAQ DNA polymerase	0.25
ddH_2O	20.25
Total	**25**

PCR program

Temperature (°C)	Time	Cycles
98	30 sec	
98	30 sec	
66	30 sec	35
72	45 sec	
72	10 min	
4	∞	

PCR product was analyzed using 1% agarose gel electrophoresis. The colonies containing the BCAT1-v6 insert were used for small scale plasmid preparation. 3 mL LB medium containing ampicillin were inoculated with a pipette tip containing a picked bacterial colony and incubated overnight at 37°C with shaking. Plasmid isolation followed using a QIAprep® spin Minikit (Qiagen) according to the manufacturers' protocol. Concentrations were determined using a NanoDrop ND-1000 spectrophotometer.

The sequences of pGEM-He-Juel-BCAT1-v6 plasmid was verified by Sanger sequencing using a BigDye® Terminator v3.1 Cycle sequencing kit. 2 µL T7 sequencing primer (2.1.12) (10µM) or 2 µL BCAT1_h_HindIII reverse primer (10 µM) (2.1.12), 1 µL BigDye® terminator mix, 2 µL 5X sequencing buffer were added to 300 ng of plasmid DNA (1.2 µL) and ddH_2O up to 21 µL. PCR sequencing was performed accordingly to the table below:

PCR program

Temperature (°C)	Time	Cycles
96	3 min	
96	30 sec	
51	15 sec	25
60	4 min	
4	∞	

PCR products were purified by precipitation with 27.5 µL absolute ethanol and 1.1 µL 3M sodium acetate, with subsequent centrifugation at 13000 rpm 30 min at RT. The precipitated pellet was washed with 100 µL 60% ethanol and centrifuged at 13000 rpm 14 min. The precipitated pellet was dried at 37°C and dissolved in 11 µL formamid. Sequencing was performed using ABI PRISM 3100 genetic analyzer.

After confirming the sequence of the plasmid, large scale plasmid preparation was performed by inoculating 300 mL LB medium supplemented with ampicillin with *E.coli* (transformed with the pGEM-He-Juel-BCAT1-v6 plasmid) glycerol stocks and incubated at 37°C ON with agitation (200 rpm). For plasmid isolation the Qiagen Maxiprep Kit was used according to the manufacturers' protocol. Concentrations were determined using a NanoDrop ND-1000 spectrophotometer.

2.2.7.2. Heterologous protein expression in Xenopus oocytes

The generated pGEM-He-Juel-BCAT1-v6 plasmid was sent to Holger Becker for following heterologous expression of human BCAT1 in the *Xenopus* oocytes. In addition, plasmid DNA of MCT1, MCT4 or NBCe1 cloned into pGEM-He-Juel, which contains the 5' and the 3' untranscribed regions of the *Xenopus β*-globin flanking the multiple cloning site, was used. DNA was linearized with SalI and transcribed *in vitro* with T7 RNA-polymerase (mMessage mMachine, Ambion Inc., USA) as described earlier (Becker et al., 2004).

Oocytes at stages V were injected with 5 ng of cRNA coding for rat MCT1 or rat MCT4, 12 ng of cRNA coding for human BCAT1, 7 ng cRNA coding for human NBCe1, 5 ng of cRNA for rat MCT1 or MCT4 and 12 ng of cRNA for human BCAT1 5 days before the experiments.

Native oocytes or oocytes expressing the specified proteins were stimulated with BCAAs (1 nmol L-Valin, 1 nmol L-Leucin, 1 nmol L-Isoleucin) and α-ketoglutarate (3 nmol) for 2h at RT. After the incubation time, culture medium was removed and stored for posterior analysis by UPLC (2.2.3) and cells were lysed by pipetting and the lysate was centrifuged for 10 min at 10 000 g at 4°C and stored before analysis by UPLC (2.2.3).

Batches of 10 oocytes were used per condition and the experiment was performed 3 times.

2.2.8 MCT1 inhibition

A total of 1 x 10^5 U87nt or U87shBCAT1, U251nt or U251shBCAT1 and 0.4 x 10^5 LN-229 cells were seeded onto 12-well plates, medium was replaced after 16 hours and fresh medium with AR-C155858 (Tocris) or DMSO was added and cells were incubated at 37°C 10%CO_2 for 24 hours. U87 and LN-229 cells were treated with 1 µM AR-C155858 whereas for U251 cells 2 µM AR-C155858 was used. Supernatants from U87nt, U87shBCAT1, U251nt, U251shBCAT1 and LN-229 cells treated with MCT1 inhibitor (AR-C155858) or DMSO were centrifuged at 2000 rpm for 5 min and filtered using 0.22µm filters and analyzed by UPLC. Cells were harvested by trypsinization, centrifuged at 1000 rpm for 5 min and washed once with ice-cold 0.9% NaCl, and the cells pellets were frozen at -80°C before analysis by UPLC (2.2.3).

2.2.9 Cell proliferation analysis

To assess the effect of MCT1 inhibitor (AR-C155858, Tocris) on proliferation of glioblastoma cells the Click-iT EdU cell proliferation assay (Invitrogen) was used following the manufacturer's instructions. The cells were incubated with 10 µM of the nucleoside analog EdU for 8-10h. Quantification of cells that incorporated EdU was performed using a FACS Canto II (BD Biosciences).

2.2.10 MCT4 and MCT1 siRNA mediated knockdown

A total of 2.5 x 10^5 U87nt, U251nt or LN-229 cells were seeded onto 6-well plates in medium without P/S and incubated at 37°C 10%CO_2 ON. Cells were transfected using DharmaFECT 1 transfection reagent (Dharmacon) with 25nmol of MCT4 siRNA (sc45892, Santa Cruz) (siMCT4 1), MCT4 siRNA smart pool (M-005126-04-0005, Dharmacon) (siMCT4 2), 25nmol of MCT1 siRNA (M-007402-02-0005, Dharmacon) or non-target (nt) #2 siRNA pool (D-001206-14-05, Dharmacon). Control cells were incubated with Opti-MEM medium (Gibco) and DharmaFECT1 (no siRNA added). Cells were incubated at 37°C 10%CO_2 for 48h with medium change at 24h post transfection. At 48h post transfection, cells were harvested for RNA isolation (RNeasy Microkit, Qiagen) and protein extraction (using RIPA buffer) and the knockdown efficiency was evaluated by qPCR (2.2.6) and western-blot (2.2.5). Supernatants from U87nt or U251nt cells

48h post transfection using non target siRNA or MCT4 siRNAs were centrifuged at 2000 rpm for 5 min and filtered using 0.22 µm filters and analyzed by UPLC for BCKAs determination (2.2.3).

2.2.11 *In situ* proximity ligation assay (PLA)

In situ PLA was performed in the U87nt and U251nt cells using the Duolink *in situ* proximity ligation assay (Olink Bioscience, Uppsala, Sweden) accordingly to manufacturer's protocol.
In short, cells were seeded onto 8-well chamber slides (Lab-TekII, Thermo Scientific Nunc) and incubated ON at 37°C 10%CO_2. Cells were fixed with 4% paraformaldehyde solution for 15 min at RT, permeabilized with PBS 0.1% TritonX100 for 15 min at RT and dehydrated using a ethanol series (70%, 85%, 100%) for 2 min at RT. Before the blocking step cells were rehydrated with PBS1X for 15 min at RT. Blocking solution (Olink Bioscience) was added and slides were incubated for 30 min at 37°C. The primary antibodies used were anti-BCAT1 (rabbit polyclonal antibody, Insight Biotechnology limited (Wembley, UK)) (provided by Myra Conway), anti-MCT1 (ab90582, Abcam), anti-MCT4 (376140, Santa Cruz) at 1:100 dilution in Antibody diluent (Olink Bioscience) and anti-PGK1 antibody (GTX107614, GeneTex) was used at 1:200 dilution. Cells incubated without primary antibodies or with only one of each of the antibodies tested in combination were used as procedure controls. The results were visualized using Axioplan 2 imaging (Zeiss) microscope and Hokawo software. The images were processed and PLA signals/cell were quantified using ImageJ software.

2.2.12 Tumor conditioned medium generation

2.2.12.1 Human serum cultures

A total of 0.3 x 10^6 U87nt and a total of 0.6 x 10^6 U87shBCAT1 cells were seeded onto 6-well plates in DMEM (D5921, Sigma) supplemented with 10% Human Serum (HS), type AB (MP Biomedicals) 1%P/S and glutamine (0.5 mM) with doxycycline (0.1 µg/mL) and incubated for 96h at 37°C 10%CO_2 with medium change at 48h. After 96 hours culture medium was harvested and centrifuged at 1200 rpm 10 min at RT and 3000 rpm 10 min at RT and stored at -80°C. Cells were harvested for RNA extraction (RNeasy Microkit, Qiagen) and cell number was determined using Vi-cell Counter (Beckman Coulter). Tumor conditioned medium (TCM) from three independent collections was pooled immediately before use.

2.2.12.2 No human serum cultures

U87nt or U87shBCAT1 cells after doxycycline induction for at least 3 days were cultured in DMEM (D5921, Sigma) supplemented with 10% Tet-free FBS, 1%P/S and glutamine (0.5 mM) with doxycycline (0.1 µg/mL) for 2-3 days. Supernatants were then harvested and centrifuged at 1200 rpm 10 min at RT and 3000 rpm 10 min at RT and stored at -80°C before use. Cells were harvested for RNA extraction (RNeasy Microkit, Qiagen) to confirm BCAT1 knockdown efficiency.

2.2.13 Isolation of peripheral blood mononuclear cells (PBMCs) from buffy coats

Human PBMCs were isolated from buffy coats from normal donors obtained from the Institut für Klinische Transfusionsmedizin und Zelltherapie (IKTZ) (Heidelberg, Germany) by density gradient using via Ficoll density separation. In short, 15 mL Biocoll (Biochrom) separation solution was applied to Leucosep™ tubes, which were centrifuged at 2000 rpm for 5 min. Blood buffy coat samples were diluted 1:3 in PBS and transferred to Leucosep™ tubes, adding 30 mL per tube to obtain a total volume of 45 mL. Samples were centrifuged at 2200 rpm for 20 min at RT without break. Four layers were obtained (from top to bottom): plasma layer, PBMC interphase, Biocoll layer and erythrocyte/granulocyte pellet. Using a pipet, the PBMC interphase was carefully transferred to a new 50 mL Falcon tube, avoiding excess transfer of plasma and Biocoll solution. PBMCs were washed twice in PBS and centrifuged at 1200 rpm for 10 min, prior to resuspension in RPMI 1640 and cell counting using Vi-cell counter. Assuming that 10% of PBMCs are monocytes, respective cell numbers, as needed for downstream experiments, were applied to further either positive selection of $CD14^+$ monocytes or enrichment of monocyte population by plastic adhesion.

2.2.13.1 Isolation of monocytes from PBMCs isolated from buffy coats

$CD14^+$ magnetic sorting

$CD14^+$ monocytes were purified from healthy donors' mononuclear cells by CD14 microbeads magnetic cell sorting, according to the manufacturer's instructions (Miltenyi Biotec). In brief, cells were centrifuged at 1200 rpm 10 min and resuspended in ice-cold MACS buffer (80 µL per

1 x 10^7 cells) and CD14 MicroBeads (20 µL per 1 x 10^7 cells). Samples were incubated at 4°C for 15 min, prior to additional washing with MACS buffer and centrifugation at 1200 rpm for 10 min. Cells were resuspended in ice-cold MACS buffer (10^8 cells in 500 µL of buffer) and applied to LS MACS columns previously equilibrated with ice-cold MACS buffer. Flow through was discarded and magnetic columns were washed 3 times with ice-cold MACS buffer. $CD14^+$ monocytes were eluted in 5 mL ice-cold MACS buffer and column-based purification was repeated one additional time. Subsequently monocytes were counted and resuspended in RPMI 1640 before cell counting using Vi-cell counter. Purity of the cells was accessed by FACS Canto II (BD Biosciences) using anti-CD14 FITC antibody and it was 95–99%. Cellular debris and dead cells were excluded from the analysis based on scatter signals.

Enrichment by plastic adhesion

Monocytes were enriched from the PBMCs by plastic adhesion for 2h at 37°C 5%CO_2. PBMCs were plated in 6-well plates (2x10^7 cells/mL) in RPMI and incubated for 2h at 37°C 5%CO_2. After incubation, cells were washed two times with PBS and fresh medium was added to cells and incubated ON at 37°C 5%CO_2. On the next day, cells were washed with PBS and fresh medium was added. For M-CSF differentiation, DMEM 5796 supplemented with 10%FCS and 1%P/S was used and M-CSF was added at a final concentration of 20 ng/mL for 7-10 days with supplementation every 2 days.

2.2.14 Microarray analysis

Tumor conditioned medium (TCM) differentiated macrophages

CD14 sorted monocytes were plated in 6-well plates (1.5x10^6 cells/mL) using RPMI and incubated for 2h at 37°C 5%CO_2. After incubation, medium was removed and DMEM 5921 supplemented with 10%HS 1%P/S and glutamine (0.5 mM) or TCM supplemented with 10%HS was added to cells and incubated at 37°C 10%CO_2. At day 4 ½ of fresh medium or TCM supplemented with 10%HS was added to the cells. At day 7 medium was changed and fresh medium or TCM supplemented with 10%HS was added to the cells. At day 11 cells were lysed using RLT buffer (RNeasy Minikit, Qiagen) and transferred to QiAschreder columns (Qiagen) and centrifuged at 13000rpm for 2min. RNA was extracted using RNeasy Minikit, Qiagen

following manufacturers' instructions. RNA was hybridized in Illumina HumanHT-12 Chip by the Genomics and Proteomics Core Facility (GPCF) at DKFZ, Heidelberg, Germany. Monocytes were isolated from four different donors.

M-CSF differentiated macrophages exposed to BCKAs

Monocyte-derived macrophages differentiated M-CSF during 7 days and treated with 300 µM BCKAs (KIV, KIC, KMV) or without BCKAs for 24h at 37°C 10%CO_2. After treatment, RNA was extracted from cells using RNeasy Mini Kit according to the manufacturer's protocol. RNA was hybridized in Illumina HumanHT-12 Chip by the GPCF at DKFZ, Heidelberg, Germany. Monocytes were isolated from four different donors.

U87 cells expressing normal and low BCAT1 levels

U87nt and U87shBCAT1 cells were grown in the presence of medium supplemented with 10%HS and doxycycline (2.2.12.1) and RNA was extracted using RNeasy Mini Kit according to the manufacturer's protocol. RNA was hybridized in Illumina HumanHT-12 Chip by the Genomics and Proteomics core facility (GPCF) at DKFZ, Heidelberg, Germany.

2.2.15. BCKAs uptake studies in monocyte-derived macrophages

Monocytes were isolated from the PBMCs and enriched by plastic adhesion (2.2.13.1) for 2h at 37°C 5%CO_2 and differentiated either in the presence of U87nt TCM or U87shBCAT1 TCM supplemented with 10% HS for 11 days or with 20 ng/mL human M-CSF for 7 days. For TCM differentiated macrophages, after differentiation, medium was replaced by DMEM 5921 10%HS 1%P/S and glutamine (0.5 mM) with 100 µM or 300 µM KIV, KIC and KMV and cells were incubated for 24h at 37°C 10%CO_2. For M-CSF differentiated macrophages, after differentiation, medium was replaced by DMEM 6046 10%FCS 1%P/S with 100 µM or 300 µM KIV, KIC and KMV and cells were incubated for 24h at 37°C 10%CO_2. After 24h incubation supernatants were collected, centrifuged at 2000 rpm for 5 min, filtered using 0.22 µm filters and analyzed by UPLC (2.2.3). Monocytes were isolated from two different donors.

2.2.16. ^{13}C-BCKA tracing experiments in monocyte-derived macrophages

Monocytes were isolated from the PBMCs and enriched by plastic adhesion for 2h at 37°C 5%CO_2 and differentiated either in the presence of U87nt TCM or U87shBCAT1 TCM supplemented with 10%HS for 12 days or in the presence of 20 ng/mL human M-CSF for 7-10 days. After differentiation, medium was replaced by DMEM 5921 1%HS 1%P/S and glutamine (0.5 mM) with 100 µM or 300 µM ^{13}C α-KIV (13C5, 98%, Cambridge Isotope Laboratories) and 100 µM or 300 µM ^{13}C α-KIC (1,2-13C2, 99%, Cambridge Isotope Laboratories) and cells were incubated for 48h at 37°C 10%CO_2. After 48h cells were collected and intracellular metabolites were extracted for Gas Chromatography-Mass Spectrometry (GC-MS) analysis. From M-CSF-differentiated macrophages, cell culture medium was also harvested and analyzed using GC-MS. Monocytes were isolated from two different donors.

2.2.17. Extraction of intracellular metabolites for Gas Chromatography-Mass Spectrometry (GC-MS)

Extraction of intracellular metabolites for GC-MS was according to Sapcariu et al, 2014 (Sapcariu et al., 2014). Briefly, cells were cultivated in 6-well plates, medium was retained for quantification of extracellular metabolites and cells washed with 2 mL of 0.9% NaCl. Then quenched with 0.2 mL of -20°C methanol and after adding an equal volume of 4°C cold water, cells were collected with a cell scraper and transferred to tubes containing 0.2 mL -20°C chloroform. The extracts were shaken at 1400 rpm for 20 min at 4°C and centrifuged at 16 000 g for 5 min at 4°C. 0.2mL of the upper aqueous (polar) phase was collected and stored at -80°C. After collecting polar phase the non-polar phase was also collected. Interphase was washed with 0.3 mL -20°C methanol and centrifuged at 16 000 g for 10 min at 4°C. After removing the methanol, 50 µL of methanol were added and interphase was stored at -80°C. Polar phase was subsequently subjected to GC-MS analysis.
Extraction of metabolites from cell culture medium was according to Sapcariu et al, 2014.

2.2.18. Gas chromatography-mass spectrometry (GC-MS)

Derivatization was performed with a Gerstel autosampler directly before measurement on the GC-MS. Dried metabolites were dissolved in 15 µL of 2% methoxyamine hydrochloride in pyridine at a temperature of 40°C for 60 min. Then, 15 µL of 2,2,2-trifluoro-N-methyl-N-trimethylsilyl-acetamide + 1% chloro-trimethyl-silane was added and incubated at 40°C for 30 min. The metabolite extracts were measured on an Agilent 7890 GC containing with a 30 m DB-35MS capillary column. The GC was connected to an Agilent 5975C MS operating in electron ionization (EI) at 70 eV. 1µL of derivatized sample was hot injected at 270°C in splitless mode. Helium was used as the carrier gas at a flow rate of 1 mL=min. The GC oven temperature was kept constant at 100°C for 2 min and then increased to 300°C at 10°C/min, where it was held for 4 min. The total GC-MS run time of one sample was 26 min. For relative quantification of metabolite levels, an alkane mix was run with the experimental sequence in order to provide retention index calibration for the experimental samples. The MS source was kept at a constant temperature of 230°C and the quadrupole at 150°C. For relative quantification of metabolite levels, the detector was operated in scan mode with an m/z range of 70 to 800. For analysis of stable isotope labeling, the detector was operated in selected ion monitoring (SIM) mode. Relative abundance of each mass isotopomer (M) was determined using mass isotopomer distribution analysis.

2.2.19. Phagocytosis assay

Monocyte-derived macrophages differentiated in the presence of 20 ng/mL human M-CSF (Miltenyi Biotec) (2.2.13.1) previously incubated in the absence or presence of 300 µM BCKAs (KIV, KIC, KMV) at 37°C for 24h were incubated with 1 µm diameter fluorescent biotin-labeled beads (F8768, Molecular probes, Life technologies) at a ratio of 50 beads/cell at 37°C for 2h. After 2h, medium was removed and cells were washed 5X with 1X PBS and cells were stained with Cell Mask stain (Molecular probes, Life Technologies) for 10min at 37°C prior to fixation in 4% paraformaldehyde for 20 min at RT. In parallel cells were stained with Streptavidin Phycoerythrin (PE) (554061, BD Biosciences) at 1:200 dilution for 30 min at 4°C prior to fixation in 4% paraformaldehyde for 20 min at RT. Hoechst dye (Molecular probes, Invitrogen) was used to stain cell nuclei. Phagocytosis of fluorescent beads was examined by fluorescence microscopy (Cell Observer, Zeiss). The number of beads engulfed by each cell was quantified

using ImageJ software. Cells were isolated from two different donors and 3-4 fields per condition were examined.

2.2.20. Differentiation of macrophages using U87 TCM

Primary cells

Macrophages were differentiated from monocytes isolated from PBMCs via enrichment by plastic adhesion (2.2.13.1) using U87nt/U87shBCAT1 TCM (2.2.12.2) or medium supplemented with M-CSF for 7 days. After differentiation, photos were taken using Leica DM IRBE microscope.

U937 model

U937 cells ($10x10^5$ cells/mL) were plated in 6-well plates and differentiated in the presence of 5 nM PMA either in DMEM 5921 10%Tet-free FBS 1% P/S and glutamine (0.5 mM) or U87nt/ U87shBCAT1 TCM (2.2.12.2) for 48h. After 48h, cells were harvested by incubation with accutase during 20 min at RT and cell number was determined using Vi-cell counter.

2.2.21. Cytokine array U87 TCM

Supernatants collected from U87nt or U87shBCAT1 cells cultured in the presence of 10%HS (TCM) (2.2.12.1) were collected and human cytokine antibody array (ab133998, Abcam) was performed accordingly to manufacturer's instructions. In short, membrane was blocked using 1X blocking buffer at RT for 30 min and incubated with 2 mL TCM at 4°C ON under gentle agitation followed by washing steps with Wash buffer 1 and 2. Next, membrane was incubated with 1mL 1X Biotin-Conjugated anti-cytokines for 2h at RT. Washing steps with Wash buffer 1 and 2 were performed before incubation with 2 mL of 1X HRP-Conjugated Streptavidin for 2h at RT. Membrane was washed once more before chemiluminescence detection using Fusion solo S (Vilber Lourmat) equipment.

2.2.22. Monocyte migration *in vitro* assay

Monocyte migration was assessed in transwell migration assays using 24-well transwell inserts with 5 µm pore size. Monocytes were isolated from PBMCs by $CD14^+$ magnetic sorting (2.2.13.1) (purity >94%) and $5.5x10^6$ cells/mL were resuspended in DMEM 5921 10%HS and

seeded in the upper wells. The lower chamber contained U87nt/U87shBCAT1 TCM (2.2.12.1) or 200 ng/mL CCL2 in DMEM as a positive control. The cells were allowed to migrate for 2h at 37°C. After incubation, upper culture inserts were carefully removed and cells migrated to bottom chambers were harvested and counted using Vi-cell counter. Monocytes were isolated from two different donors.

2.2.23. T cell proliferation assay

To further investigate the impact of BCAT1 knockdown in the tumor cells on T cell proliferation we used tumor conditioned medium collected from U87-MG cells expressing normal (nt) or reduced BCAT1 (shBCAT1) levels (2.2.12.1) and performed a T cell proliferation assay. PBMCs were isolated from the blood via Ficoll density separation (2.2.13) and T cells were isolated by negative selection using MagniSort® Human T cell Enrichment Kit (eBioscience) accordingly to manufacturer's protocol. After total T cell harvest, $CD4^+$ T-helper cells were separated from the rest with the MACS human CD4 Microbeads (Miltenyi Biotec) accordingly to manufacturer's protocol. $CD8^+$ population was stained with CFSE (Life Technologies) and staining efficiency was verified by FACS. 300 000 $CD8^+$ T cells were seeded in each well of 96-well plate and 125 µL of tumor conditioned medium was added per well. Cells were then stimulated with IL-2 and PHA and incubated at 37°C for 6 days. At the end of incubation, FACS analysis for CFSE staining using FACS Canto II instrument was performed. Average mean fluorescent intensity (MFI) and percentage of proliferating cells were calculated.

2.2.24. Statistical analysis

Statistical analysis was performed using GraphPad Prism software. Differences in means as determined by Student's t-test or Mann-Whitney test was considered statistically significant at $p<0.05$. Furthermore, the following convention was used: *$p < 0.05$, **$p < 0.01$, ***$p < 0.001$, ****$p < 0.0001$.

3. Results

3.1. MCT1-mediated excretion of glioblastoma cell branched-chain ketoacids modulates macrophage phagocytosis [1]

3.1.1. Glioblastoma cells excrete BCKAs

To quantify the content of the branched chain ketoacids α-ketoisocaproate (KIC), α-ketoisovalerate (KIV) and α-keto-methylvalerate (KMV) in biologic extracts, an ultra-performance liquid chromatography (UPLC) protocol in which ketoacids were derivatized with either O-Phenylendiamine (OPD) or 1,2-diamino-4,5-methylendioxybenzene (DMB) was established. While the very sensitive DMB method allows for the analysis of the usually low intracellular BCKA concentrations, the less sensitive OPD method was used to quantify the levels of BCKAs and pyruvate in cell culture supernatants (Figure 7A and B). Analysis of cell culture media from three glioblastoma cell lines, U87-MG, U251-MG and LN-229, revealed accumulation of BCKAs to concentrations of up to 85 µM over a period of 24 hours (Figure 7C) indicating that glioblastoma cells are producing and excreting large amounts of BCKAs. To further support our observation, we performed shRNA-mediated knockdown in two cell lines of the metabolic enzyme BCAT1 (Figure 7D), which generates BCKAs by transamination of BCAAs in the cytoplasm. BCAT1 knockdown resulted in reduction of BCKAs excretion of about 70% and 50% in U87-MG and U251-MG, respectively (Figure 7E and F). These data identify BCAT1 as the predominant source of BCKAs excreted by glioblastoma cells.

[1] This chapter is the subject of a manuscript entitled “MCT1-mediated excretion of glioblastoma cell branched-chain ketoacids modulates macrophage phagocytosis” which is currently submitted at *EMBO Reports*, and of which I am the first author and has been originally written by myself.

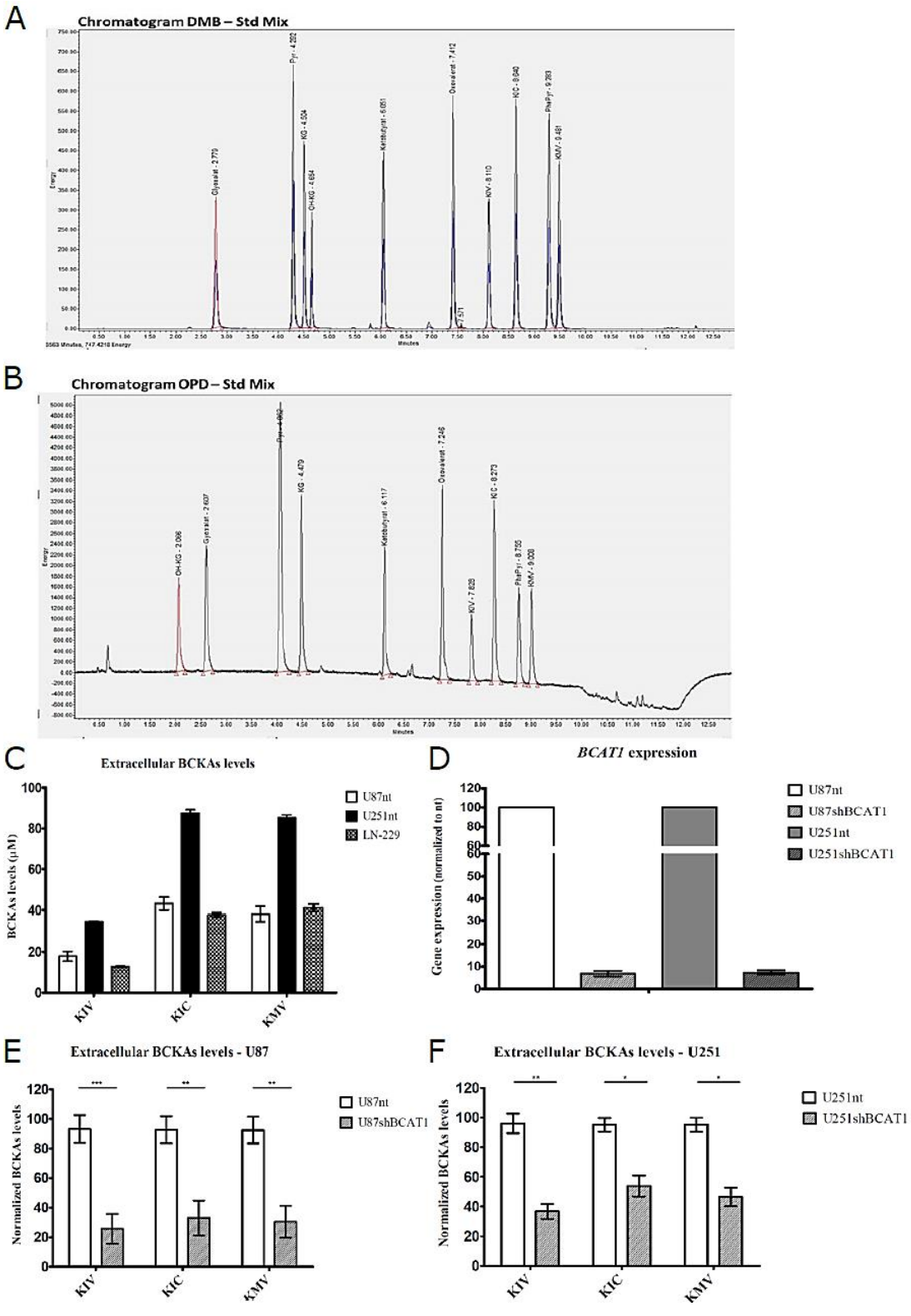

(Figure legend on the next page)

Figure 7 – Glioblastoma cells excrete BCKAs.

BCKAs (KIV, KIC, KMV) are detected by Ultra Performance Liquid Chromatography (UPLC) coupled to fluorescence detection in cell extracts using the derivatization with DMB **(A)** or in cell culture supernatants using the OPD derivatization reagent **(B)**. **(C)** BCKAs (KIV, KIC, KMV) levels (µM) detected in supernatants from U87-MG and U251-MG cells expressing normal BCAT1 levels, U87nt and U251nt, respectively, and from LN-229 cells. **(D)** BCAT1 mRNA expression in U87-MG and U251-MG cells after BCAT1 knockdown. Expression levels are normalized to those from cells expressing normal BCAT1 levels (nt: non-target). Values are mean ± SD of three technical replicates. BCKAs levels after BCAT1 knockdown in supernatants from U87 **(E)** and U251 **(F)** cells. Values are mean ± SD of three technical replicates. **(E)** and **(F)** BCKAs levels are normalized to the detected levels in U87nt or U251nt cells, respectively. *Data generated with support of Dr. Gernot Poschet, COS, University of Heidelberg, Heidelberg, Germany.* KIV: α-ketoisovalerate. KIC: α-ketoisocaproate. KMV: α-keto-β-methylvalerate. unpaired t-test; * p<0.05 ** p<0.01 *** p<0.001

3.1.2. MCTs expression in glioblastoma

To determine which of the monocarboxylate transporters could be responsible for BCKA excretion from glioblastoma cells, we analyzed their RNA expression in published data of primary untreated glioblastoma (n=480; TCGA dataset). *SLC16A1* (MCT1) and *SLC16A3* (MCT4) both were significantly overexpressed in glioblastoma compared to normal brain (NB) tissue (Figure 8A). *SLC16A7* (MCT2) and *SLC16A8* (MCT3) expression were variable but on average lower in tumor than in normal tissue (Figure 8A). Comparing glioblastoma subtypes, MCT4 expression was significantly higher in mesenchymal tumors than in others (Figure 8B). Expression of MCT1 and MCT4 on RNA (Figure 8C) and protein (Figure 8D) levels was confirmed in three glioblastoma cell lines, U87-MG, U251-MG and LN-229, which commonly are used as *in vitro* models.

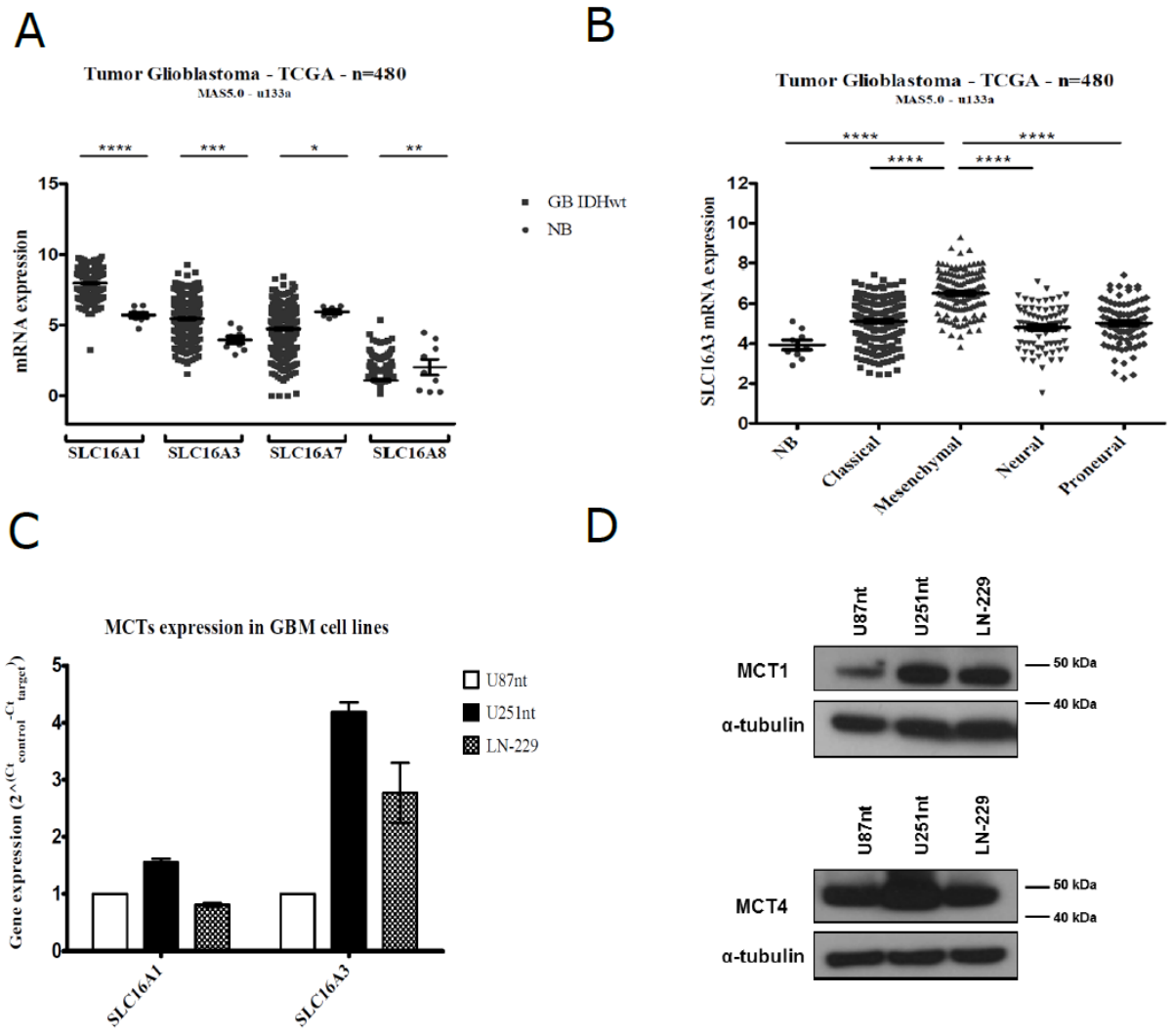

Figure 8 – MCT1 and MCT4 are upregulated in glioblastoma.

mRNA expression of *SLC16A1* (MCT1), *SLC16A3* (MCT4), *SLC16A7* (MCT2), *SLC16A8* (MCT3) in glioblastoma (GB IDHwt) (n=480) compared to normal brain (NB) tissue (n=9) in samples from the TCGA dataset **(A). (B)** mRNA expression of *SLC16A3* in the four different subtypes of glioblastoma (n=480) defined by gene expression patterns compared to normal brain (NB) tissue (n=9) in samples from the TCGA dataset. Values are mean ± SEM. unpaired t-test * p< 0.05; ** p< 0.01 *** p< 0.001; **** p< 0.0001. Expression of MCT1 and MCT4 in the glioblastoma cell lines U87nt (nt: non-target), U251nt (nt: non-target) and LN-229, at mRNA **(C)** and protein level **(D). (C)** Values are mean ±SD and are normalized to the levels detected for U87nt. **(D)** α-tubulin was used as loading control.

3.1.3. MCT1 and MCT4 transport BCKAs across cell membranes

To test whether MCT1 and MCT4 are capable of transporting BCKAs across the membranes of living cells, heterologous expression in *Xenopus* oocytes (Hardwick and Philpott, 2015) was used as a rapid, accessible and easy to manipulate model system. To evaluate the function of individual protein components of BCKA transport, the respective cRNAs were injected into *Xenopus* oocytes, stimulated the oocytes with BCAAs and αKG, and determined changes in intra- and extracellular BCKA levels. Since the concentrations of BCKAs were expected to be lower than in the tumor cells the quantification of BCKAs in cell lysates as well as in the supernatants from oocyte cultures by UPLC was performed using the DMB derivatization agent. Expression of BCAT1 alone led to a significant increase in the intracellular levels of all three BCKAs compared to native oocytes or oocytes that expressed rat MCT1, rat MCT4 or the sodium/bicarbonate cotransporter (NBCe1) which was included to control for non-specific excretion of BCKAs. When BCAT1 was co-expressed with either MCT1 or MCT4, intracellular BCKA concentrations significantly dropped (Figure 9A), suggesting that the MCTs mediated the excretion of the BCKAs produced by BCAT1.

To further support this hypothesis, BCKA levels in the supernatants of the very same batches of oocytes (Figure 9B) were analyzed. Expression of the NBCe1 control did not affect BCKAs levels. Much larger increases of extracellular BCKA levels, however, were observed upon co-expression of human BCAT1 and either rat MCT1 or rat MCT4. BCKA concentrations in the supernatants reached about 25µM within 2 hours indicating that MCT1 and MCT4 can efficiently transport BCKAs across the membranes of living cells.

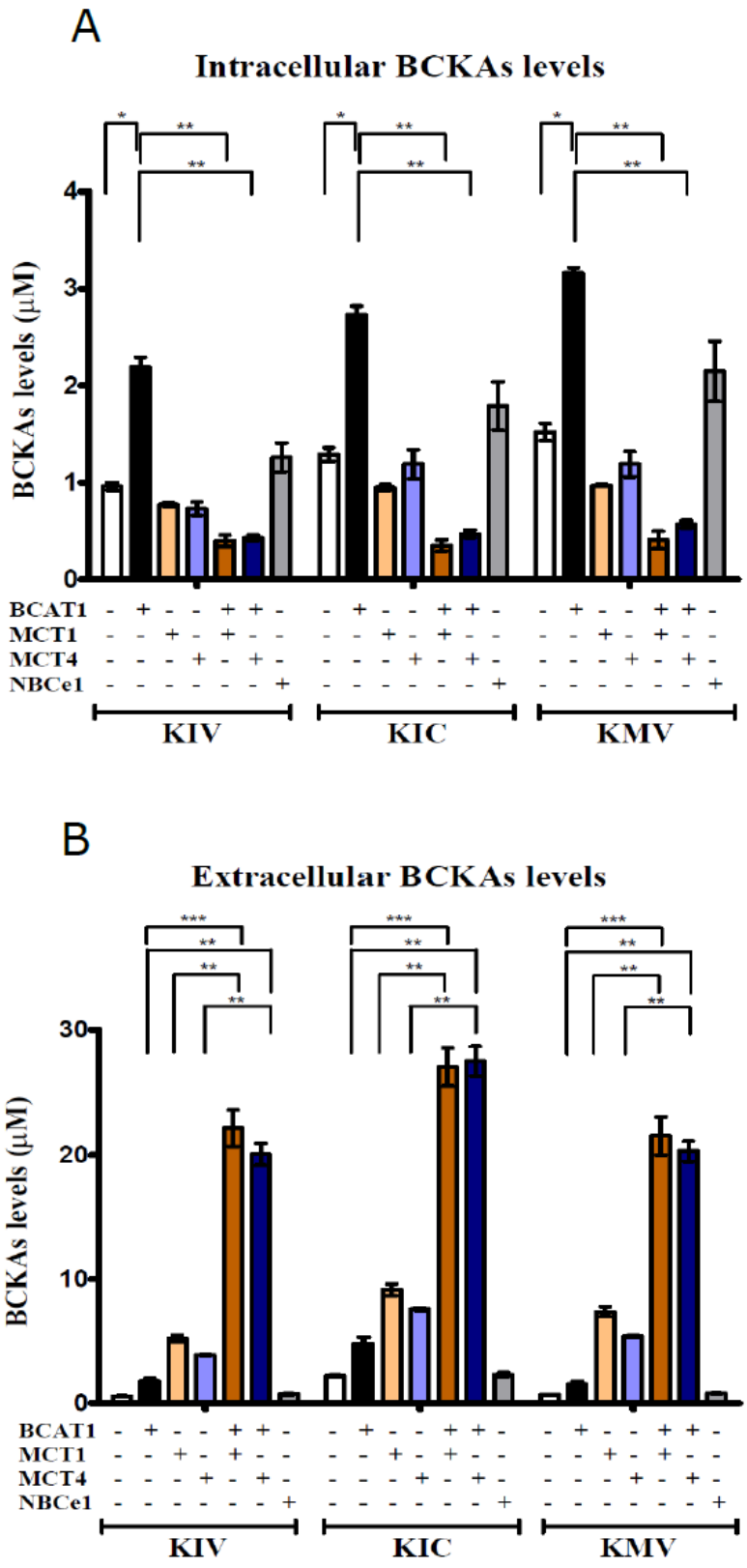

(Figure legend on the next page)

Figure 9 – Co-expression of BCAT1 and either MCT1 or MCT4 facilitates the excretion of BCKAs from *Xenopus* oocytes.

BCKAs (KIV, KIC, KMV) levels detected by Ultra Performance Liquid Chromatography (UPLC) coupled to fluorescence detection in native oocytes or oocytes expressing BCAT1, MCT1, MCT4, NBCe1 or co-expressing MCT1 or MCT4 and BCAT1 stimulated with BCAAs (1 nmol L-Valin, 1 nmol L-Leucin, 1 nmol L-Isoleucin) and α-ketoglutarate (3 nmol) for 2 h at RT **(A)** and in the oocytes culture medium **(B).** Heterologous expression of the human or rat proteins in the oocytes was performed by injection of the respective cRNA into the oocyte. The cRNA concentrations used were: 5 ng rat MCT1, 5 ng rat MCT4, 12 ng human BCAT1, 7 ng human NBCe1 or 5 ng MCT1 or MCT4 and 12 ng BCAT1. Batches of 10 oocytes were used per condition. Values are mean ± SD of three biological replicates. *Data generated with support of Prof. Holger M. Becker, TU Kaiserslautern, Kaiserslautern Germany*. KIV: α-ketoisovalerate. KIC: α-ketoisocaproate. KMV: α-keto-β-methylvalerate. NBCe1: sodium/bicarbonate cotransporter. unpaired t-test * p<0.05; ** p<0.01; *** p<0.001

3.1.4. Inhibition of MCT1 but not MCT4 reduces BCKA excretion from glioblastoma cells

To investigate the role of MCTs in the transport of BCKAs in glioblastoma cells, we manipulated MCT function in the U87-MG, U251-MG and LN-229 cell lines by pharmacologic inhibition of MCT1 with the MCT1/MCT2-specific inhibitor AR-C155858 at concentrations that did not affect cell proliferation (Figure 10).

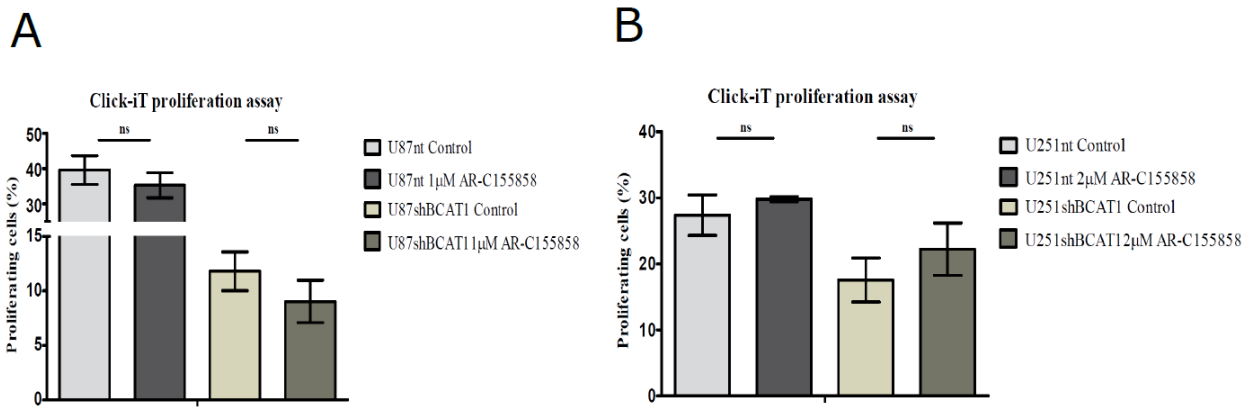

Figure 10 – MCT1 inhibition does not impact on cell proliferation.

Effect of MCT1 inhibitor AR-C155858 on cell proliferation of U87nt and U87shBCAT1 **(A)** and of U251nt and U251shBCAT1 **(B)** cells determined using the Click-iT proliferation assay. Values are mean ± SD for n = 2-3 technical replicates. unpaired t-test; ns: not significant

Application of AR-C155858 reduced the excretion of individual BCKAs 20% and 80% in U87-MG and LN-229, respectively (Figure 11A and B) while intracellular BCKA concentrations showed concurrent increases (Figure 11D and E). For unknown reasons, the effects of inhibition were less clear in U251-MG cells where in most cases we could only observe trends for decreases of excreted and increases of intracellular BCKAs, respectively (Figure 11C and F). Furthermore, consistently with the MCT1 inhibitor data, siRNA mediated knockdown of MCT1 resulted in decreased excretion of BCKAs in the three glioblastoma cell lines (Figure 12). Inhibition of MCT1 also significantly decreased the excretion of pyruvate in all three cell lines (Figure 13A). This suggests that U251-MG potentially can compensate suppression of MCT1-mediated transport of BCKAs but not pyruvate through another carrier system. Together these data indicate that MCT1 is an important mediator of the excretion of BCKAs as well as pyruvate by glioblastoma cells.

To examine the role of MCT4 in BCKA transport in glioblastoma cells, siRNA-mediated knockdown was used since no specific inhibitors of MCT4 are commercially available. Despite good knockdown efficiencies in U87-MG and U251-MG cells using two different siRNA pools (Figure 14A), no significant changes in the levels of BCKAs in the cell culture media were observed (Figure 14B and C). To exclude the possibility that MCT4-mediated transport activity lost due to the siRNA knockdown was compensated by increased activity of MCT1, MCT4 knockdown was performed with and without concurrent MCT1 inhibition in U87-MG cells. The combined inhibition of both MCTs did not result in any additive effect on BCKA excretion beyond that caused by MCT1 inhibition alone except for KIC (Figure 15).

Furthermore, knockdown of MCT4 also did not reduce pyruvate excretion (Figure 13B and C). Together the data suggest that MCT4 has very limited transport capacities for BCKAs and pyruvate in glioblastoma cells.

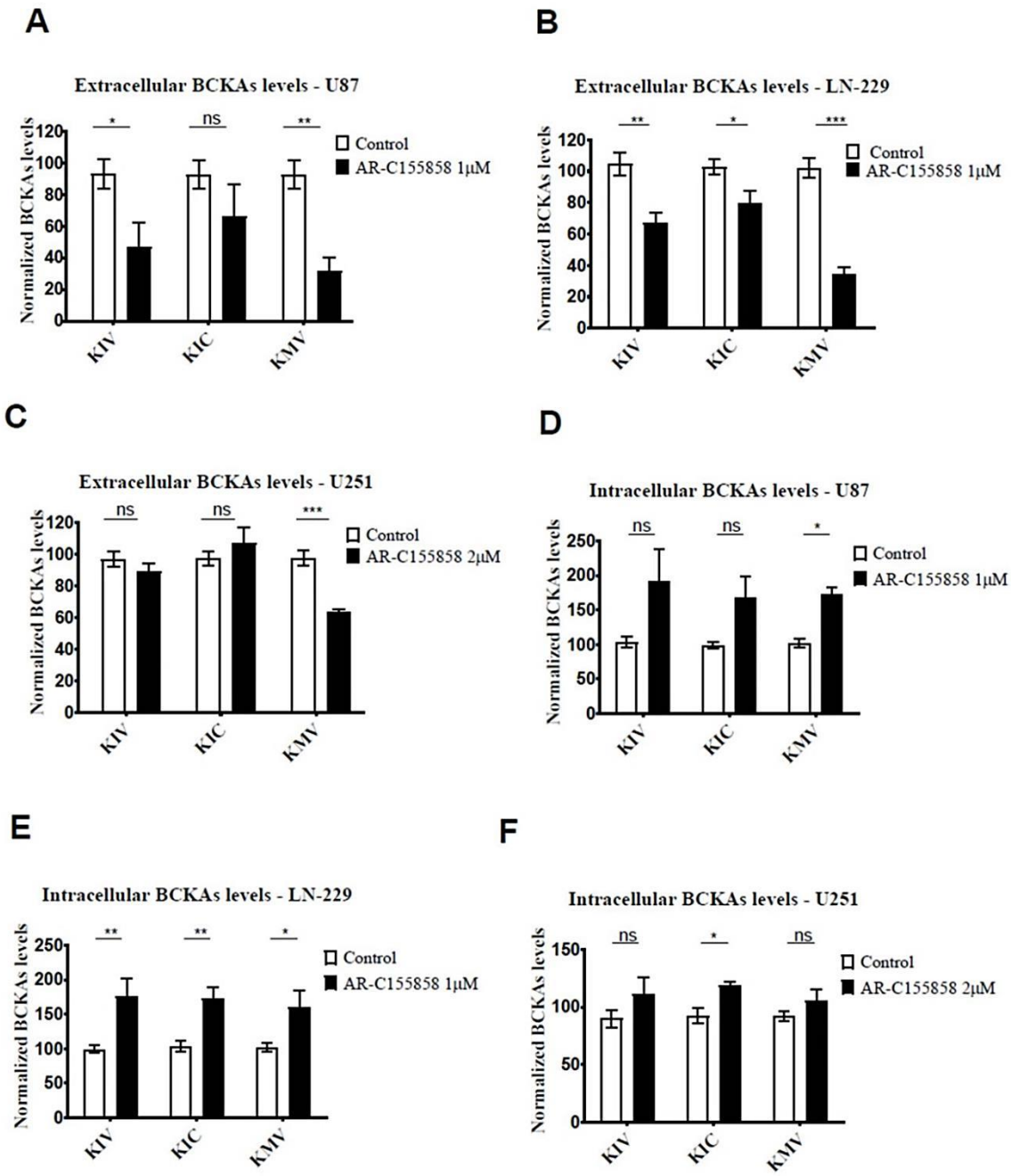

Figure 11 – Inhibition of MCT1 transporter decreases BCKAs excretion in glioblastoma cells.

BCKAs (KIV, KIC, KMV) levels were determined by Ultra Performance Liquid Chromatography (UPLC) coupled to fluorescence detection in supernatants from U87nt **(A)** , LN-229 **(B)** and U251nt **(C)** cells as well as in cell extracts **(D, E, F)** treated with AR-C155858 for 24h at 37°C 10%CO_2. BCKAs levels were normalized to total protein content and to the detected levels in the respective cells treated with DMSO (Control). **(A, B, C, E)** Values are mean ± SD of three independent experiments, run in triplicates. **(D, F)** Values are mean ± SD of two independent experiments, run in triplicates. *Data generated with support of Dr. Gernot Poschet, COS, University of Heidelberg, Heidelberg, Germany*. KIV: α-ketoisovalerate. KIC: α-ketoisocaproate. KMV: α-keto-β-methylvalerate. unpaired t-test; ns: not significant * p<0.05 ** p<0.01 *** p<0.001

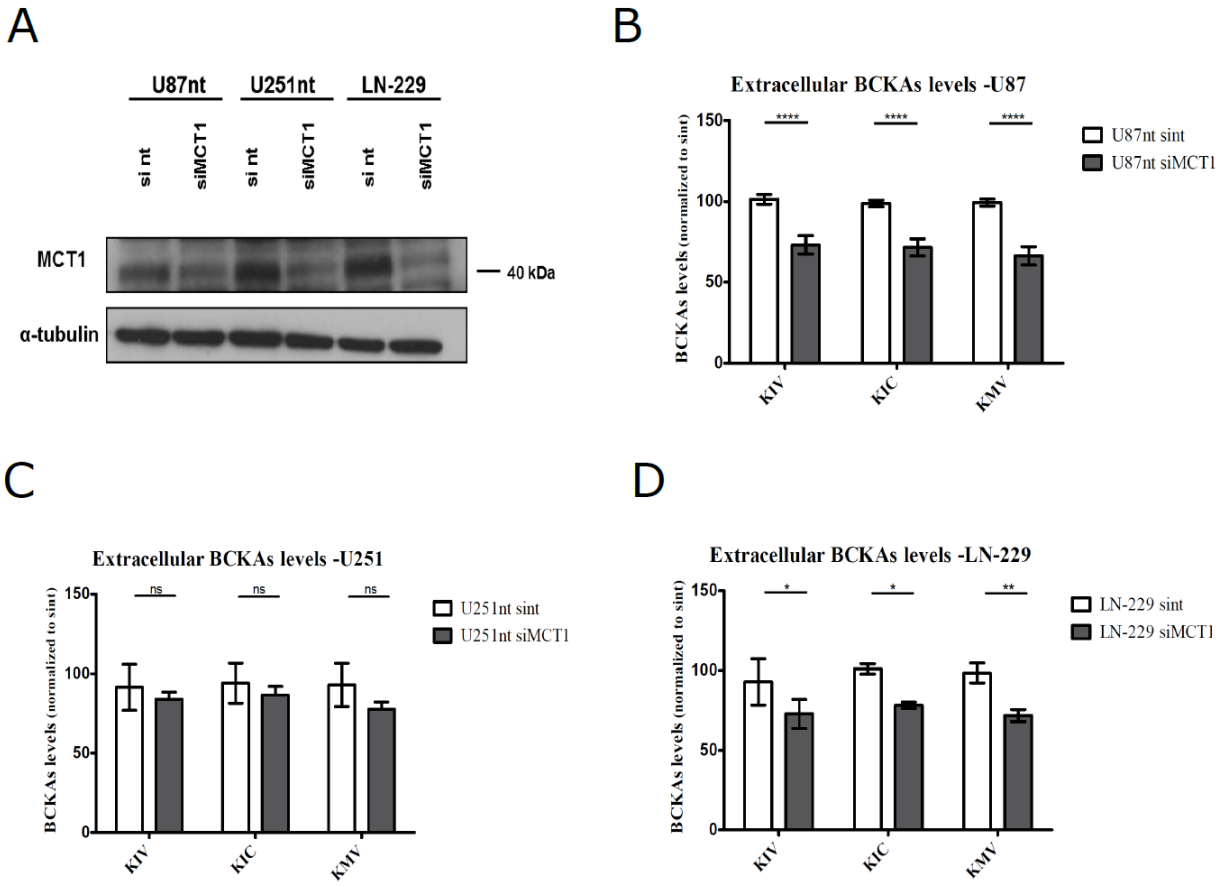

Figure 12 – MCT1 knockdown reduces BCKAs excretion.

(A) Western blot analysis of MCT1 levels in U87-MG cells, U251-MG expressing normal levels of BCAT1 (U87nt and U251nt) and LN-229 cells 48h post transfection using of MCT1 siRNA (Dharmacon) or non-target siRNA (sint) (Dharmacon). Anti-MCT1 (AB3538P, Millipore) antibody was used at 1:500 dilution. α-tubulin was used as loading control. BCKAs (KIV, KIC, KMV) levels were determined by Ultra Performance Liquid Chromatography (UPLC) coupled to fluorescence detection in supernatants from U87nt **(B)**, U251nt **(C)** and LN-229 **(D)** cells 48h after transfection. BCKAs levels were normalized to total protein content and to the levels detected in U87nt, U251nt or LN-229 cells transfected with non-target (nt) siRNA (U87nt sint, U251nt sint or LN-229 sint, respectively). Levels are mean ± SD for n = 3 technical replicates. *Data generated with support of Dr. Gernot Poschet, COS, University of Heidelberg, Heidelberg, Germany*. KIV: α-ketoisovalerate. KIC: α-ketoisocaproate. KMV: α-keto-β-methylvalerate. unpaired t-test; ns: not significant * $p<0.05$ ** $p<0.01$ **** $p<0.0001$

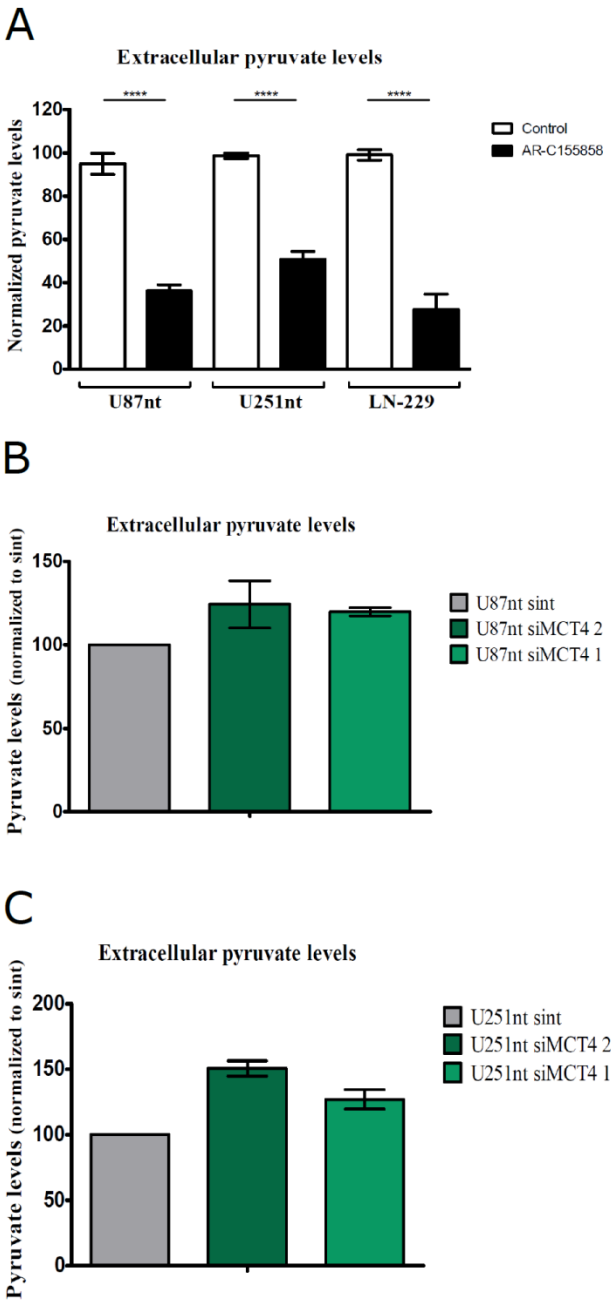

Figure 13 – MCT1 inhibition reduces pyruvate excretion.

Pyruvate levels were determined by UPLC in supernatants from U87nt, U251nt and LN-229 cells treated with AR-C155858 for 24h at 37°C 10%CO_2 **(A)** and from U87nt **(B)** or U251nt **(C)** cells expressing normal MCT4 levels (sint) or low MCT4 levels (siMCT4). Pyruvate levels were normalized to total protein content and to the detected levels in the respective cells treated with DMSO (Control) or to the detected levels in cells expressing normal MCT4 levels (sint), respectively. **(A)** Values are mean ± SD for n = 3 technical replicates. **(B, C)** Values are mean ± SD of two biological replicates. unpaired t-test; **** p< 0.0001. *Data generated with support of Dr. Gernot Poschet, COS, University of Heidelberg, Heidelberg, Germany*.

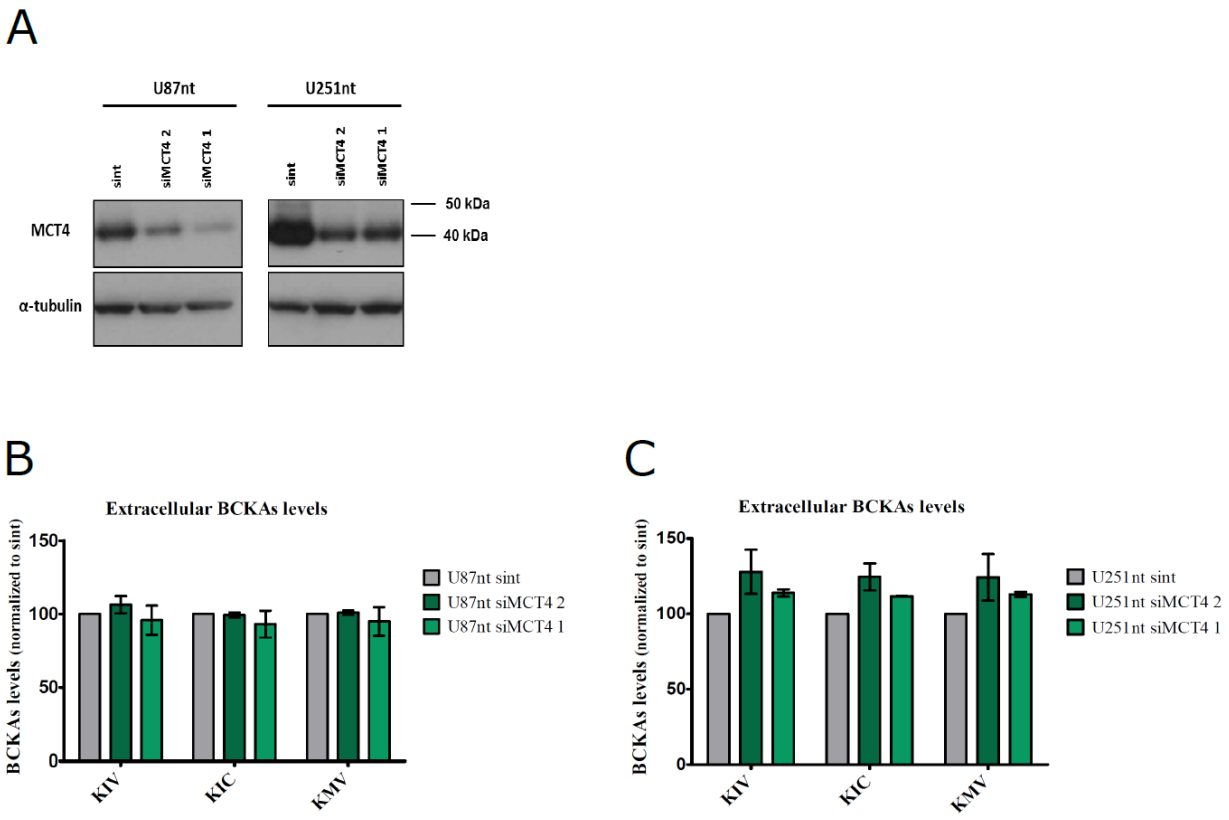

Figure 14 – MCT4 knockdown does not impact on BCKAs excretion.

(A) Western blot analysis of MCT4 levels in U87-MG cells and U251-MG expressing normal levels of BCAT1 (U87nt and U251nt) 48h post transfection using MCT4 siRNA (Santa Cruz) (siMCT4 1), MCT4 siRNA (Dharmacon) (siMCT4 2), or non-target siRNA (sint) (Dharmacon). Anti-MCT4 sc 50329 (Santa Cruz) antibody was used at 1:1000 dilution. α-tubulin was used as loading control. BCKAs (KIV, KIC, KMV) levels were determined by Ultra Performance Liquid Chromatography (UPLC) coupled to fluorescence detection in supernatants from U87nt **(B)** and U251nt **(C)** cells 48h after transfection. BCKAs levels were normalized to total protein content and to the levels detected in U87nt or U251nt cells transfected with non-target siRNA (U87nt sint or U251nt sint, respectively). Levels are mean ± SD of two biological replicates. *Data generated with support of Dr. Gernot Poschet, COS, University of Heidelberg, Heidelberg, Germany*. KIV: α-ketoisovalerate. KIC: α-ketoisocaproate. KMV: α-keto-β-methylvalerate

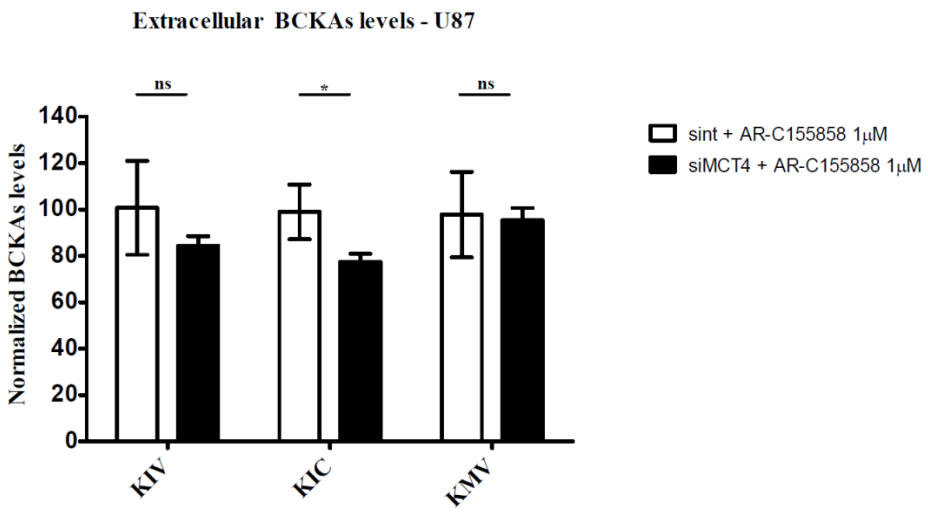

Figure 15 – MCT4 knockdown does not potentiate the effect of MCT1 inhibition on BCKAs excretion.
BCKAs (KIV, KIC, KMV) levels were determined by Ultra Performance Liquid Chromatography (UPLC) coupled to fluorescence detection in supernatants from U87 cells expressing normal MCT4 levels (sint) or low MCT4 levels (siMCT4) treated with AR-C155858 for 24h at 37°C 10%CO2. BCKAs levels were normalized to total protein content and to the detected levels in cells expressing normal MCT4 levels (sint) treated with the MCT1 inhibitor. Values are mean ± SD for n = 3 technical replicates. unpaired t-test; ns: not significant; * $p<0.05$. *Data generated with support of Dr. Gernot Poschet, COS, University of Heidelberg, Heidelberg, Germany*. KIV: α-ketoisovalerate. KIC: α-ketoisocaproate. KMV: α-keto-β-methylvalerate

3.1.5. BCAT1 and MCTs are in close proximity in glioblastoma cells

It has previously been shown that lactate-transport activities of MCT1 and MCT4 are enhanced by their close association with carbonic anhydrases, which serve as proton donors or acceptors to help drive co-transport of protons and lactate (Jamali et al., 2015; Klier et al., 2014). Here we performed *in situ* proximity ligation assays (PLA) of MCT1, MCT4 and BCAT1 in U87-MG and U251-MG cells to test whether BCAT1, the enzyme producing the BCKAs in the cytoplasm, is located in close proximity to MCT1 and MCT4. We hypothesize that such an association might help increase local BCKA concentrations and enhance cross-membrane transport. In both cell lines we observed specific PLA signals indicating that BCAT1 and MCT1 indeed are located in close proximity to one another (Figure 16A and B). Close proximity of BCAT1 and MCT4 also was detected in U251-MG cells (Figure 16D) but not in U87-MG cells (Figure 16C). To control for non-specific association of proteins, we performed PLA with the MCTs and the cytoplasmic metabolic enzyme phosphoglycerate kinase 1 (PGK1) in place of

BCAT1 (Figure 17B). PGK1 was selected because its level of protein expression is comparable to that of BCAT1 protein in U251-MG cells (NCI60 proteome resource: http://129.187.44.58:7070/NCI60/).

Counting of the PLA signals revealed that the number of PLA signals/cell detected in the combination of anti-BCAT1 and anti-MCT1 antibodies was significantly higher than for the control combination of anti-PGK1 and anti-MCT1 antibodies in both cell lines (Figure 16E and F), suggesting specific close proximity between BCAT1 and MCT1 in glioblastoma cells.

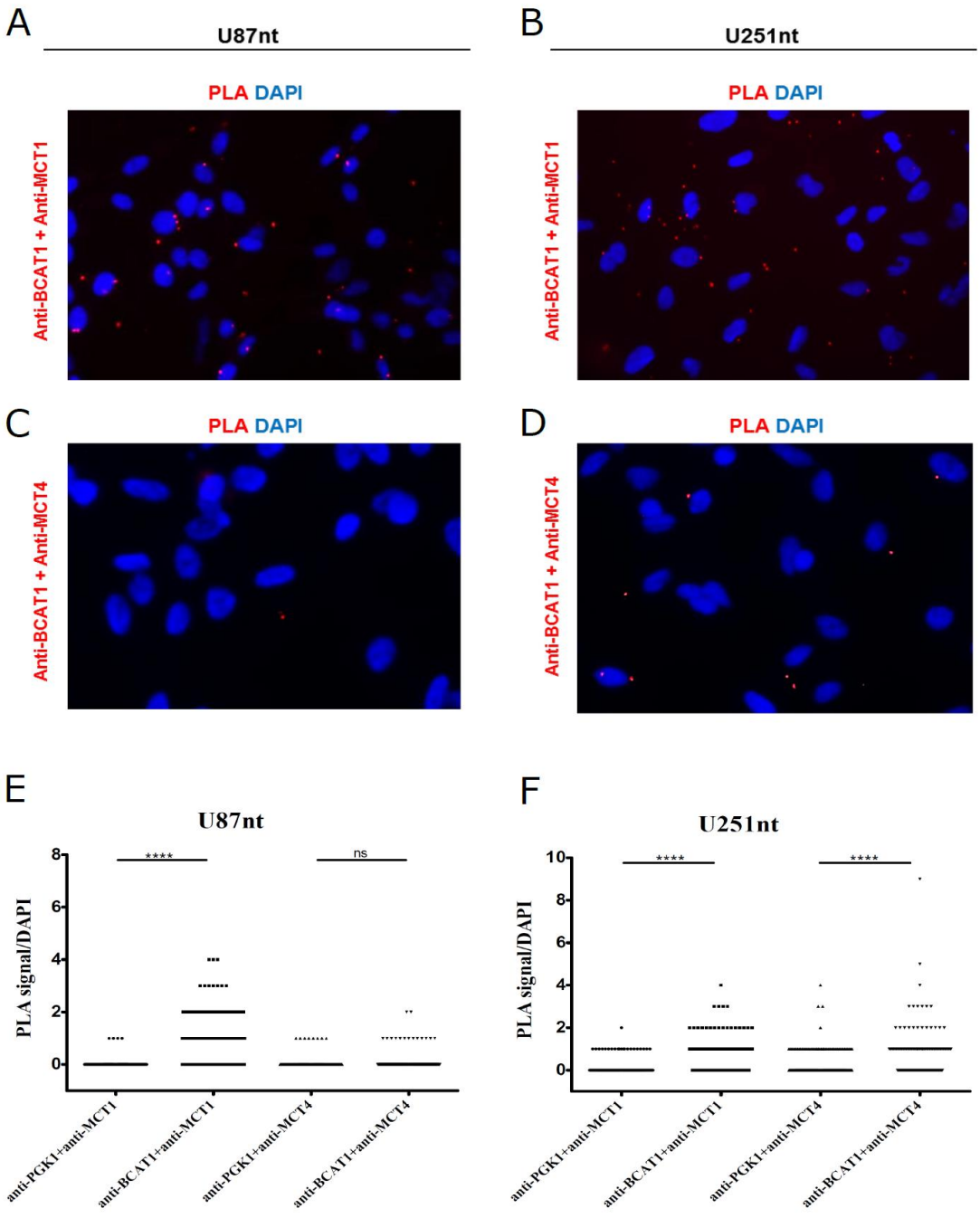

Figure 16 – BCAT1 and MCTs are in close proximity in glioblastoma cells.

Representative images of *in situ* proximity ligation assay (PLA) in the U87-MG **(A, C)** and U251-MG **(B, D)** cells expressing normal BCAT1 levels (U87nt, U251nt respectively) are shown. Cells were incubated with antibodies against BCAT1 and MCT1 or MCT4. Cells incubated PGK1 and MCT1 or MCT4 antibodies were used as control and representative pictures are shown in Figure 17B. Magnification: 200x. Red, PLA signal; blue, DAPI. Quantification of PLA signals per cell in U87nt **(E)** and U251nt cells **(F)**.

Mann Whitney test; ns: not significant ; **** p< 0.0001.

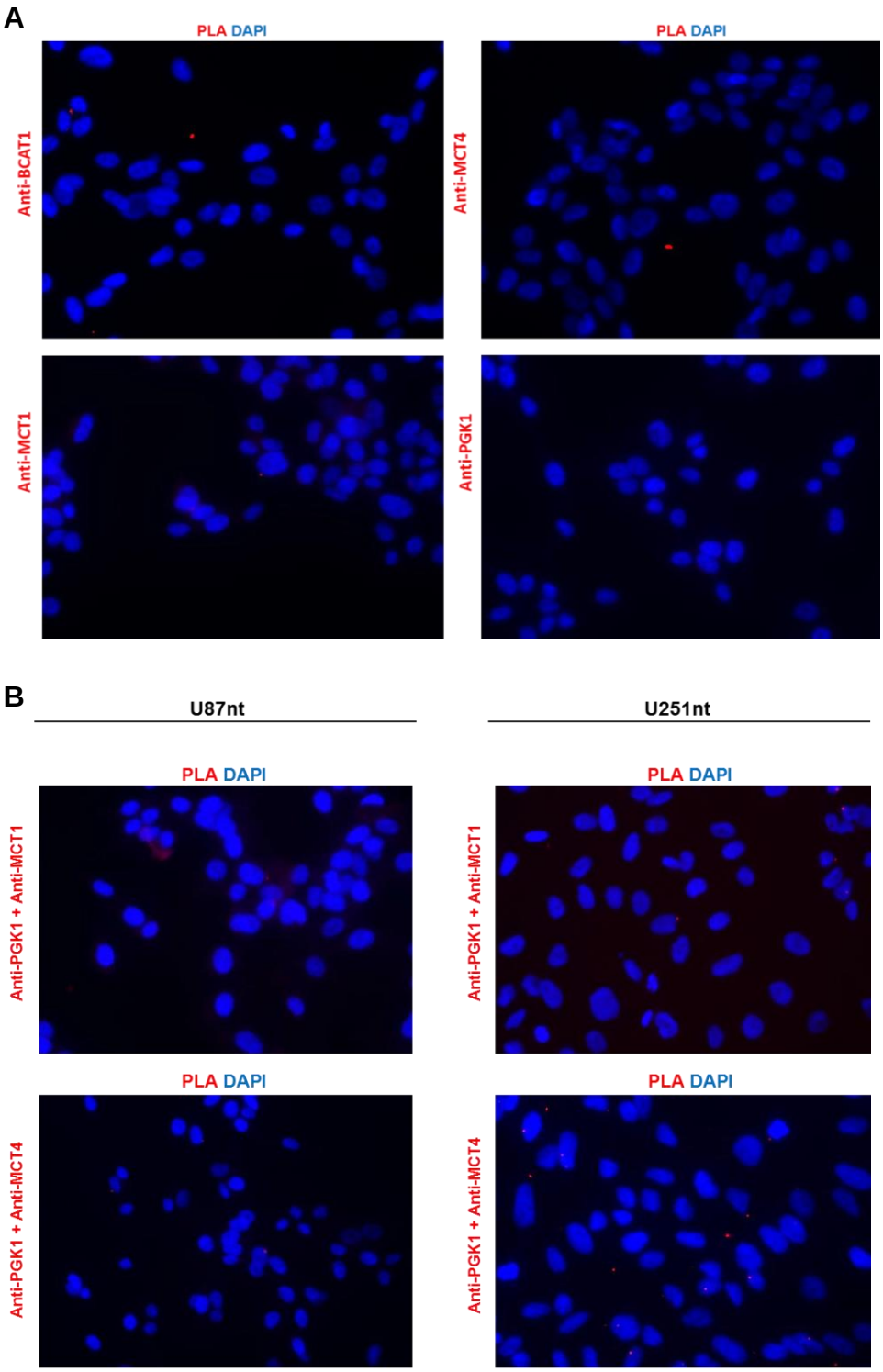

Figure 17 – *In situ* proximity ligation assay controls.

(A) Representative images of the negative controls of *in situ* proximity ligation assay (PLA) in U87nt cells. **(B)** Representative images of *in situ* PLA in the U87nt and U251nt cells. Cells were incubated with antibodies against PGK1 and MCT1 or MCT4.

Magnification: 200x. Red, PLA signal; blue, DAPI.

3.1.6. BCKAs are taken up and metabolized by macrophages

After characterizing the transport of BCKAs from glioblastoma cells I wanted to know whether the predominant cells of the glioblastoma stroma, i.e. tumor-associated macrophages, take up and catabolize tumor-secreted BCKAs, as recently had been shown for tumor-derived lactate. For this purpose, I first cultured human monocyte-derived, M-CSF-differentiated macrophages in the absence or presence of BCKAs (100 µM or 300 µM) and quantified BCKA levels in the culture media after 48 hours of culture using Ultra Performance Liquid Chromatography (UPLC). I observed that the BCKAs levels present in the culture medium of the M-CSF differentiated macrophages were not significantly changed compared to the levels detected in the medium without macrophages suggesting that the macrophages did not take up any BCKAs (Figure 18A). Second, I differentiated monocytes isolated from normal donors with U87nt and U87shBCAT1 conditioned medium (TCM) in the presence of human serum and treated them for the same 48 hours with 100 µM or 300 µM of BCKAs. These macrophages did not appear to take up the BCKAs present in the culture media (Figure 18B and C) similarly to what was observed for the M-CSF differentiated macrophages.

To test whether small amounts of tumor-derived BCKAs still might be taken up and catabolized by macrophages, tracing experiments with non-radioactively labeled BCKAs in human monocyte-derived macrophages that had been differentiated with either M-CSF or tumor-conditioned media (TCM) were performed. After adding ^{13}C-αKIC (1,2-13C2) and ^{13}C-αKIV (13C5) to the cell culture media for 48 hours, cell extracts were prepared from the macrophages and selected TCA cycle metabolites and amino acids (Table 2) analyzed by sequential gas chromatography and mass spectrometry (GC-MS). No detectable labeling in any of the analyzed metabolites was found when 100 µM of ^{13}C-αKIC and ^{13}C-αKIV were added to TCM differentiated macrophages (Table 2). However, regarding M-CSF differentiated macrophages cultured in the presence of 100 µM or 300 µM of ^{13}C-αKIC and ^{13}C-αKIV a more extensive analysis revealed M2 leucine labeling and M5 valine labeling, with increased labeling with increasing ^{13}C-BCKA concentration (Figure 19C and D). Additionally, the analysis of the supernatants from the very same macrophage cultures by GC-MS revealed a decrease in M2 KIC labeling (Figure 19A) and M5 KIV labeling (Figure 19B), comparing to the levels detected in the medium without macrophages. Together, these observations suggest that macrophages do take up BCKAs, contrasting with the data acquired using UPLC, and convert them into BCAAs. Additionally, the presence of unlabeled (M0) KIC or KIV in the supernatant from macrophage

cultures (Figure 19A and B) indicate that macrophages also synthesize and release BCKAs into the medium. The apparent discrepancy regarding the uptake of BCKAs by macrophages using the two distinct approaches mentioned above is further discussed in the discussion section of this thesis.

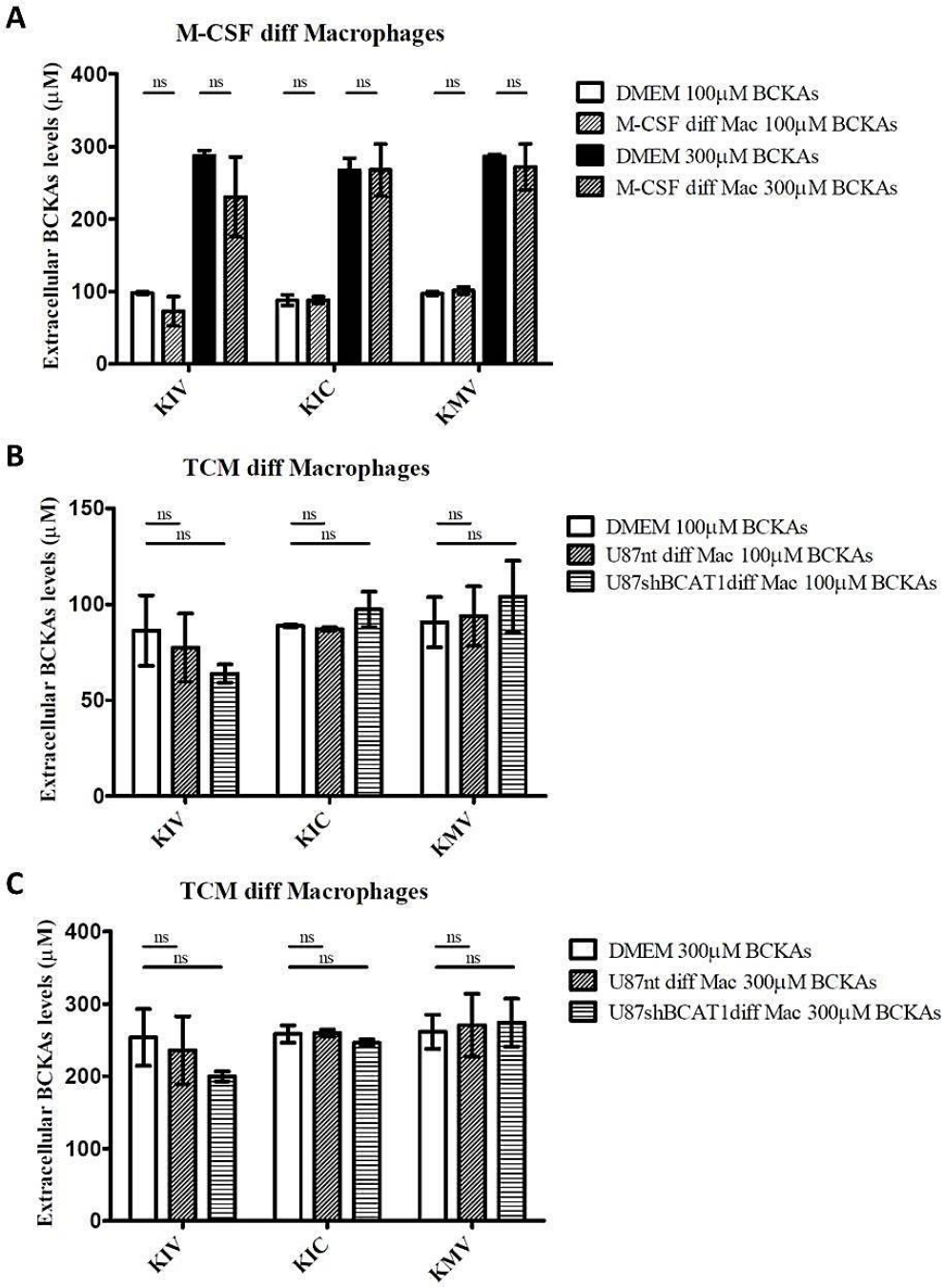

Figure 18 – Extracellular BCKA levels in BCKA-treated monocyte-derived macrophages.

BCKAs (KIV, KIC, KMV) levels were determined by Ultra Performance Liquid Chromatography (UPLC) in supernatants from M-CSF differentiated macrophages cultured with 100 µM or 300 µM of BCKAs **(A)** or from macrophages differentiated using U87nt (nt: non-target) or U87shBCAT1 conditioned medium cultured with 100 µM **(B)** or 300 µM **(C)** of BCKAs and compared to the levels detected in the culture medium (DMEM) in the absence of macrophages. *Data generated with support of Dr. Gernot Poschet, COS, University of Heidelberg, Heidelberg, Germany*. Values are mean ± SD of two independent experiments, run in triplicates. KIV: α-ketoisovalerate. KIC: α-ketoisocaproate. KMV: α-keto-β-methylvalerate. unpaired t-test; ns: not significant

Table 2 – List of intracellular metabolites analyzed by GC-MS after incubation of monocyte-derived macrophages with 100 µM or 300 µM of ^{13}C-αKIC and ^{13}C-αKIV for 48 hours.

Monocytes were isolated from two different donors and differentiated into macrophages using either U87nt /shBCAT1 tumor conditioned medium (TCM) or M-CSF. αKIC: α-ketoisocaproate. αKIV: α-ketoisovalerate.

Macrophages	[^{13}C-αKIC + ^{13}C-αKIV] (µM)	Metabolite
U8tnt TCM/U87shBCAT1 TCM	100	Pyruvate Methionine Succinate Glutamine a-Ketoglutarate Alanine Aspartate Citrate Serine Lactate
M-CSF	100/300	N-acetyl Aspartate Glycine Malate Glutamate Fumarate

A

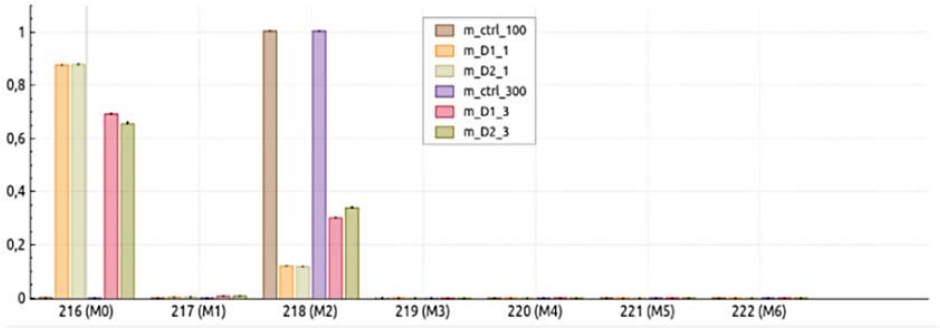

B

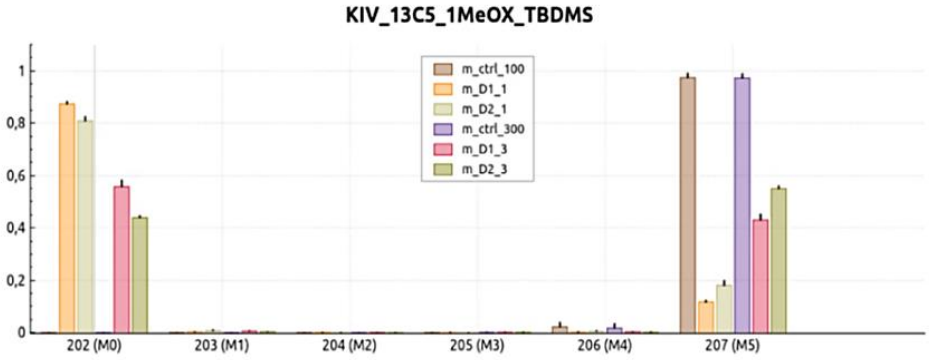

C

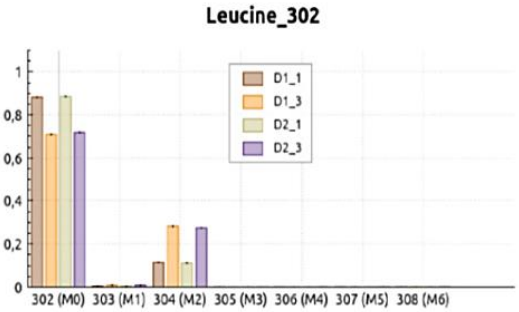

D

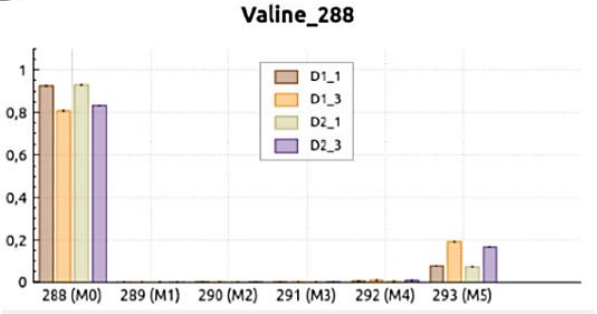

(Figure legend on the next page)

Figure 19 - BCKAs are taken up by human-monocyte derived macrophages and converted to BCAAs.

(A, B) KIC **(A)** and KIV **(B)** labeling pattern was determined by sequential gas chromatography and mass spectrometry (GC-MS) in supernatants from M-CSF differentiated macrophages cultured with 100 µM (1) or 300 µM (3) of ^{13}C-αKIC and ^{13}C-αKIV and compared to the levels detected in the medium (ctrl) with 100 µM (100) or 300 µM (300) of BCKAs in the absence of macrophages.

Leucine **(C)** and Valine **(D)** labeling pattern was determined by GC-MS in cell extracts from M-CSF differentiated macrophages cultured with 100 µM (1) or 300 µM (3) of ^{13}C-αKIC and ^{13}C-αKIV. Values are mean ± standard error of the mean of n=3 technical replicates. Monocytes were isolated from two different donors (D1, D2). Y-axis: Relative abundance of each mass isotopomer (M). M0, M1 to Mn: M is the base mass of an ion fragment and the following number from 0 to *n* (active carbon number) indicates the mass shift from M. *Data generated with support of Yannic Nonnenmacher, TU-BS, Braunschweig, Germany*.

3.1.7. BCKAs reduce macrophage phagocytosis

Glioblastoma exert strong immuno-suppressive effects on their microenvironment including the suppression of macrophage phagocytic activities (Hambardzumyan et al., 2016). It is unclear what role tumor-derived metabolites might have in this process. Here, I considered whether BCKAs could directly affect the phagocytic properties of macrophages. For this purpose the engulfment of fluorescent beads by monocyte-derived macrophages was assessed. Once the beads were biotin-labeled we first discriminated between engulfed and non-engulfed beads using streptavidin PE (Figure 20A). Considering only engulfed beads, we observed a significant decrease in the number of beads in the macrophages cultured with 300 µM of BCKAs compared to the cultures not exposed to BCKAs (Figure 20C), suggesting that tumor cell-derived BCKAs can affect the tumor microenvironment in glioblastoma by suppressing phagocytosis by tumor-associated macrophages.

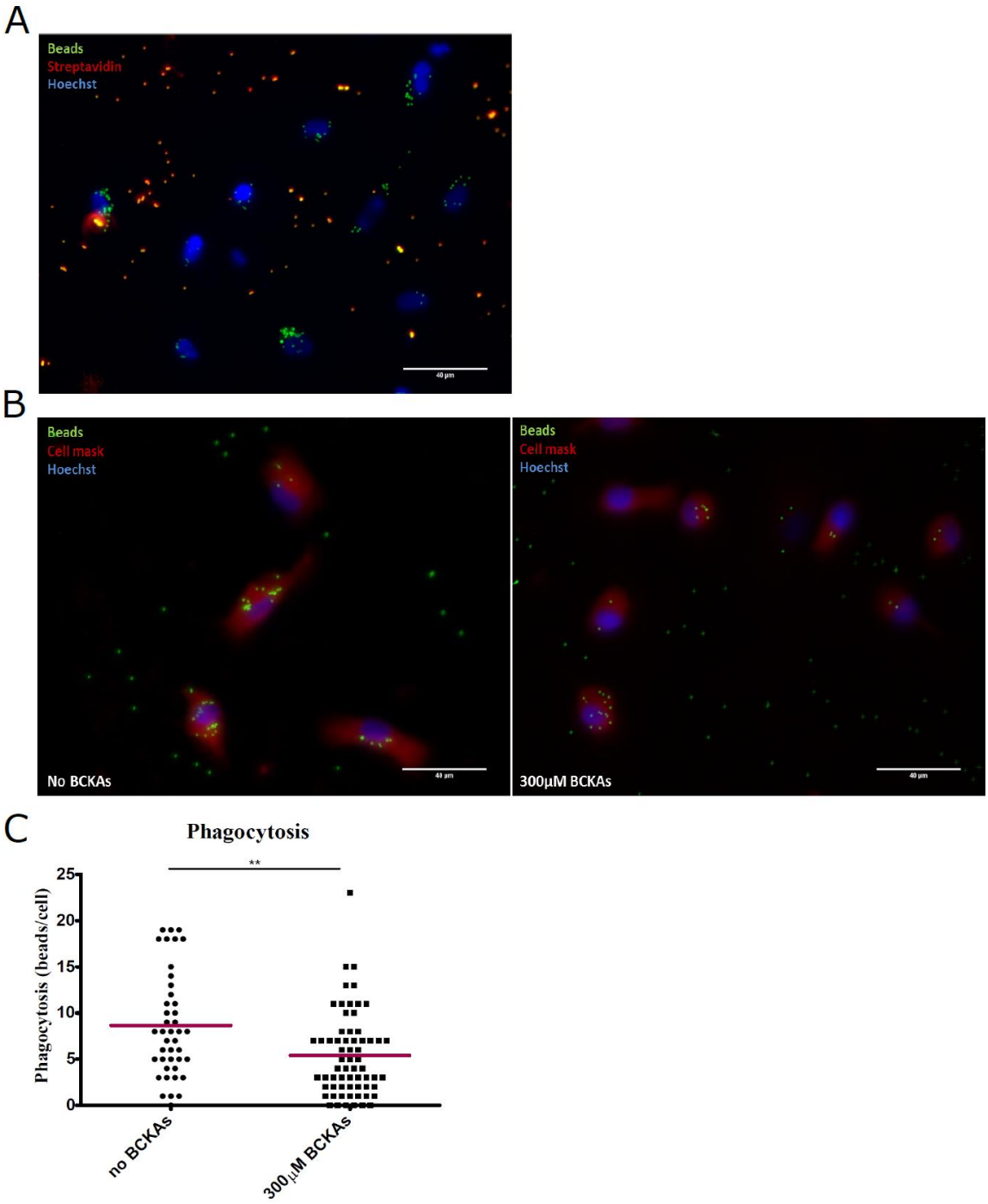

Figure 20 – BCKAs reduce macrophage phagocytosis *in vitro*.

(A) Streptavidin PE (red) binds to non-engulfed biotin-labeled fluorescent beads (green) resulting in an orange staining under fluorescence microscope. **(B)** Comparison between the number of fluorescent beads (green) engulfed by macrophages cultured with and without BCKAs was assessed using fluorescence microscopy. Plasma membrane (red) is stained with Cell Mask stain. **(A), (B)** Hoechst stains nuclei (blue). Scale bar: 40µm. **(C)** The number of beads engulfed by each cell was quantified using ImageJ software. Line represents mean (monocytes were isolated from two different donors and 3-4 fields per condition were examined). Mann Whitney test; ** $p<0.01$

Aiming to explain the observed effect on macrophage phagocytosis caused by BCKAs gene expression arrays of monocyte-derived macrophages differentiated in the presence or absence of BCKAs were performed. It was observed that BCKA treatment had a minor impact on macrophages' expression profiles. This is evident from the observed low fold-change differential expression (2.34 max.) (Supplementary table 2) (Appendix) as well as minor deviations from the diagonal evident in the X/Y-plot of BCKA-treated and control samples (Figure 21A). However, analysis of the data using gene set enrichment analysis (GSEA) revealed a significant (nominal p-value<0.01 and FDR<0.25) enrichment for genes involved in hypoxia and angiogenesis and also, less significant (nominal p-value<0.05 and FDR>0.25), in epithelial-mesenchymal-transition and glycolysis (Figure 21B-E) in macrophages treated with 300μM BCKAs in comparison to untreated (control) macrophages.

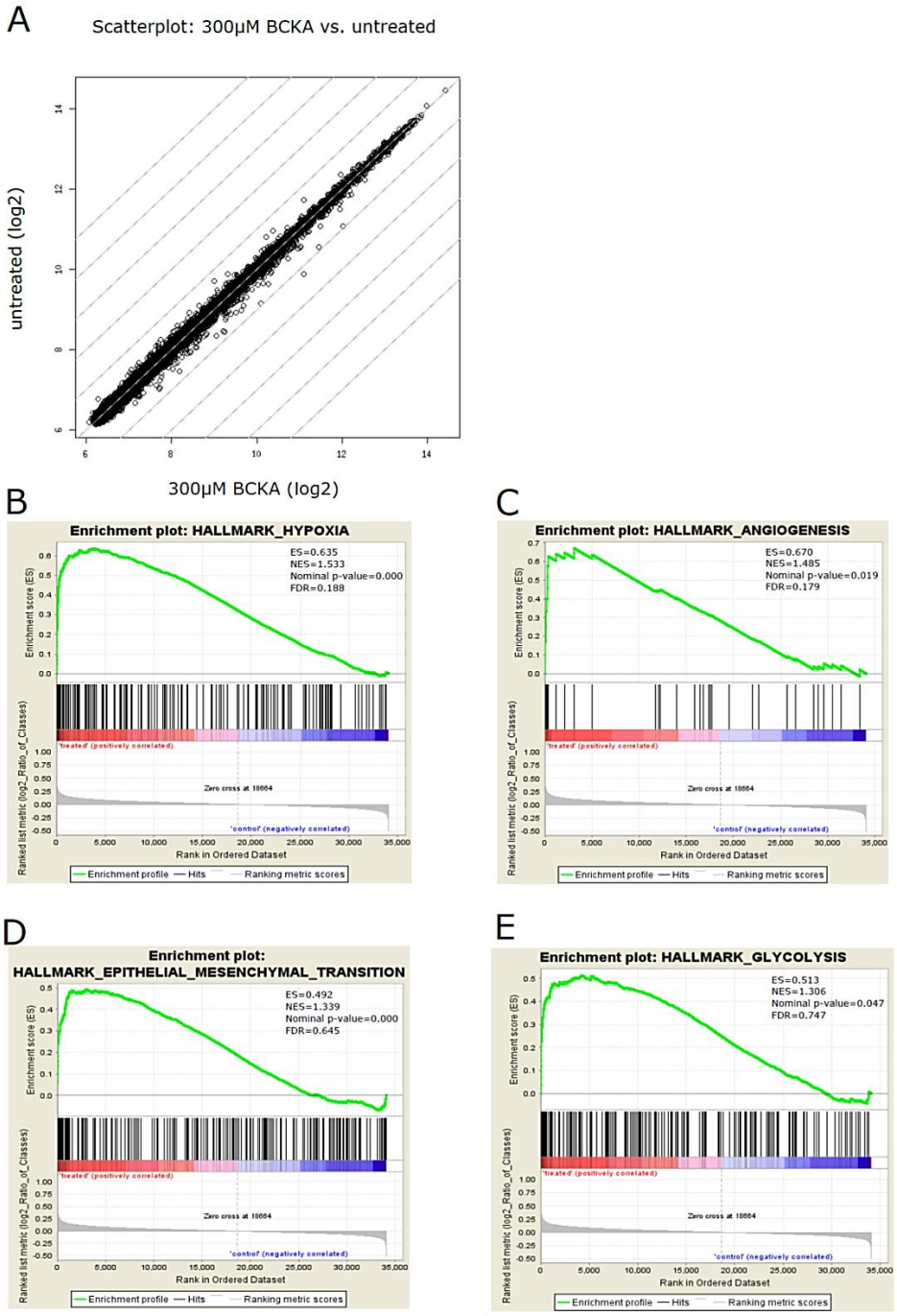

Figure 21 – Differential expression analysis (A) and Gene Set Enrichment Analysis (GSEA) (B-E) of macrophages treated with 300 µM BCKAs in comparison to untreated (control) macrophages.

(A) Scatterplot profiles of differential gene expression in macrophages treated with 300µM BCKA versus untreated macrophages. Axes represent the mean (n=4) expression values in log_2 scale. Diagonal line represent an expression ratio of 1 (similar levels of expression in BCKA-treated and untreated macrophages). Monocytes were isolated from four different donors. *Data generated jointly with Dr. Ann-Christin Gaupel, Department of Molecular Genetics, German Cancer Research Center (DKFZ), Heidelberg, Germany.* ES: enrichment score; NES: normalized enrichment score; FDR: false discovery rate

3.2. Manipulation of BCAT1 expression in the tumor compartment affects stromal cell phenotype

After studying the impact of BCKAs in the stromal cell phenotype I aimed to investigate the effects of BCAT1 knockdown in the tumor cells on the stromal cell phenotype.

3.2.1. shBCAT1 TCM promotes survival and differentiation of monocytes

The effect of manipulation of BCAT1 in the tumor compartment on the cells of the stroma compartment was assessed next. To accomplish this aim, we differentiated monocytes in the presence of conditioned medium harvested from U87 cells expressing low or normal levels of BCAT1 (2.2.12.2). In a first instance monocytes isolated from buffy coats were used and the results were also validated using the U937 monocytic cell line model. It was observed that U87shBCAT1 TCM promoted survival and differentiation of monocytes (Figure 22).

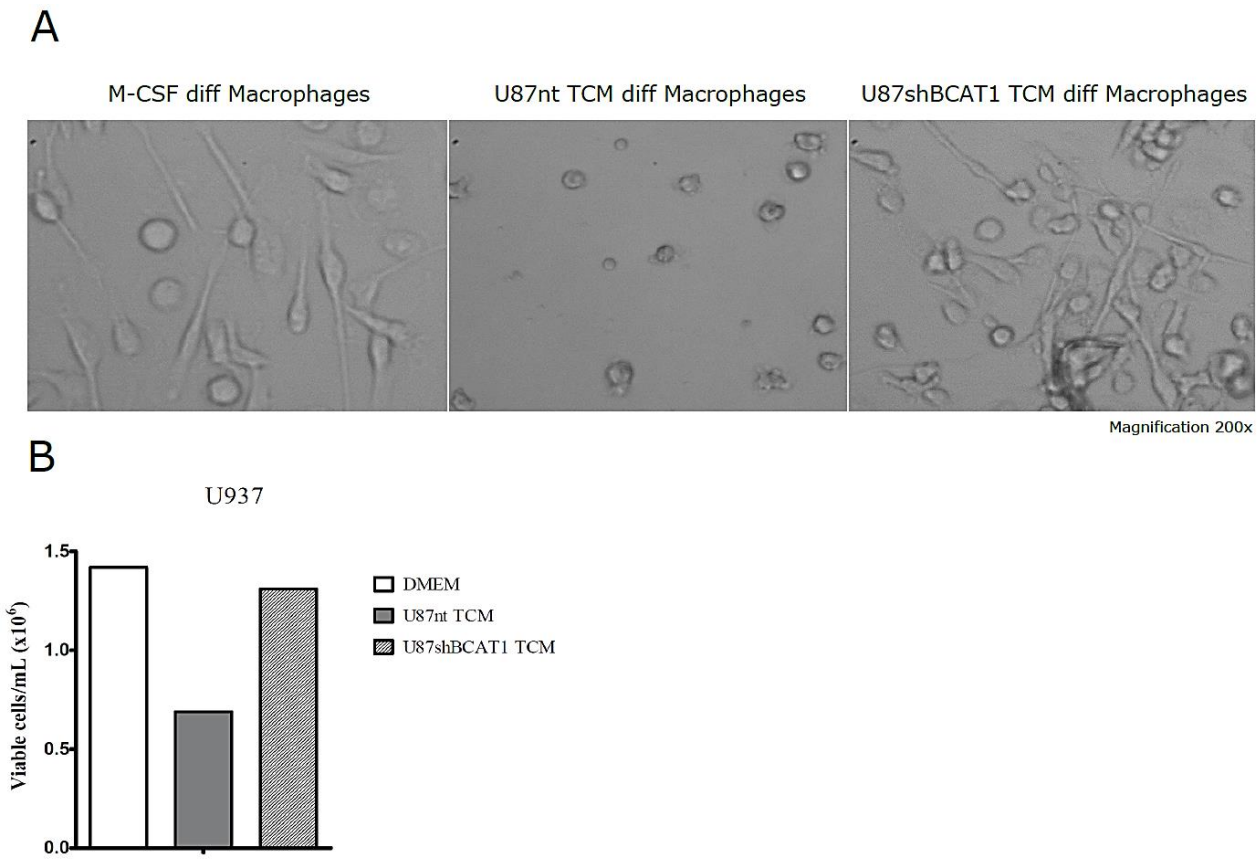

Figure 22 – BCAT1 knockdown TCM promotes monocyte survival and differentiation to macrophages.
(A) Representative pictures of monocytes differentiated in the presence of U87nt (nt: non-target) or shBCAT1 TCM in comparison to those differentiated in the presence of human M-CSF. Magnification: 200x. **(B)** U937 cells were differentiated to macrophages using 5 nM PMA in DMEM medium or in the presence of U87nt or shBCAT1 TCM for 48h. Counts of viable cells/mL were obtained using a Vi-cell counter. **(A)** Experiment was performed twice. **(B)** Experiment was performed once.

3.3.2 BCAT1 knockdown modulates monocyte-derived macrophage expression profile

Gene set enrichment analysis (GSEA) indicated a significant (nominal p-value<0.01 and FDR<0.25) positive enrichment of interferon (IFN) alpha and gamma responses in macrophages differentiated with shBCAT1 TCM (shBCAT1-M) compared to non-target (nt) TCM (nt-M) (Figure 23). This suggests that the expression of BCAT1 in the glioblastoma cells might suppress macrophage inflammatory response. Among the deregulated genes present in the interferon gamma response pathway, a downregulation of the IFN-induced ubiquitin-like protein (UBL) ISG15 – described by others as a regulator of macrophage activation and phagocytosis (Yanguez et al., 2013), was observed in TAMs exposed to nt TCM vs shBCAT1 TCM (Supplementary figure 1) (Appendix). We hypothesize that the high BCKAs levels present in the

nt TCM can decrease ISG15 expression, contributing to the observed decrease in macrophage phagocytosis.

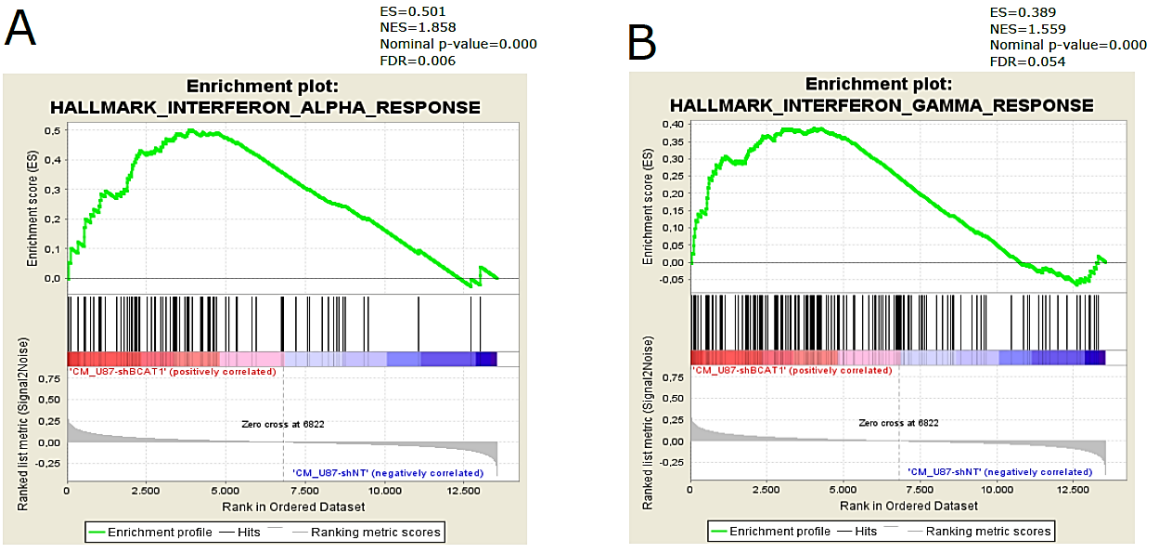

Figure 23 – Macrophages differentiated with U87 shBCAT1 medium or U87nt medium display different expression profiles.

GSEA enrichment plots for the Hallmark_Interferon_alpha_response **(A)** and Hallmark_Interferon_gamma_response **(B)** for macrophages differentiated with U87shBCAT1 medium (shBCAT1–M, n = 4) comparing to U87nt differentiated ones (nt–M, n = 4). ES: enrichment score; NES: normalized enrichment score; FDR: false discovery rate

To investigate the effect of BCAT1 knockdown in the tumor cells a gene expression array for U87 cells expressing normal (nt) or low *BCAT1* levels (shBCAT1) was performed. Differential expression analysis of the data and the investigation of the top 60 deregulated genes revealed upregulation of *CCL2* after BCAT1 knockdown (Supplementary table 3).

Next the effect of BCAT1 knockdown in the production of tumor-derived factors, specifically cytokines was investigated. An increase in the levels of MCP-1/CCL2 was observed, which is in accordance with the observed increased in gene expression, and slight increases in GRO, IL-6 and IL-8 after BCAT1 knockdown (Figure 24). The remaining cytokines present in the array (Appendix) were not affected by BCAT1 knockdown.

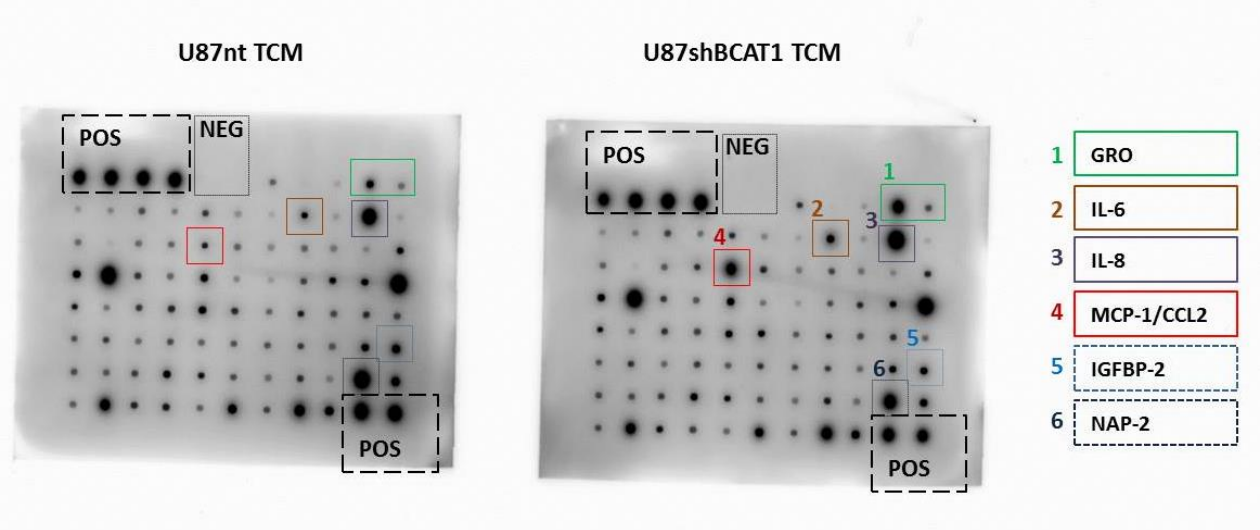

Figure 24 – Overview of the cytokine panel for the 80 cytokines including the internal assay controls and representative blots.

Positive (POS) and negative (NEG) controls are shown. Highlighted are the cytokines that were upregulated or downregulated in U87shBCAT1 TCM with solid or dashed line, respectively, comparing to U87nt TCM.

3.3.3 Monocyte migration is not affected by BCAT1 knockdown in the tumor cells

The effect of BCAT1 knockdown in the tumor cells on the migratory potential of monocytes was assessed using transwell migration assay. Application of U87shBCAT1 TCM (2.2.12.1) showed no evident chemotactic potential of monocytes comparing to U87nt TCM (Figure 25). When comparing the number of migrated cells to the tumor conditioned medium with the CCL2 it was observed that the conditioned medium has higher chemotactic potential of monocytes suggesting the involvement of other tumor-derived factors in addition to CCL2.

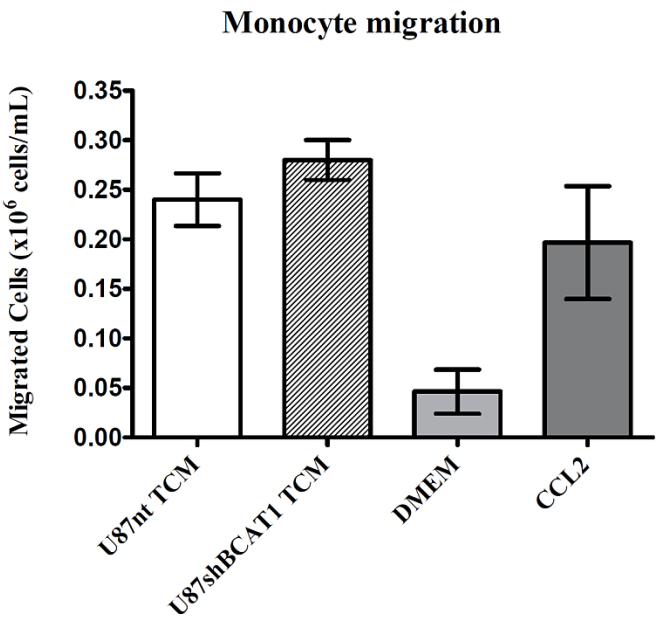

Figure 25 – Monocyte migration assay.

Transwell migration assay with monocytes seeded in upper chamber, 2h migration prior to harvest and cell counting. Indicated chemoattractants were applied in lower chamber: U87nt (nt: non-target) TCM, U87shBCAT1 TCM, DMEM, CCL2. Monocytes were isolated from three independent donors. Values are mean ± SD. *Data generated jointly with Dr. Ann-Christin Gaupel, Department of Molecular Genetics, German Cancer Research Center (DKFZ), Heidelberg, Germany.*

4. Discussion

In the current study, a comprehensive characterization of the branched-chain ketoacids transport in living cells was performed. In a first instance, the production and excretion of these metabolites was characterized in two distinct systems (tumor cell lines and *Xenopus* oocytes). MCT1 and MCT4 were identified as potential BCKAs transporters in living cells with MCT1 being involved in the excretion of BCKAs from glioblastoma cell lines. In a second instance, I evaluated the role of the BCKAs in the tumor-stroma interaction using macrophages as a model of the stromal compartment. In this model, BCKAs were taken up and catabolized by macrophages and impaired macrophage phagocytosis. Finally, I generated data characterizing the stromal cell phenotype after modulating BCAT1 expression in the tumor cell compartment.

4.1 MCT1-mediated excretion of glioblastoma cell branched-chain ketoacids modulates macrophage phagocytosis [2]

Glioblastoma cells excrete BCKAs

Glioblastoma are characterized by overexpression of the metabolic enzyme BCAT1 and associated excretion of glutamate, features that are well-conserved in cell line models (Tönjes et al., 2013). In glioma patients glutamate excretion was shown to cause tumor-associated epilepsy (Buckingham et al., 2011). In the present work I could show that BCKAs, which are generated by BCAT1 alongside glutamate, also are excreted by glioblastoma cells, resulting in the accumulation of high concentrations (in the µM range) in the culture media within 24 hours. The observation that tumor cells excrete BCKAs was intriguing since these metabolites have been reported to be important energy sources (Kainulainen et al., 2013). However, others have shown that BCKAs can be excreted from cells, i.e. during overnight fasting when BCAAs are transaminated to BCKAs in muscle cells which get excreted and transported to the liver for further oxidation (Hutson et al., 2005). In support of the idea that tumor cells might excrete

[2] This chapter is the subject of a manuscript entitled “MCT1-mediated excretion of glioblastoma cell branched-chain ketoacids modulates macrophage phagocytosis” which is currently submitted at *EMBO Reports*, and of which I am the first author and has been originally written by myself.

BCKAs for their own benefit are the observations that accumulation of toxic levels of BCAAs and BCKAs in tissues in maple syrup urine disease (MSUD), a heritable defect of BCAA catabolism, has been shown to affect cell energy metabolism and cell survival (Amaral et al., 2010; Hutson et al., 2005; Sgaravatti et al., 2003).

MCTs mediate BCKAs excretion

It has been previously described that MCTs have affinity for the transport of α-ketoacids (Manning Fox et al., 2000) and that the transport of α-ketoisocaproate (KIC), the ketoacid of leucine, in neurons involves one of the MCT proteins (Mac et al., 2000). The query of published data of primary untreated glioblastoma (n=480; TCGA dataset) revealed that both MCT1 and MCT4, but not MCT2 or MCT3, were significantly overexpressed compared to normal brain lead us to select these two members of the MCT family as potential BCKAs transporters. MCT1 and MCT4 overexpression in glioblastoma was corroborated by others (Lim et al., 2014; Miranda-Goncalves et al., 2013; Takada et al., 2016). Using *Xenopus* oocytes as a heterologous expression system showed that MCT1 and MCT4 can mediate the transport of all three BCKAs across the membranes of living cells. These data are consistent with and extend previous studies showing that uptake of KIC and KIV can be mediated by MCTs in *Xenopus* oocytes (Bröer et al., 1998; Halestrap, 2012).

Modulation of MCT1 and MCT4 transport capacity

Suppression of MCT1 by the MCT1/2-specific inhibitor AR-C155858 (Nancolas et al., 2015) in glioblastoma cell lines indicated that BCKAs are excreted from the tumor cells via MCT1. Since AR-C155858 also inhibits MCT2 when it is associated with the ancillary protein CD147 (Nancolas et al., 2015) one cannot exclude a role of MCT2 in BCKAs export *in vitro*. However, major effects on BCKAs export appear unlikely given that MCT2 rarely associates with CD147 in mammalian cells (Ovens et al., 2010) and furthermore is downregulated in tumor compared to normal brain. Inhibition of MCT1 also significantly reduced the efflux of pyruvate in all three glioblastomas cell lines consistent with similar observations reported for mammary carcinoma cell lines (Hong et al., 2016). Knockdown of MCT4 did not appear to affect the efflux of BCKAs or pyruvate in my analysis. These observations indicate that while both MCT1 and MCT4 are in principle capable of transporting BCKAs, MCT4-mediated transport appears to be attenuated in glioblastoma cells. In part this might be explained by differences in substrate-

dependent transport kinetics. Estimates of Michaelis-Menten constants for MCT1 and MCT4 mediated transport in *Xenopus* oocytes (summarized in (Halestrap, 2012)) are suggesting preferred transport of KIC, KIV and pyruvate by MCT1 (KIC, KIV and pyruvate ~ 1mM vs. lactate 3.5mM) and of lactate by MCT4 (lactate 28mM vs. KIC, KIV and pyruvate ~100-150mM). This is consistent with the idea that in cells that express both MCT1 and MCT4, BCKAs and pyruvate, which are present in the cell at lower concentrations, will preferentially be transported by the high-affinity carrier MCT1, while lactate, which is produced in vast amounts in cancer cells, will be excreted via the high-capacity transporter MCT4.

Despite the lack of evidence for the involvement of MCT4 in BCKA transport in glioblastoma, the observation that MCT4 is significantly upregulated in the mesenchymal subtype of glioblastoma is still relevant in the context of glioblastoma. This observation agrees with what others have published (Lim et al., 2014) and suggests MCT4 as a subtype specific gene in glioblastoma. MCT4 has also been identified as a subtype specific gene in other tumor entities, namely in pancreatic cancer, where MCT4 defines a glycolytic subtype of these tumors (Baek et al., 2014). In glycolytic tumors, cells produce large amounts of lactate and upregulation of MCT4 allows them to eliminate excess lactate and survive (Baek et al., 2014). These observations support our assumption that MCT4 will preferentially excrete lactate.

Transport of metabolites might be further regulated through spatial association of proteins resulting in locally increased metabolite concentrations. In this work, data from *in situ* PLA indicate that BCAT1 and MCTs are in close proximity in glioblastoma cells. Hypothetically, this might serve to further optimize BCKA transport by increasing local BCKA concentrations in the vicinity of the MCTs. Previous studies have provided evidence for an analogous mechanism that the proximity of Carbonic Anhydrase II (CAII) to MCT1 and MCT4 supports the proton/lactate co-transport with CAII acting as a "H^+-collecting antenna" and increasing the concentration of protons in the vicinity of MCTs (Becker et al., 2011; Noor et al., 2015; Stridh et al., 2012).

A similar pattern of metabolite transport as observed in this study was recently reported for mammary carcinoma (Hong et al., 2016). In triple negative breast cancer (TNBC) cell lines, the authors found a segregation of metabolite excretion, with pyruvate and lactate export being exclusively mediated by MCT1 and MCT4, respectively. Further, suppression of MCT1-mediated transport switched tumor metabolism to a more oxidative state and blocked mammary carcinoma growth *in vitro* and in a xenograft model (Hong et al., 2016). A query of published microarray data (GSE76675) of the three breast cancer cell lines (HS578T, SUM149 and

SUM159) used in this study revealed all as having high levels of *BCAT1* expression. Interestingly, it has been shown that in TNBC, BCAT1 almost always is highly overexpressed and is essential for tumor growth in cell line and animal models (Thewes et al., 2017), suggesting that TNBC likely will secrete BCKAs in addition to lactate and pyruvate. This raises the interesting possibility that intracellular accumulation of BCKAs in addition to pyruvate might be causing the growth inhibition that was observed following MCT1 suppression in several studies (Hong et al., 2016; Takada et al., 2016). It will be difficult to address this question since transport of pyruvate and BCKAs via MCT1 might co-occur in many tumors. However, the effects of accumulation of BCKAs in MSUD patients on cell energy metabolism and cell survival (Amaral et al., 2010; Jouvet et al., 2000; Sgaravatti et al., 2003) suggest that blocked BCKA export might be responsible for at least part of the observed phenotype (growth inhibition).

These results expand upon a growing literature on MCT1 involvement in the transport of tumor-derived metabolites and provide further evidence for the eminent role of BCAA catabolism in glioblastomas. Furthermore, the anti-proliferative effects of MCT1 knockdown observed by others (Hong et al., 2016; Takada et al., 2016) might be in part due to intracellular accumulation of BCKAs in addition to pyruvate, adding additional support for the concept of using MCT1 inhibitors as anti-cancer therapeutic drugs.

BCKAs are taken up by macrophages and metabolized to BCAAs

After characterizing the transport of BCKAs from glioblastoma cells I wanted to know whether the predominant cells of the glioblastoma stroma, i.e. tumor associated macrophages, take up and catabolize tumor-secreted BCKAs, as recently had been shown for tumor-derived lactate in mammary carcinoma (Nakajima and Van Houten, 2013). In this model, lactate is produced and excreted via MCT4 by CAFs and taken up by oxygenated tumor cells via MCT1 for ATP production. An analogous exchange of metabolites, in this case the amino acids glutamate/glutamine and a BCAT cycle has been proposed to occur in the normal brain for nitrogen balance maintenance (Bak et al., 2013; Leke et al., 2011). In the present work, isotope tracing analysis provided evidence of a similar metabolite transfer, in which tumor-derived BCKAs appear to be taken up by macrophages and converted to BCAAs. Others have recently shown that in non-small cell lung cancer cells BCAAs can be directly incorporated into protein supporting the needs of rapidly proliferating cells (Mayers et al., 2016). However, the metabolic fate of BCAAs in macrophages, considered as non-proliferative cells *in vitro*, remains poorly described.

Intriguingly, the quantification of BCKAs in BCKA-treated macrophage supernatants using UPLC did not reveal significant reduction of BCKAs levels compared to those detected in the medium without macrophages, failing to support the isotope tracing data that suggest that macrophages take up labeled BCKAs. However, isotope tracing experiments also revealed the presence of high levels of unlabeled (M0) KIC and KIV in the 13C2-KIC- and 13C5-KIV-treated macrophage supernatants, respectively, suggesting that macrophages are able to produce and secrete BCKAs. Given that in the UPLC experiments total BCKAs levels present in the supernatant after 24 hours of BCKA treatment are detected, we hypothesize that the decrease in BCKAs levels is not observed due to the concurrent secretion of BCKAs by macrophages.

BCKAs decrease macrophage phagocytosis

The impact of BCKAs in the cells from the stromal compartment has not been studied so far. In the present study it was shown that macrophages cultured in the presence of 300μM of BCKAs display reduced phagocytic capacity *in vitro*. Reduced phagocytic activity has been associated with an immunosuppressive phenotype of infiltrating macrophages that can be induced by glioma (Hussain et al., 2006; Li and Graeber, 2012). At the expression level, BCKAs did not induce evident changes of the macrophage expression profile, hampering the identification of the mechanism by which these metabolites affect phagocytosis. Interestingly, in this study it was provided evidence for BCKA uptake by macrophages and their conversion to BCAAs. These observations raise the question whether the observed effect of BCKAs-treatment on macrophage phagocytosis is directly mediated by BCKAs or dependent on their catabolism to BCAAs. Nevertheless, the observation that exposure of monocytes to U87 or U251 conditioned medium, which I showed here contains high levels of BCKAs, reduced their phagocytic ability (Rodrigues et al., 2010) is supporting the hypothesis that BCKAs are affecting phagocytosis by glioma-associated macrophages.

Analysis of gene expression arrays of macrophage cultured in the presence or absence of BCKAs using gene set enrichment analysis (GSEA) revealed an enrichment of genes involved in glycolysis in BCKA-treated macrophages. Others have shown that TAMs generated *in vitro* exhibit a pronounced glycolytic signature in a metabolic flux assay, corresponding with elevated glycolytic gene transcript levels that correlated with pro-metastatic phenotype (Penny et al., 2016). However, the factors, present in the conditioned medium that could be responsible

for promoting the phenotype, were not identified (Penny et al., 2016). Here, the data suggest that BCKAs can be one of the tumor-derived factors with impact on macrophage phenotype.

4.2 Manipulation of BCAT1 expression in the tumor compartment affects the stromal cell phenotype

Here I showed that conditioned medium from U87 cells expressing low BCAT1 levels impacted stromal cell, specifically, monocyte and macrophage phenotype. However, the tumor-derived factors involved in this process remain poorly understood, since alterations in BCKAs levels are only one among several consequences of BCAT1 knockdown. This is a very interesting topic but given the complexity of studying tumor-stroma interactions *in vitro* only preliminary data were generated. Gene set enrichment analysis of monocyte-derived macrophages differentiated in the presence of tumor conditioned medium indicated significant positive enrichment of interferon (IFN) alpha and gamma responses in macrophages differentiated with U87shBCAT1 TCM compared to U87nt TCM. The data suggest that BCAT1 expression, associated with production and secretion of BCKAs and other factors by the tumor cells, suppresses macrophage inflammatory response supporting tumor progression. Others showed that IFN-gamma priming of macrophages repressed part of the inflammatory program and attenuated neutrophil recruitment to inflammatory sites (Hoeksema et al., 2015). Moreover, it was shown that normal human monocytes exposed to malignant glioma cells, expressing BCAT1, adopt an immunosuppressive phenotype characterized by reduced phagocytic/antigen presenting ability and increased ability to induce apoptosis in activated T cells (Rodrigues et al., 2010). Among the deregulated genes present in the interferon gamma response pathway a downregulation of the IFN-induced ubiquitin-like protein (UBL) ISG15, described by others as a regulator of macrophage activation and phagocytosis (Yanguez et al., 2013), was observed in TAMs exposed to nt TCM *vs* shBCAT1 TCM. I hypothesize that the high BCKAs levels present in the nt TCM can decrease ISG15 expression, contributing to the observed decrease in macrophage phagocytosis. In agreement with these data, others have shown that $ISG15^{-}/^{-}$ macrophages displayed reduced activation and phagocytic capacity comparing to the $ISG15^{+}/^{+}$ cells (Yanguez et al., 2013). However, using the BCAT1-knockdown conditioned medium, the effect of factors other than BCKAs in the observed modulation of macrophage phagocytosis cannot be excluded.

In addition, I showed that conditioned medium from U87 cells expressing low BCAT1 levels promoted survival and differentiation of monocytes. However, an important aspect that

has to be considered is that the generation of U87nt and shBCAT1 conditioned medium used in the assays where macrophages survival and differentiation was assessed, did not take into account the differences in cell proliferation caused by BCAT1 knockdown (Tönjes et al., 2013). Thus, an impact of different nutrient availability in the alterations observed in the survival and differentiation of monocytes cannot be excluded.

Aiming to further characterize the impact of BCAT1 knockdown in the tumor cells on the stromal cell phenotype, the migration of monocytes towards tumor-cell conditioned medium was investigated. An increase in the expression of CCL2 at the RNA and protein level that was translated into higher secretion of CCL2 after BCAT1 knockdown in U87 cells was observed. CCL2 is a clinically relevant cytokine in glioblastoma supported by the observation that in clinical specimens of glioblastoma, elevated levels of CCL2 expression correlated with reduced overall survival of patients (Chang et al., 2016a). Moreover, given the previous reports suggesting an important role of CCL2 in mediating the dialog between glioma cells and microglia (Zhang et al., 2012) and its role as monocyte/macrophage chemoattractant (Bonapace et al., 2014; Pena et al., 2015), the chemoattractant properties of U87 BCAT1-knockdown conditioned medium in comparison to U87nt medium were evaluated. However, the application of BCAT1-knockdown medium in comparison to U87nt medium did not show any evident change of the chemotactic potential of monocytes. In mammary tumors, estrogen receptor (ER)-α^+ tumors that are characterized by low BCAT1 expression (Thewes et al., 2017) have reduced immune cell infiltration compared to ER- and progesterone receptor (PR)-negative subtypes (Sousa et al., 2015). Since the tumor conditioned medium displayed higher chemotactic potential of monocytes than CCL2, one can hypothesize that monocyte migration is in the scenario being affected by other factors present in the conditioned medium, and independently of BCAT1 knockdown. Others have recently shown that periostin is a glioma-secreted factor that promotes recruitment of monocytes and macrophages (Guo et al., 2016; Zhou et al., 2015).

Moreover, the impact of tumor-derived CCL2 in the stromal cell compartment may involve cell types other than monocytes demonstrating the complexity of the tumor-stroma interaction. Others have recently shown that glioma microenvironment-derived CCL2 recruits regulatory T cells and myeloid-derived suppressor cells (Chang et al., 2016a).

The study of metabolite exchange in the tumor-stroma interaction *in vitro* is demanding and has the limitation that it represents only a subtype of the stromal cell compartment at a time. Besides the effect of tumor-secreted BCKAs in the macrophage phenotype such as phagocytosis, in the complex tumor-stroma interaction it has been shown that promotion of phagocytosis can in turn impact on other cells from the stromal compartment. It has been

recently shown that butyrate, a microbial-derived metabolite, promoted phagocytosis in IL-4-induced macrophages that can limit T-cell production of IL-17A revealing an important aspect of bacterial-host interaction in the regulation of intestinal homeostasis (Fernando et al., 2016).

5. Outlook

In future studies the mechanism through which tumor-secreted BCKAs contribute to the observed decrease in macrophages phagocytosis needs to be clarified in detail to determine whether, as suggested by the data reported here, this phenotype is induced through signals that do not involve alterations in the gene expression of the macrophages.

Regarding the role of tumor-secreted BCKAs in tumor progression it would be intriguing to quantify BCKAs secretion in triple negative breast cancer cell lines that also depend on high BCAT1 expression for sustained growth. This will help to evaluate the hypothesis that the anti-proliferative effects of MCT1 knockdown observed by others might be related to the blocked excretion of BCKAs.

Furthermore, it would be of great interest to extend the work on the effects of BCAT1 knockdown in the tumor compartment on the stroma compartment to other cell types such as T cells, given that preliminary results (Supplementary figure 2) (Appendix) suggested that culture medium from U87 cells after BCAT1 knockdown stimulated $CD8^+$ T cell proliferation *in vitro*. These data imply that BCAT1-knockdown conditioned media are less immunosuppressive than control media, adding additional support for the concept of using BCAT1 inhibitors as anti-cancer therapeutics.

As the modulation of the tumor-stroma interaction *in vitro* has proven to be very complex and the data obtained difficult to interpret, these studies could benefit from the establishment of *in vivo* models to further characterize the impact of metabolite exchange between tumor and stromal cell compartments and the consequences to tumor progression.

6. References

Amaral, A.U., Leipnitz, G., Fernandes, C.G., Seminotti, B., Schuck, P.F., and Wajner, M. (2010). Alpha-ketoisocaproic acid and leucine provoke mitochondrial bioenergetic dysfunction in rat brain. Brain Res *1324*, 75-84.

Baek, G., Tse, Y.F., Hu, Z., Cox, D., Buboltz, N., McCue, P., Yeo, C.J., White, M.A., DeBerardinis, R.J., Knudsen, E.S.*, et al.* (2014). MCT4 defines a glycolytic subtype of pancreatic cancer with poor prognosis and unique metabolic dependencies. Cell Rep *9*, 2233-2249.

Bak, L.K., Waagepetersen, H.S., Sorensen, M., Ott, P., Vilstrup, H., Keiding, S., and Schousboe, A. (2013). Role of branched chain amino acids in cerebral ammonia homeostasis related to hepatic encephalopathy. Metab Brain Dis *28*, 209-215.

Balkwill, F., Charles, K.A., and Mantovani, A. (2005). Smoldering and polarized inflammation in the initiation and promotion of malignant disease. Cancer Cell *7*, 211-217.

Balkwill, F., and Mantovani, A. (2001). Inflammation and cancer: back to Virchow? The Lancet *357*, 539-545.

Balss, J., Meyer, J., Mueller, W., Korshunov, A., Hartmann, C., and von Deimling, A. (2008). Analysis of the IDH1 codon 132 mutation in brain tumors. Acta Neuropathol *116*, 597-602.

Becker, H.M., Broer, S., and Deitmer, J.W. (2004). Facilitated lactate transport by MCT1 when coexpressed with the sodium bicarbonate cotransporter (NBC) in Xenopus oocytes. Biophys J *86*, 235-247.

Becker, H.M., Klier, M., Schuler, C., McKenna, R., and Deitmer, J.W. (2011). Intramolecular proton shuttle supports not only catalytic but also noncatalytic function of carbonic anhydrase II. Proc Natl Acad Sci U S A *108*, 3071-3076.

Bingle, L., Brown, N.J., and Lewis, C.E. (2002). The role of tumour-associated macrophages in tumour progression: implications for new anticancer therapies. J Pathol *196*, 254-265.

Boidot, R., Vegran, F., Meulle, A., Le Breton, A., Dessy, C., Sonveaux, P., Lizard-Nacol, S., and Feron, O. (2012). Regulation of monocarboxylate transporter MCT1 expression by p53 mediates inward and outward lactate fluxes in tumors. Cancer Res *72*, 939-948.

Bola, B.M., Chadwick, A.L., Michopoulos, F., Blount, K.G., Telfer, B.A., Williams, K.J., Smith, P.D., Critchlow, S.E., and Stratford, I.J. (2014). Inhibition of monocarboxylate transporter-1 (MCT1) by AZD3965 enhances radiosensitivity by reducing lactate transport. Mol Cancer Ther *13*, 2805-2816.

Bonapace, L., Coissieux, M.M., Wyckoff, J., Mertz, K.D., Varga, Z., Junt, T., and Bentires-Alj, M. (2014). Cessation of CCL2 inhibition accelerates breast cancer metastasis by promoting angiogenesis. Nature *515*, 130-133.

Brantley, E.C., Guo, L., Zhang, C., Lin, Q., Yokoi, K., Langley, R.R., Kruzel, E., Maya, M., Kim, S.W., Kim, S.-J.*, et al.* (2010). Nitric Oxide-Mediated Tumoricidal Activity of Murine Microglial Cells. Translational Oncology *3*, 380-388.

Bröer, S., Schneider, H.P., Broer, A., Rahman, B., Hamprecht, B., and Deitmer, J.W. (1998). Characterization of the monocarboxylate transporter 1 expressed in Xenopus laevis oocytes by changes in cytosolic pH. Biochem J *333 (Pt 1)*, 167-174.

Buckingham, S.C., Campbell, S.L., Haas, B.R., Montana, V., Robel, S., Ogunrinu, T., and Sontheimer, H. (2011). Glutamate release by primary brain tumors induces epileptic activity. Nat Med *17*, 1269-1274.

Butt, S.A., Sogaard, L.V., Magnusson, P.O., Lauritzen, M.H., Laustsen, C., Akeson, P., and Ardenkjaer-Larsen, J.H. (2012). Imaging cerebral 2-ketoisocaproate metabolism with hyperpolarized (13)C magnetic resonance spectroscopic imaging. J Cereb Blood Flow Metab *32*, 1508-1514.

Cairns, R.A., Harris, I.S., and Mak, T.W. (2011). Regulation of cancer cell metabolism. Nat Rev Cancer *11*, 85-95.

Ceccarelli, M., Barthel, F.P., Malta, T.M., Sabedot, T.S., Salama, S.R., Murray, B.A., Morozova, O., Newton, Y., Radenbaugh, A., Pagnotta, S.M.*, et al.* (2016). Molecular Profiling Reveals Biologically Discrete Subsets and Pathways of Progression in Diffuse Glioma. Cell *164*, 550-563.

Chang, A.L., Miska, J., Wainwright, D.A., Dey, M., Rivetta, C.V., Yu, D., Kanojia, D., Pituch, K.C., Qiao, J., Pytel, P.*, et al.* (2016a). CCL2 Produced by the Glioma Microenvironment Is Essential for the Recruitment of Regulatory T Cells and Myeloid-Derived Suppressor Cells. Cancer Res *76*, 5671-5682.

Chang, I.W., Wu, W.J., Wang, Y.H., Wu, T.F., Liang, P.I., He, H.L., Yeh, B.W., and Li, C.F. (2016b). BCAT1 overexpression is an indicator of poor prognosis in patients with urothelial carcinomas of the upper urinary tract and urinary bladder. Histopathology *68*, 520-532.

Charles, N.A., Holland, E.C., Gilbertson, R., Glass, R., and Kettenmann, H. (2012). The brain tumor microenvironment. Glia *60*, 502-514.

Chiche, J., Le Fur, Y., Vilmen, C., Frassineti, F., Daniel, L., Halestrap, A.P., Cozzone, P.J., Pouyssegur, J., and Lutz, N.W. (2012). In vivo pH in metabolic-defective Ras-transformed fibroblast tumors: key role of the monocarboxylate transporter, MCT4, for inducing an alkaline intracellular pH. Int J Cancer *130*, 1511-1520.

Colegio, O.R., Chu, N.Q., Szabo, A.L., Chu, T., Rhebergen, A.M., Jairam, V., Cyrus, N., Brokowski, C.E., Eisenbarth, S.C., Phillips, G.M.*, et al.* (2014). Functional polarization of tumour-associated macrophages by tumour-derived lactic acid. Nature *513*, 559-563.

Coussens, L.M., and Werb, Z. (2002). Inflammation and cancer. Nature *420*, 860-867.

D'Alessandro, G., Catalano, M., Sciaccaluga, M., Chece, G., Cipriani, R., Rosito, M., Grimaldi, A., Lauro, C., Cantore, G., Santoro, A.*, et al.* (2013). KCa3.1 channels are involved in the infiltrative behavior of glioblastoma in vivo. Cell Death Dis *4*, e773.

Daikhin, Y., and Yudkoff, M. (2000). Compartmentation of brain glutamate metabolism in neurons and glia. J Nutr *130*, 1026S-1031S.

Dang, C.V. (2012). Links between metabolism and cancer. Genes Dev *26*, 877-890.

De Simone, R., Vissicchio, F., Mingarelli, C., De Nuccio, C., Visentin, S., Ajmone-Cat, M.A., and Minghetti, L. (2013). Branched-chain amino acids influence the immune properties of microglial cells and their responsiveness to pro-inflammatory signals. Biochim Biophys Acta *1832*, 650-659.

DeAngelis, L.M. (2001). Brain tumors. N Engl J Med *344*, 114-123.

Dimmer, K.S., Friedrich, B., Lang, F., Deitmer, J.W., and Broer, S. (2000). The low-affinity monocarboxylate transporter MCT4 is adapted to the export of lactate in highly glycolytic cells. Biochemical Journal *350*, 219-227.

Draoui, N., and Feron, O. (2011). Lactate shuttles at a glance: from physiological paradigms to anti-cancer treatments. Dis Model Mech *4*, 727-732.

Eilertsen, M., Andersen, S., Al-Saad, S., Kiselev, Y., Donnem, T., Stenvold, H., Pettersen, I., Al-Shibli, K., Richardsen, E., Busund, L.T.*, et al.* (2014). Monocarboxylate Transporters 1-4 in NSCLC: MCT1 Is an Independent Prognostic Marker for Survival. Plos One *9*.

Fais, S., De Milito, A., You, H., and Qin, W. (2007). Targeting vacuolar H+-ATPases as a new strategy against cancer. Cancer Res *67*, 10627-10630.

Fang, J., Quinones, Q.J., Holman, T.L., Morowitz, M.J., Wang, Q., Zhao, H., Sivo, F., Maris, J.M., and Wahl, M.L. (2006). The H+-linked monocarboxylate transporter (MCT1/SLC16A1): a potential therapeutic target for high-risk neuroblastoma. Mol Pharmacol *70*, 2108-2115.

Fernando, M.R., Saxena, A., Reyes, J.-L., and McKay, D.M. (2016). Butyrate enhances antibacterial effects while suppressing other features of alternative activation in IL-4-induced macrophages. American Journal of Physiology - Gastrointestinal and Liver Physiology *310*, G822-G831.

Feron, O. (2009). Pyruvate into lactate and back: from the Warburg effect to symbiotic energy fuel exchange in cancer cells. Radiother Oncol *92*, 329-333.

Franklin, R.A., Liao, W., Sarkar, A., Kim, M.V., Bivona, M.R., Liu, K., Pamer, E.G., and Li, M.O. (2014). The cellular and molecular origin of tumor-associated macrophages. Science *344*, 921-925.

Fujiwara, S., Wada, N., Kawano, Y., Okuno, Y., Kikukawa, Y., Endo, S., Nishimura, N., Ueno, N., Mitsuya, H., and Hata, H. (2015). Lactate, a putative survival factor for myeloma cells, is incorporated by myeloma cells through monocarboxylate transporters 1. Exp Hematol Oncol *4*, 12.

Gabrusiewicz, K., Rodriguez, B., Wei, J., Hashimoto, Y., Healy, L.M., Maiti, S.N., Thomas, G., Zhou, S., Wang, Q., Elakkad, A.*, et al.* (2016). Glioblastoma-infiltrated innate immune cells resemble M0 macrophage phenotype. JCI Insight *1*.

Galic, S., Schneider, H.P., Broer, A., Deitmer, J.W., and Broer, S. (2003). The loop between helix 4 and helix 5 in the monocarboxylate transporter MCT1 is important for substrate selection and protein stability. Biochemical Journal *376*, 413-422.

Garcia-Espinosa, M.A., Wallin, R., Hutson, S.M., and Sweatt, A.J. (2007). Widespread neuronal expression of branched-chain aminotransferase in the CNS: implications for leucine/glutamate metabolism and for signaling by amino acids. J Neurochem *100*, 1458-1468.

Garcia, C.K., Goldstein, J.L., Pathak, R.K., Anderson, R.G., and Brown, M.S. (1994). Molecular characterization of a membrane transporter for lactate, pyruvate, and other monocarboxylates: implications for the Cori cycle. Cell *76*, 865-873.

Green, C.R., Wallace, M., Divakaruni, A.S., Phillips, S.A., Murphy, A.N., Ciaraldi, T.P., and Metallo, C.M. (2016). Branched-chain amino acid catabolism fuels adipocyte differentiation and lipogenesis. Nat Chem Biol *12*, 15-21.

Guo, X., Xue, H., Shao, Q., Wang, J., Guo, X., Chen, X., Zhang, J., Xu, S., Li, T., Zhang, P.*, et al.* (2016). Hypoxia promotes glioma-associated macrophage infiltration via periostin and subsequent M2 polarization by upregulating TGF-beta and M-CSFR. Oncotarget.

Halestrap, A.P. (2012). The monocarboxylate transporter family--Structure and functional characterization. IUBMB Life *64*, 1-9.

Halestrap, A.P. (2013). The SLC16 gene family - structure, role and regulation in health and disease. Mol Aspects Med *34*, 337-349.

Halestrap, A.P., and Meredith, D. (2004). The SLC16 gene family-from monocarboxylate transporters (MCTs) to aromatic amino acid transporters and beyond. Pflugers Arch *447*, 619-628.

Halestrap, A.P., and Price, N.T. (1999). The proton-linked monocarboxylate transporter (MCT) family: structure, function and regulation. Biochem J *343 Pt 2*, 281-299.

Hambardzumyan, D., Gutmann, D.H., and Kettenmann, H. (2016). The role of microglia and macrophages in glioma maintenance and progression. Nat Neurosci *19*, 20-27.

Hanahan, D., and Weinberg, R.A. (2011). Hallmarks of cancer: the next generation. Cell *144*, 646-674.

Hardwick, L.J., and Philpott, A. (2015). An oncologists friend: How Xenopus contributes to cancer research. Dev Biol *408*, 180-187.

Hoeksema, M.A., Scicluna, B.P., Boshuizen, M.C., van der Velden, S., Neele, A.E., Van den Bossche, J., Matlung, H.L., van den Berg, T.K., Goossens, P., and de Winther, M.P. (2015). IFN-gamma priming of macrophages represses a part of the inflammatory program and attenuates neutrophil recruitment. J Immunol *194*, 3909-3916.

Hong, C.S., Graham, N.A., Gu, W., Espindola Camacho, C., Mah, V., Maresh, E.L., Alavi, M., Bagryanova, L., Krotee, P.A., Gardner, B.K.*, et al.* (2016). MCT1 Modulates Cancer Cell Pyruvate Export and Growth of Tumors that Co-express MCT1 and MCT4. Cell Rep *14*, 1590-1601.

Hu, F., a Dzaye, O.D., Hahn, A., Yu, Y., Scavetta, R.J., Dittmar, G., Kaczmarek, A.K., Dunning, K.R., Ricciardelli, C., Rinnenthal, J.L.*, et al.* (2015). Glioma-derived versican promotes tumor expansion via glioma-associated microglial/macrophages Toll-like receptor 2 signaling. Neuro Oncol *17*, 200-210.

Hussain, S.F., Yang, D., Suki, D., Aldape, K., Grimm, E., and Heimberger, A.B. (2006). The role of human glioma-infiltrating microglia/macrophages in mediating antitumor immune responses. Neuro Oncol *8*, 261-279.

Hutson, S.M., Sweatt, A.J., and Lanoue, K.F. (2005). Branched-chain [corrected] amino acid metabolism: implications for establishing safe intakes. J Nutr *135*, 1557S-1564S.

Hwang, S.Y., Yoo, B.C., Jung, J.W., Oh, E.S., Hwang, J.S., Shin, J.A., Kim, S.Y., Cha, S.H., and Han, I.O. (2009). Induction of glioma apoptosis by microglia-secreted molecules: The role of nitric oxide and cathepsin B. Biochim Biophys Acta *1793*, 1656-1668.

Izumi, H., Takahashi, M., Uramoto, H., Nakayama, Y., Oyama, T., Wang, K.Y., Sasaguri, Y., Nishizawa, S., and Kohno, K. (2011). Monocarboxylate transporters 1 and 4 are involved in the invasion activity of human lung cancer cells. Cancer Sci *102*, 1007-1013.

Izumi, H., Torigoe, T., Ishiguchi, H., Uramoto, H., Yoshida, Y., Tanabe, M., Ise, T., Murakami, T., Yoshida, T., Nomoto, M*., et al.* (2003). Cellular pH regulators: potentially promising molecular targets for cancer chemotherapy. Cancer Treatment Reviews *29*, 541-549.

Jain, M., Nilsson, R., Sharma, S., Madhusudhan, N., Kitami, T., Souza, A.L., Kafri, R., Kirschner, M.W., Clish, C.B., and Mootha, V.K. (2012). Metabolite profiling identifies a key role for glycine in rapid cancer cell proliferation. Science *336*, 1040-1044.

Jamali, S., Klier, M., Ames, S., Barros, L.F., McKenna, R., Deitmer, J.W., and Becker, H.M. (2015). Hypoxia-induced carbonic anhydrase IX facilitates lactate flux in human breast cancer cells by non-catalytic function. Sci Rep *5*, 13605.

Jouvet, P., Rustin, P., Taylor, D.L., Pocock, J.M., Felderhoff-Mueser, U., Mazarakis, N.D., Sarraf, C., Joashi, U., Kozma, M., Greenwood, K*., et al.* (2000). Branched chain amino acids induce apoptosis in neural cells without mitochondrial membrane depolarization or cytochrome c release: Implications for neurological impairment associated with maple syrup urine disease. Mol Biol Cell *11*, 1919-1932.

Kainulainen, H., Hulmi, J.J., and Kujala, U.M. (2013). Potential role of branched-chain amino acid catabolism in regulating fat oxidation. Exerc Sport Sci Rev *41*, 194-200.

Kees, T., Lohr, J., Noack, J., Mora, R., Gdynia, G., Todt, G., Ernst, A., Radlwimmer, B., Falk, C.S., Herold-Mende, C*., et al.* (2012). Microglia isolated from patients with glioma gain antitumor activities on poly (I:C) stimulation. Neuro Oncol *14*, 64-78.

Kennedy, K.M., and Dewhirst, M.W. (2010). Tumor metabolism of lactate: the influence and therapeutic potential for MCT and CD147 regulation. Future Oncol *6*, 127-148.

Kim, J., and Bae, J.S. (2016). Tumor-Associated Macrophages and Neutrophils in Tumor Microenvironment. Mediators Inflamm *2016*, 6058147.

Kirk, P., Wilson, M.C., Heddle, C., Brown, M.H., Barclay, A.N., and Halestrap, A.P. (2000). CD147 is tightly associated with lactate transporters MCT1 and MCT4 and facilitates their cell surface expression. Embo J *19*, 3896-3904.

Klier, M., Andes, F.T., Deitmer, J.W., and Becker, H.M. (2014). Intracellular and extracellular carbonic anhydrases cooperate non-enzymatically to enhance activity of monocarboxylate transporters. J Biol Chem *289*, 2765-2775.

Klier, M., Schuler, C., Halestrap, A.P., Sly, W.S., Deitmer, J.W., and Becker, H.M. (2011). Transport activity of the high-affinity monocarboxylate transporter MCT2 is enhanced by extracellular carbonic anhydrase IV but not by intracellular carbonic anhydrase II. J Biol Chem *286*, 27781-27791.

Koppenol, W.H., Bounds, P.L., and Dang, C.V. (2011). Otto Warburg's contributions to current concepts of cancer metabolism. Nat Rev Cancer *11*, 325-337.

Koukourakis, M.I., Giatromanolaki, A., Harris, A.L., and Sivridis, E. (2006). Comparison of metabolic pathways between cancer cells and stromal cells in colorectal carcinomas: a metabolic survival role for tumor-associated stroma. Cancer Res *66*, 632-637.

Leke, R., Bak, L.K., Anker, M., Melo, T.M., Sorensen, M., Keiding, S., Vilstrup, H., Ott, P., Portela, L.V., Sonnewald, U.*, et al.* (2011). Detoxification of ammonia in mouse cortical GABAergic cell cultures increases neuronal oxidative metabolism and reveals an emerging role for release of glucose-derived alanine. Neurotox Res *19*, 496-510.

Lenting, K., Verhaak, R., Ter Laan, M., Wesseling, P., and Leenders, W. (2017). Glioma: experimental models and reality. Acta Neuropathol *133*, 263-282.

Li, R., Li, H.L., Yan, W., Yang, P., Bao, Z.S., Zhang, C.B., Jiang, T., and You, Y.P. (2015). Genetic and clinical characteristics of primary and secondary glioblastoma is associated with differential molecular subtype distribution. Oncotarget *6*, 7318-7324.

Li, W., and Graeber, M.B. (2012). The molecular profile of microglia under the influence of glioma. Neuro Oncol *14*, 958-978.

Lim, K.S., Lim, K.J., Price, A.C., Orr, B.A., Eberhart, C.G., and Bar, E.E. (2014). Inhibition of monocarboxylate transporter-4 depletes stem-like glioblastoma cells and inhibits HIF transcriptional response in a lactate-independent manner. Oncogene *33*, 4433-4441.

Louis, D.N., Ohgaki, H., Wiestler, O.D., Cavenee, W.K., Burger, P.C., Jouvet, A., Scheithauer, B.W., and Kleihues, P. (2007). The 2007 WHO classification of tumours of the central nervous system. Acta Neuropathol *114*, 97-109.

Louis, D.N., Perry, A., Reifenberger, G., von Deimling, A., Figarella-Branger, D., Cavenee, W.K., Ohgaki, H., Wiestler, O.D., Kleihues, P., and Ellison, D.W. (2016). The 2016 World Health Organization Classification of Tumors of the Central Nervous System: a summary. Acta Neuropathol *131*, 803-820.

Mac, M., Nehlig, A., Nalecz, M.J., and Nalecz, K.A. (2000). Transport of alpha-ketoisocaproate in rat cerebral cortical neurons. Arch Biochem Biophys *376*, 347-353.

Manning Fox, J.E., Meredith, D., and Halestrap, A.P. (2000). Characterisation of human monocarboxylate transporter 4 substantiates its role in lactic acid efflux from skeletal muscle. J Physiol *529 Pt 2*, 285-293.

Manoharan, C., Wilson, M.C., Sessions, R.B., and Halestrap, A.P. (2006). The role of charged residues in the transmembrane helices of monocarboxylate transporter 1 and its ancillary protein basigin in determining plasma membrane expression and catalytic activity. Mol Membr Biol *23*, 486-498.

Mantovani, A., Sozzani, S., Locati, M., Allavena, P., and Sica, A. (2002). Macrophage polarization: tumor-associated macrophages as a paradigm for polarized M2 mononuclear phagocytes. Trends Immunol *23*, 549-555.

Mayers, J.R., Torrence, M.E., Danai, L.V., Papagiannakopoulos, T., Davidson, S.M., Bauer, M.R., Lau, A.N., Ji, B.W., Dixit, P.D., Hosios, A.M.*, et al.* (2016). Tissue of origin dictates branched-chain amino acid metabolism in mutant Kras-driven cancers. Science *353*, 1161-1165.

Migneco, G., Whitaker-Menezes, D., Chiavarina, B., Castello-Cros, R., Pavlides, S., Pestell, R.G., Fatatis, A., Flomenberg, N., Tsirigos, A., Howell, A.*, et al.* (2010). Glycolytic cancer associated fibroblasts promote breast cancer tumor growth, without a measurable increase in angiogenesis: evidence for stromal-epithelial metabolic coupling. Cell Cycle *9*, 2412-2422.

Miranda-Goncalves, V., Honavar, M., Pinheiro, C., Martinho, O., Pires, M.M., Pinheiro, C., Cordeiro, M., Bebiano, G., Costa, P., Palmeirim, I.*, et al.* (2013). Monocarboxylate transporters (MCTs) in gliomas: expression and exploitation as therapeutic targets. Neuro Oncol *15*, 172-188.

Muller, A., Brandenburg, S., Turkowski, K., Muller, S., and Vajkoczy, P. (2015). Resident microglia, and not peripheral macrophages, are the main source of brain tumor mononuclear cells. Int J Cancer *137*, 278-288.

Nakajima, E.C., and Van Houten, B. (2013). Metabolic symbiosis in cancer: refocusing the Warburg lens. Mol Carcinog *52*, 329-337.

Nakayama, T., Yao, L., and Tosato, G. (2004). Mast cell-derived angiopoietin-1 plays a critical role in the growth of plasma cell tumors. J Clin Invest *114*, 1317-1325.

Nancolas, B., Sessions, R.B., and Halestrap, A.P. (2015). Identification of key binding site residues of MCT1 for AR-C155858 reveals the molecular basis of its isoform selectivity. Biochem J *466*, 177-188.

Noor, S.I., Dietz, S., Heidtmann, H., Boone, C.D., McKenna, R., Deitmer, J.W., and Becker, H.M. (2015). Analysis of the binding moiety mediating the interaction between monocarboxylate transporters and carbonic anhydrase II. J Biol Chem *290*, 4476-4486.

Noushmehr, H., Weisenberger, D.J., Diefes, K., Phillips, H.S., Pujara, K., Berman, B.P., Pan, F., Pelloski, C.E., Sulman, E.P., Bhat, K.P*., et al.* (2010). Identification of a CpG island methylator phenotype that defines a distinct subgroup of glioma. Cancer Cell *17*, 510-522.

Ohgaki, H., and Kleihues, P. (2013). The definition of primary and secondary glioblastoma. Clin Cancer Res *19*, 764-772.

Ohka, F., Natsume, A., and Wakabayashi, T. (2012). Current trends in targeted therapies for glioblastoma multiforme. Neurol Res Int *2012*, 878425.

Ovens, M.J., Davies, A.J., Wilson, M.C., Murray, C.M., and Halestrap, A.P. (2010). AR-C155858 is a potent inhibitor of monocarboxylate transporters MCT1 and MCT2 that binds to an intracellular site involving transmembrane helices 7-10. Biochem J *425*, 523-530.

Parsons, D.W., Jones, S., Zhang, X., Lin, J.C., Leary, R.J., Angenendt, P., Mankoo, P., Carter, H., Siu, I.M., Gallia, G.L*., et al.* (2008). An integrated genomic analysis of human glioblastoma multiforme. Science *321*, 1807-1812.

Patel, B.B., Ackerstaff, E., Serganova, I.S., Kerrigan, J.E., Blasberg, R.G., Koutcher, J.A., and Banerjee, D. (2017). Tumor stroma interaction is mediated by monocarboxylate metabolism. Exp Cell Res.

Pellerin, L. (2003). Lactate as a pivotal element in neuron–glia metabolic cooperation. Neurochemistry International *43*, 331-338.

Pena, C.G., Nakada, Y., Saatcioglu, H.D., Aloisio, G.M., Cuevas, I., Zhang, S., Miller, D.S., Lea, J.S., Wong, K.K., DeBerardinis, R.J*., et al.* (2015). LKB1 loss promotes endometrial cancer progression via CCL2-dependent macrophage recruitment. J Clin Invest *125*, 4063-4076.

Penny, H.L., Sieow, J.L., Adriani, G., Yeap, W.H., See Chi Ee, P., San Luis, B., Lee, B., Lee, T., Mak, S.Y., Ho, Y.S*., et al.* (2016). Warburg metabolism in tumor-conditioned macrophages promotes metastasis in human pancreatic ductal adenocarcinoma. Oncoimmunology *5*, e1191731.

Perez-Escuredo, J., Van Hee, V.F., Sboarina, M., Falces, J., Payen, V.L., Pellerin, L., and Sonveaux, P. (2016). Monocarboxylate transporters in the brain and in cancer. Biochim Biophys Acta *1863*, 2481-2497.

Pertega-Gomes, N., Vizcaino, J.R., Attig, J., Jurmeister, S., Lopes, C., and Baltazar, F. (2014). A lactate shuttle system between tumour and stromal cells is associated with poor prognosis in prostate cancer. BMC Cancer *14*, 352.

Pertega-Gomes, N., Vizcaino, J.R., Felisbino, S., Warren, A.Y., Shaw, G., Kay, J., Whitaker, H., Lynch, A.G., Fryer, L., Neal, D.E*., et al.* (2015). Epigenetic and oncogenic regulation of SLC16A7 (MCT2) results in protein over-expression, impacting on signalling and cellular phenotypes in prostate cancer. Oncotarget *6*, 21675-21684.

Philp, N.J., Yoon, H.Y., and Lombardi, L. (2001). Mouse MCT3 gene is expressed preferentially in retinal pigment and choroid plexus epithelia. Am J Physiol-Cell Ph *280*, C1319-C1326.

Pinheiro, C., Longatto-Filho, A., Pereira, S.M., Etlinger, D., Moreira, M.A., Jube, L.F., Queiroz, G.S., Schmitt, F., and Baltazar, F. (2009). Monocarboxylate transporters 1 and 4 are associated with CD147 in cervical carcinoma. Dis Markers *26*, 97-103.

Pinheiro, C., Longatto-Filho, A., Scapulatempo, C., Ferreira, L., Martins, S., Pellerin, L., Rodrigues, M., Alves, V.A., Schmitt, F., and Baltazar, F. (2008). Increased expression of monocarboxylate transporters 1, 2, and 4 in colorectal carcinomas. Virchows Arch *452*, 139-146.

Polanski, R., Hodgkinson, C.L., Fusi, A., Nonaka, D., Priest, L., Kelly, P., Trapani, F., Bishop, P.W., White, A., Critchlow, S.E*., et al.* (2014). Activity of the monocarboxylate transporter 1 inhibitor AZD3965 in small cell lung cancer. Clin Cancer Res *20*, 926-937.

Pollard, J.W. (2004). Tumour-educated macrophages promote tumour progression and metastasis. Nat Rev Cancer *4*, 71-78.

Poole, R.C., and Halestrap, A.P. (1997). Interaction of the erythrocyte lactate transporter (monocarboxylate transporter 1) with an integral 70-kDa membrane glycoprotein of the immunoglobulin superfamily. J Biol Chem *272*, 14624-14628.

Price, N.T., Jackson, V.N., and Halestrap, A.P. (1998). Cloning and sequencing of four new mammalian monocarboxylate transporter (MCT) homologues confirms the existence of a transporter family with an ancient past. Biochem J *329 (Pt 2)*, 321-328.

Ries, C.H., Cannarile, M.A., Hoves, S., Benz, J., Wartha, K., Runza, V., Rey-Giraud, F., Pradel, L.P., Feuerhake, F., Klaman, I.*, et al.* (2014). Targeting tumor-associated macrophages with anti-CSF-1R antibody reveals a strategy for cancer therapy. Cancer Cell *25*, 846-859.

Rodrigues, J.C., Gonzalez, G.C., Zhang, L., Ibrahim, G., Kelly, J.J., Gustafson, M.P., Lin, Y., Dietz, A.B., Forsyth, P.A., Yong, V.W*., et al.* (2010). Normal human monocytes exposed to glioma cells acquire myeloid-derived suppressor cell-like properties. Neuro Oncol *12*, 351-365.

Sapcariu, S.C., Kanashova, T., Weindl, D., Ghelfi, J., Dittmar, G., and Hiller, K. (2014). Simultaneous extraction of proteins and metabolites from cells in culture. MethodsX *1*, 74-80.

Sarkar, S., Doring, A., Zemp, F.J., Silva, C., Lun, X., Wang, X., Kelly, J., Hader, W., Hamilton, M., Mercier, P.*, et al.* (2014). Therapeutic activation of macrophages and microglia to suppress brain tumor-initiating cells. Nat Neurosci *17*, 46-55.

Schioppa, T., Uranchimeg, B., Saccani, A., Biswas, S.K., Doni, A., Rapisarda, A., Bernasconi, S., Saccani, S., Nebuloni, M., Vago, L.*, et al.* (2003). Regulation of the chemokine receptor CXCR4 by hypoxia. J Exp Med *198*, 1391-1402.

Semenza, G.L. (2008). Tumor metabolism: cancer cells give and take lactate. J Clin Invest *118*, 3835-3837.

Sgaravatti, A.M., Rosa, R.B., Schuck, P.F., Ribeiro, C.A.J., Wannmacher, C.M.D., Wyse, A.T.S., Dutra-Filho, C.S., and Wajner, M. (2003). Inhibition of brain energy metabolism by the α-keto acids accumulating in maple syrup urine disease. Biochimica et Biophysica Acta (BBA) - Molecular Basis of Disease *1639*, 232-238.

Sonveaux, P., Vegran, F., Schroeder, T., Wergin, M.C., Verrax, J., Rabbani, Z.N., De Saedeleer, C.J., Kennedy, K.M., Diepart, C., Jordan, B.F*., et al.* (2008). Targeting lactate-fueled respiration selectively kills hypoxic tumor cells in mice. J Clin Invest *118*, 3930-3942.

Sousa, S., Brion, R., Lintunen, M., Kronqvist, P., Sandholm, J., Monkkonen, J., Kellokumpu-Lehtinen, P.L., Lauttia, S., Tynninen, O., Joensuu, H.*, et al.* (2015). Human breast cancer cells educate macrophages toward the M2 activation status. Breast Cancer Res *17*, 101.

Stridh, M.H., Alt, M.D., Wittmann, S., Heidtmann, H., Aggarwal, M., Riederer, B., Seidler, U., Wennemuth, G., McKenna, R., Deitmer, J.W*., et al.* (2012). Lactate flux in astrocytes is enhanced by a non-catalytic action of carbonic anhydrase II. J Physiol *590*, 2333-2351.

Sturm, D., Witt, H., Hovestadt, V., Khuong-Quang, D.A., Jones, D.T., Konermann, C., Pfaff, E., Tonjes, M., Sill, M., Bender, S*., et al.* (2012). Hotspot mutations in H3F3A and IDH1 define distinct epigenetic and biological subgroups of glioblastoma. Cancer Cell *22*, 425-437.

Suryawan, A., Hawes, J.W., Harris, R.A., Shimomura, Y., Jenkins, A.E., and Hutson, S.M. (1998). A molecular model of human branched-chain amino acid metabolism. Am J Clin Nutr *68*, 72-81.

Sweatt, A.J., Wood, M., Suryawan, A., Wallin, R., Willingham, M.C., and Hutson, S.M. (2004). Branched-chain amino acid catabolism: unique segregation of pathway enzymes in organ systems and peripheral nerves. Am J Physiol Endocrinol Metab *286*, E64-76.

Szulzewsky, F., Pelz, A., Feng, X., Synowitz, M., Markovic, D., Langmann, T., Holtman, I.R., Wang, X., Eggen, B.J., Boddeke, H.W*., et al.* (2015). Glioma-associated microglia/macrophages display an expression profile different from M1 and M2 polarization and highly express Gpnmb and Spp1. PLoS One *10*, e0116644.

Takada, T., Takata, K., and Ashihara, E. (2016). Inhibition of monocarboxylate transporter 1 suppresses the proliferation of glioblastoma stem cells. J Physiol Sci *66*, 387-396.

Thewes, V., Simon, R., Hlevnjak, M., Schlotter, M., Schroeter, P., Schmidt, K., Wu, Y., Anzeneder, T., Wang, W., Windisch, P.*, et al.* (2017). The branched-chain amino acid transaminase 1 sustains growth of antiestrogen-resistant and ERalpha-negative breast cancer. Oncogene.

Tönjes, M., Barbus, S., Park, Y.J., Wang, W., Schlotter, M., Lindroth, A.M., Pleier, S.V., Bai, A.H., Karra, D., Piro, R.M.*, et al.* (2013). BCAT1 promotes cell proliferation through amino acid catabolism in gliomas carrying wild-type IDH1. Nat Med *19*, 901-908.

Ullah, M.S., Davies, A.J., and Halestrap, A.P. (2006). The plasma membrane lactate transporter MCT4, but not MCT1, is up-regulated by hypoxia through a HIF-1alpha-dependent mechanism. J Biol Chem *281*, 9030-9037.

Verhaak, R.G., Hoadley, K.A., Purdom, E., Wang, V., Qi, Y., Wilkerson, M.D., Miller, C.R., Ding, L., Golub, T., Mesirov, J.P.*, et al.* (2010). Integrated genomic analysis identifies clinically relevant subtypes of glioblastoma characterized by abnormalities in PDGFRA, IDH1, EGFR, and NF1. Cancer Cell *17*, 98-110.

Viswanath, P., Najac, C., Izquierdo-Garcia, J.L., Pankov, A., Hong, C.B., Eriksson, P., Costello, J.F., Pieper, R.O., and Ronen, S.M. (2016). Mutant IDH1 expression is associated with down-regulation of monocarboxylate transporters. Oncotarget *7*, 34942-34955.

Wang, Z.Q., Faddaoui, A., Bachvarova, M., Plante, M., Gregoire, J., Renaud, M.C., Sebastianelli, A., Guillemette, C., Gobeil, S., Macdonald, E.*, et al.* (2015). BCAT1 expression associates with ovarian cancer progression: possible implications in altered disease metabolism. Oncotarget *6*, 31522-31543.

Warburg, O. (1924). Verbesserte Methode zur Messung der Atmung und Glykolyse. Biochem Zeitschr *152* 51–63

Warburg, O. (1956). On respiratory impairment in cancer cells. Science *124*, 269–270

Wilson, M.C., Meredith, D., Fox, J.E., Manoharan, C., Davies, A.J., and Halestrap, A.P. (2005). Basigin (CD147) is the target for organomercurial inhibition of monocarboxylate transporter isoforms 1 and 4: the ancillary protein for the insensitive MCT2 is EMBIGIN (gp70). J Biol Chem *280*, 27213-27221.

Wyckoff, J., Wang, W.G., Lin, E.Y., Wang, Y.R., Pixley, F., Stanley, E.R., Graf, T., Pollard, J.W., Segall, J., and Condeelis, J. (2004). A paracrine loop between tumor cells and macrophages is required for tumor cell migration in mammary tumors. Cancer Research *64*, 7022-7029.

Xu, M., Liu, Q., Jia, Y., Tu, K., Yao, Y., Liu, Q., and Guo, C. (2016). BCAT1 promotes tumor cell migration and invasion in hepatocellular carcinoma. Oncol Lett *12*, 2648-2656.

Yan, H., Parsons, D.W., Jin, G., McLendon, R., Rasheed, B.A., Yuan, W., Kos, I., Batinic-Haberle, I., Jones, S., Riggins, G.J.*, et al.* (2009). IDH1 and IDH2 mutations in gliomas. N Engl J Med *360*, 765-773.

Yanguez, E., Garcia-Culebras, A., Frau, A., Llompart, C., Knobeloch, K.P., Gutierrez-Erlandsson, S., Garcia-Sastre, A., Esteban, M., Nieto, A., and Guerra, S. (2013). ISG15 regulates peritoneal macrophages functionality against viral infection. PLoS Pathog *9*, e1003632.

Zhang, J., Sarkar, S., Cua, R., Zhou, Y., Hader, W., and Yong, V.W. (2012). A dialog between glioma and microglia that promotes tumor invasiveness through the CCL2/CCR2/interleukin-6 axis. Carcinogenesis *33*, 312-319.

Zhou, W., Ke, S.Q., Huang, Z., Flavahan, W., Fang, X., Paul, J., Wu, L., Sloan, A.E., McLendon, R.E., Li, X.*, et al.* (2015). Periostin secreted by glioblastoma stem cells recruits M2 tumour-associated macrophages and promotes malignant growth. Nat Cell Biol *17*, 170-182.

7. Publications

Silva LS, Becker HM, Poschet G, Nonnenmacher Y, Sapcariu S, Gaupel AC, Kneisel N, Hell R, Hiller K, Lichter P, Radlwimmer B. (submitted). MCT1-mediated excretion of glioblastoma cell branched-chain ketoacids modulates macrophage phagocytosis. EMBO Rep.

8. Appendix

Supplementary table 1 – Metabolite levels detected by Ultra Performance Liquid Chromatography (UPLC) in cell extracts (pmol/million cells) using the DMB derivatization method and in cell culture supernatants and in commercial DMEM (µM) using the OPD derivatization method.
KIV: α-ketoisovalerate. KIC: α-ketoisocaproate. KMV: α-keto-β-methylvalerate; n.d not detected

	DMB method	**OPD method**	
Metabolite	**Levels (pmol/mio cells) - cell extracts**	**Levels (µM) - cell culture supernatants**	**Levels (µM) - DMEM**
KIV	3-16	20-40	n.d
KIC	5-35	40-85	n.d
KMV	7-28	40-85	n.d
Pyruvate	high background	30-130	2-3.5

Plasmid maps

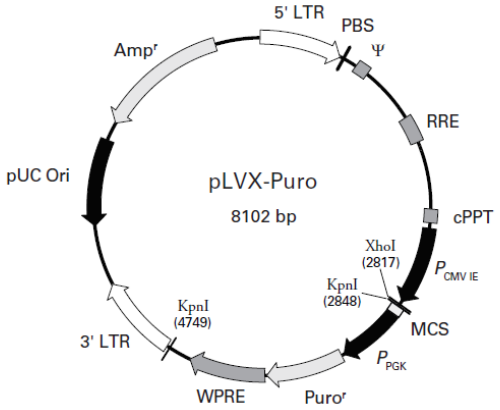

EcoRI SmaI
XhoI BstBI ApaI BamHI
2811 CAGATCTCGA GCTCAAGCTT CGAATTCTGC AGTCGACGGT ACCGCGGGCC CGGGATCCCG
GTCTAGAGCT CGAGTTCGAA GCTTAAGACG TCAGCTGCCA TGGCGCCCGG GCCCTAGGGC
XbaI
2871 CGACTCTAGA
GCTGAGATCT

pLVX-Puro Vector Map and Multiple Cloning Site (MCS).

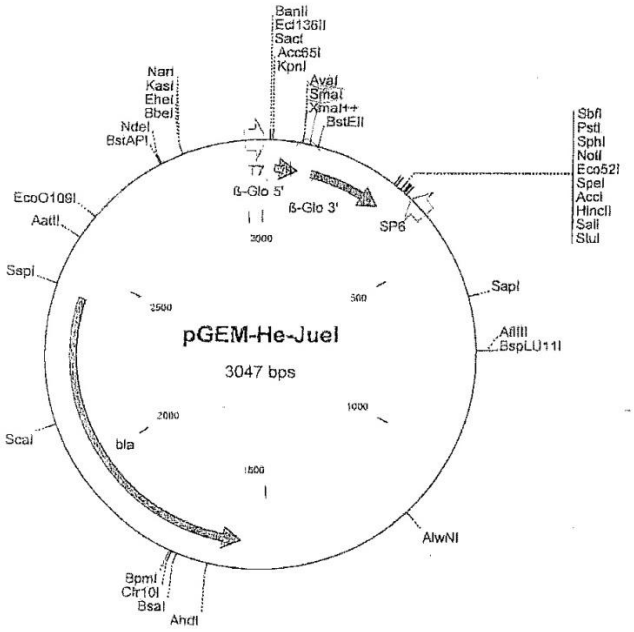

Human Cytokine array maps

	A	B	C	D	E
1	Pos	Pos	Pos	Pos	Neg
2	I-309	IL-1α	IL-1β	IL-2	IL-3
3	IL-12 p40/p70	IL-13	IL-15	IFN-γ	MCP-1
4	MIP-1δ	RANTES	SCF	SDF-1	TARC
5	Oncostatin M	Thrombopoietin	VEGF	PDGF-BB	Leptin
6	FGF-4	FGF-6	FGF-7	FGF-9	Flt-3 Ligand
7	IGFBP-3	IGFBP-4	IL-16	IP-10	LIF
8	NT-4	Osteopontin	Osteoprotegerin	PARC	PIGF

	F	G	H	I	J	K
1	Neg	ENA-78	GCSF	GM-CSF	GRO	GRO-α
2	IL-4	IL-5	IL-6	IL-7	IL-8	IL-10
3	MCP-2	MCP-3	MCSF	MDC	MIG	MIP-1b
4	TGF-β1	TNF-α	TNF-β	EGF	IGF-I	Angiogenin
5	BDNF	BLC	Ck β 8-1	Eotaxin	Eotaxin-2	Eotaxin-3
6	Fractalkine	GCP-2	GDNF	HGF	IGFBP-1	IGFBP-2
7	LIGHT	MCP-4	MIF	MIP-3α	NAP-2	NT-3
8	TGF-β2	TGF-β3	TIMP-1	TIMP-2	Pos	Pos

Supplementary table 2 – List of top20 fold changes after differential analysis of BCKA-treated macrophages in comparison to untreated (control) macrophages.

Gene	**BCKAs** mean	**Control** mean	**BCKAs *vs.* control fold change**
IL8	2207.41	945.35	2.34
PPBP	4151.8	2144.08	1.94
TACSTD2	1095.33	570.95	1.92
ADM	2820.33	1499.69	1.88
IL8	610.98	348.23	1.75
	596.14	352.29	1.69
SLC39A8	509.17	837.15	0.61
CXCL1	289.65	176.7	1.64
MMP12	211.67	132.47	1.6
P4HA1	792.79	504.84	1.57
CXCL5	1235.6	792.93	1.56
LGMN	2201.06	3361.13	0.65
CLLU1OS	826.85	543.41	1.52
DDIT4	732.43	483.95	1.51
LGMN	1189.13	1792.21	0.66
C1QC	1334	1996.87	0.67
CKS2	640.58	944.8	0.68
HSPA6	386.66	264.13	1.46

PLOD2	200.48	137.7	1.46
SLC2A1	346.6	241.58	1.43

Supplementary figure 1 – Macrophages differentiated with U87 shBCAT1 medium or U87nt medium display different expression profiles.

Expression heat map for the Hallmark_Interferon_gamma_response for macrophages differentiated with U87shBCAT1 medium (shBCAT1–M, n = 4) comparing to U87nt differentiated ones (nt–M, n = 4).

Supplementary table 3 – List of top60 fold changes after differential analysis of U87shBCAT1 cells in comparison to U87nt cells.

Gene	**U87shBCAT1** mean	**U87nt** mean	**U87shBCAT1 *vs.* U87nt fold change**
SCG2	2214.709045	93.7519299	23.62307685
TMEM119	1867.096884	177.5250351	10.51737228
STMN3	1268.235829	157.5570893	8.049373307
TGFB3	2413.012782	406.9095429	5.930096317
SIDT2	1684.941689	291.8235467	5.773837335
CYBASC3	3619.178513	702.120406	5.154640831
AKR1B10	1872.710438	365.0159129	5.130489855
CRYGS	535.1100999	106.6719332	5.016409508
HCP5	426.2150221	85.29204986	4.997124853
COL5A2	1755.644119	354.3781855	4.954154039
HSPB3	981.7110333	202.7276716	4.842511264
FAIM2	972.5626291	202.2311702	4.809162841
ADM	5127.621376	1068.379013	4.799440381
CFI	853.8071751	179.8272414	4.747930115
FLVCR2	1601.064901	355.8925179	4.498731557
LEPREL1	1112.246014	254.0379938	4.378266406
C21orf121	591.3750387	141.8482592	4.169068004
CGNL1	452.6282723	111.6604066	4.053614759

HCFC1R1	1008.938194	255.5521201	3.948072095
AQP9	2878.543802	742.8528873	3.874985009
LRRC17	376.318448	99.01885862	3.800472489
KIAA1199	1248.086765	329.3962752	3.789012988
CCL2	303.9872724	82.89332119	3.667210676
MFAP4	3306.271114	913.4494159	3.619544834
RFTN2	388.2066049	107.6924908	3.60476949
NR2F1	714.9705606	199.35044	3.58650104
SAT1	2101.40227	596.7404039	3.521468056
IGFBP3	641.1040215	183.4349582	3.49499369
YPEL2	370.7232405	107.3666429	3.452871678
MAFB	2054.280586	603.3873107	3.404580358
BCAT1	141.3169487	1548.897745	0.091237107
VIL2	273.0487683	1778.057293	0.153565787
EZR	470.1618591	3002.889203	0.156569832
AXL	428.2370133	2326.603799	0.184060996
CEP55	262.8478785	1426.851578	0.184215291
CNIH4	508.5440192	2343.739705	0.216979735
PPM1F	254.2078691	1149.688747	0.221110166
HSP90AB1	632.2350851	2811.79346	0.224851183
CDC20	1150.506112	5000.668044	0.230070483

PRC1	439.1861322	1883.370878	0.233191528
HNRNPD	1472.76046	6207.606031	0.237250955
TOP2A	473.7013864	1996.562486	0.237258483
GINS2	340.3335287	1412.161193	0.241001899
FAM83D	183.4983346	749.9322767	0.244686541
PBK	266.8714535	1062.323111	0.251214956
PODXL	102.7769012	402.2733125	0.25549023
UBE2C	599.0872027	2312.296924	0.259087488
NSMAF	229.9038071	886.5380559	0.259327623
CCNB2	460.265289	1761.01402	0.261363785
TRIB3	187.2138635	714.1019904	0.262166842
LSM14A	269.2634046	1011.462163	0.266212039
CDCA5	331.971421	1230.618649	0.269759784
MCM3	847.2450178	3126.139472	0.271019584
CDCA7	191.2168573	699.9084426	0.273202673
DLGAP5	339.0962419	1234.001528	0.274794021
FJX1	358.0659257	1298.194984	0.275818294
TRIP13	320.4616059	1156.371166	0.277126943
MELK	328.2925602	1181.273456	0.277914109
AURKB	197.7867771	704.897095	0.280589576
CDCA4	160.1998057	560.077708	0.286031391

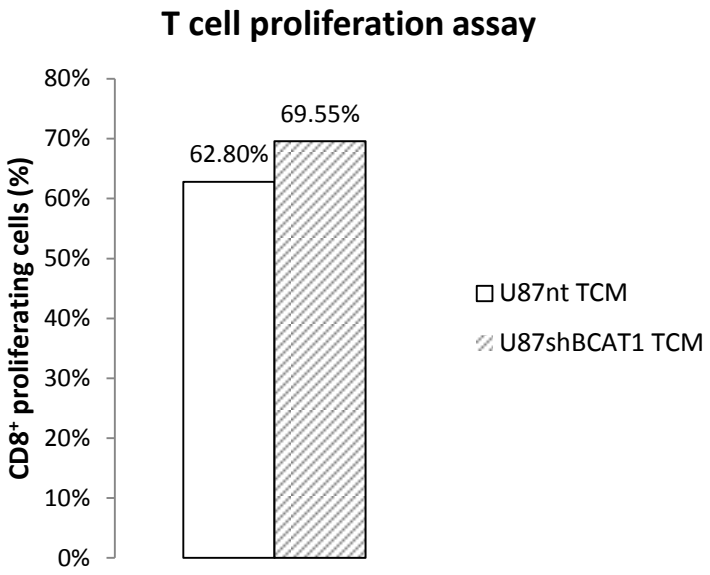

Supplementary figure 2 – U87shBCAT1 conditioned medium stimulates T cell proliferation.

T cells were enriched out of the total PBMCs isolated from a healthy donor using a negative selection protocol (Miltenyi Biotec). Isolated T cells were cultured with conditioned medium from U87-MG cells expressing normal BCAT1 levels (nt) or decreased BCAT1 levels (shBCAT1) and stimulated with IL-2 and PHA for 6 days**.** Proliferation was determined by CFSE dilution. Values are mean of two technical replicates. *Data generated jointly with Soumya Mohapatra and Dr. Christiane Opitz, Brain Cancer Metabolism Group, German Cancer Research Center (DKFZ), Heidelberg, Germany.*

9. Acknowledgments

The work presented in this PhD thesis would not have been possible to do without the support and guidance that I received from many people, to whom I express my gratitude:

Dr. Bernhard Radlwimmer for the direct supervision of my PhD thesis work, for giving me the opportunity to develop my project in his group and for all the ongoing support and helpful discussions.

Prof. Dr. Peter Lichter for providing me the opportunity to integrate his division and for all the helpful discussions throughout my PhD. I highly appreciate that you always took time to discuss my PhD project and give positive and fruitful input regarding experiments and publication-related issues.

Prof. Dr. Rüdiger Hell for his scientific input and support as the first examiner of my PhD thesis and member of my TAC committee.

Dr. Christiane Opitz for her valuable contributions as member of my TAC committee and as the second examiner of my PhD thesis.

Prof. Dr. Peter Angel for his willingness to evaluate my PhD thesis and his contribution as member of my examination committee.

Prof. Holger Becker for a great collaboration and all the input and work performed on *Xenopus* oocytes.

Dr. Gernot Poschet for a great collaboration, fruitful discussions regarding UPLC experiments. I am thankful for your openness to exchange expertise regarding techniques and analysis of the data.

Yannic Nonnenmacher, Sean Sapcariu and Prof. Dr. Karsten Hiller for performing GC-MS experiments, analysis of the data and their input on this topic.

All the members from the B06x division for providing a great working atmosphere.

Michaela Kirchgäßner and Magdalena Schlotter for their excellent technical support during this work.

Dr. Martina Seiffert for helpful discussions and scientific input on the tumor microenvironment.

Members of the Tumor Metabolism group for helpful scientific discussions and excellent working environment.

Tumor Metabolism group alumni – Irene Helbing for the great support in the beginning of this work and for introducing me to the PLA, Martje Barbus for all the advices and help inside and outside the lab and Ann-Christin Gaupel for helpful discussions and her experimental contribution to this work.

Yonghe Wu for all the helpful scientific discussions, encouragement and for listening to all my complaints.

Jasmin Mangei for the great help in writing the German summary of this work and for all the great times inside and outside the lab.

Liliana and Laura for the great Spanish-Portuguese environment, all the support inside and outside the lab and the good times.

My family for the ongoing support. My parents for their incentive, for all the words of affection, and encouragement, for being always there!

My boyfriend Duarte for his emotional (and technical) support, dedication, patience throughout this whole time and for always believing in me and in my work.